האוניברסיטה העברית בירושלים
THE HEBREW UNIVERSITY OF JERUSALEM
THE ROBERT H. SMITH FACULTY OF AGRICULTURE, FOOD AND ENVIRONMENT

Electroflocculation of a model colloidal suspension: coagulation/flocculation mechanisms and their impact on flux in membrane ultrafiltration

Thesis Submitted for the Degree of "Doctor of Philosophy"

by

Tali Harif

Submitted to the Senate of the Hebrew University in Jerusalem in 2006

This thesis was performed under the supervision of

Professor Avner Adin

Acknowledgements

Professor Avner Adin for his supervision and guidance

Yoav for his unlimited support and devotion

Moti for doing his share so well

Dr. Rivka Amit from the Geological Survey of Israel for kindly allowing use of the Malvern Mastersizer Microplus and supplemental instrumentation

Professor David Avnir from the Chemistry Department at the Hebrew University of Jerusalem for enlightening discussions on the fractal dimension

Dr. Yaniv Soffer for supporting and understanding

In dedication of my father

And did you get what
you wanted from this life, even so?
I did.
And what did you want?
To call myself beloved, to feel myself
beloved on the earth.

"Late Fragment" by Raymond Carver

All experiments were conducted using a model kaolin suspension of 15-60mg/l, prepared in distilled water, conductivity increased and pH corrected to 5, 6.5 or 8. Various EF cells were designed, depending on the requirements of each section of research. All cells were operated in batch mode, and comprised two electrodes – a stainless steel cathode and an aluminum anode. The electrodes were connected to a DC external power source. The cell was operated in galvanostatic mode: the current was set and the potential found its own value at a predetermined rate, defined by Faraday's law.

Changes in ζ potential and pH were monitored. Fractal analysis was used in conjunction with image analysis and particle size distributions to gain a comprehensive analysis of the aggregates/flocs formed in the EF process. Size and structural evolution measurements were performed utilizing static light scattering techniques.

The membrane unit used was a stirred cell type, and the membranes were flat sheet hydrophilic polyethersulfone ultrafiltration membranes. The effect of suspension pretreatment on membrane fouling was measured by flux decline at constant pressure.

This study has identified key mechanisms dictating coagulation and flocculation behavior in EF, and gained an understanding of differences in these mechanisms compared to those in CF. The pH of the suspension is a vital parameter dictating coagulation and flocculation behavior and in EF, unlike CF, its final value will always be higher than its initial value. This rise is continuous and results in the shifting of coagulation mechanisms while the current is applied. The degree of pH change, however, can be controlled by adequate mixing conditions, and standard velocity gradient values were found to be sufficient for this.

The passage of current was found to affect particle transport. This could be due to the electrical field induced as enhanced aggregation of primary particles was observed without applying a velocity gradient for suspensions with high conductivity suspensions in which the diffusion barrier between primary particles was lowered.

In EF the sweep floc range is wider than in CF. Thus, EF is able to produce flocs over a wide range of doses and pH values. This versatility produces a range of floc "types", depending on conditions of operation.

The growth patterns of floc in EF were of sigmoidal behavior, and unlike CF were attained for all currents applied. This behavior was observed in CF only within optimal dose limits.

Floc growth in EF is quicker than in CF which EF shows a dependency of growth rate on current (dose), with higher growth rates obtained at higher currents. This dependency also depends on the initial pH, and a higher dependency exists for enhanced precipitation zones (pH 6.5).

Differences in structural evolution patterns between the two processes have also been identified. For adequate flocculation conditions (i.e sufficient growth) in CF the growth is into a more porous structure. In EF, however, the evolution is generally from a less compact structure into a more compact one. EF produces flocs which initially are more porous than those formed in CF, but are more fragile and more susceptible to shear forces. Thus they undergo compaction and in some cases structural fluctuation.

It appears that the flocculation mechanism in EF is of a diffusion limited type, whereas in CF it is more of a reaction limited nature. This can explain differences in floc growth rate and floc structural evolution between the two processes.

Floc size growth was found to be independent of current density, although these were found to be correlated to current application times.

EF was found to serve as an efficient pretreatment to membrane ultrafiltration with enhanced flux observed at pH 6.5 for higher currents, where sweep floc dominates and more porous floc structures are obtained. The major fouling factor is cake formation although results indicate that a degree of pore blocking occurs. The differences in critical flux can be attributed to cake properties, such as thickness and porosity, which are a function of the quantity of precipitate in solution and floc structure, respectively.

This thesis has provided conceptual development and experimental justification which unravel the mechanisms of EF. Thus EF is shown to be a versatile and reliable technology, which can serve as an alternative to conventional processes and has considerable potential for water treatment and reuse.

List of publications

T. Harif, M. Hai and A. Adin. "Electroflocculation as potential pretreatment in colloid ultrafiltration", 2006, *Water Science and Technology/WaterSupply* 1(6): 69-78.

T. Harif and A. Adin. "Characteristics of aggregates formed by electroflocculation of a colloidal suspension", 2006 (submitted to *Water Research*).

T. Harif, M. Hai and A. Adin. "Size and structure evolution of kaolin-$Al(OH)_3$ flocs in the electroflocculation process: A study using static light scattering", 2006 (submitted to *Environmental Science and Technology*).

T. Harif, M. Hai and A. Adin. "Comparing electroflocculation to conventional flocculation: coagulation/flocculation mechanisms and resulting floc characteristics", 2006 (in preparation).

Table of contents

List of figures

List of tables

Nomenclature

Alphanumeric notations

Δb	distance between electrodes
ΔG^0	Standard Gibb's free energy of formation
ΔP	pressure gradient
b	growth factor
C_D	drag coefficient of particle
CF	conventional flocculation
C_i	concentration of specie i
$D(V,0.5)$	volume mean diameter
D_2	two-dimensional fractal dimension
DC	direct current
D_f	(number) fractal dimension
d_i	particles of size i
d_j	particles of size j
dp	pore diameter
P_T	applied pressure
du/dy	velocity gradient of fluid
E	actual electrode half potential (mV or V)
E^0	standard electrode half potential
E_0	The equilibrium potential
$E^0{}_A$	standard anode potential
$E^0{}_C$	standard cathode potential
E_a	anode half cell potential
E_c	cathode half cell potential
EF	electroflocculation
E_l	loss potential

E_s	solution potential
F	Faraday's constant (96,486 $Cmol^{-1}$)
F_{BT}	back-transport drag force
F_y	filtrate flow drag force
G	root mean velocity gradient (sec^{-1})
I	current intensity (A)
$I(q)$	angular scattering intensity
i_c	current density
J	flux through membrane
J_0	initial flux
J_p	flux through membrane
K	Boltzman's constant
K	empirical aggregation constant
K	fitting parameter
K_A	aggregation constant
K_B	floc breakup constant
l	diameter of sphere
L	length of the scattering body
L	resolution or size of square (box counting technique)
m	metal dissolving (gr)
m	number of compartments (completely mixed reactors in series)
m	relative refractive index of the primary particles
Me	metal
MF	microfiltration
MW	molecular weight of metal (gr/mol)
n	absolute refractive index
n	number of moles

N_0	initial particle count
n_1^0, n_1^m	number concentrations of primary particles in initial water and in m_{th} compartment
NF	nanofiltration
n_i	particle concentration of particles of size i
n_j	particle concentration of particles of size j
n_k	particle concentration of particles of size k
N_l	number of particles
N_t	total particle count at time t
P(q)	form factor
PSD	particle size distribution
q	wave number
R	The gas constant ($8.314 Jmol^{-1}K^{-1}$)
R_a	resistance from adsorption inside pores
R_c	resistance from cake formation
R_{cp}	resistance from concentration polarization
R_m	initial membrane resistance
RO	reverse osmosis
R_p	resistance from pore blocking
r_s	primary particle/scatterer radius
S(q)	structure factor
SE	scattering exponent
SHE	standard hydrogen electrode
T	absolute temperature of the fluid (^oK)
T	time (Argaman and Kaufman equation for flocculator)
t	time (min or sec)
UF	ultrafiltration
v_{BT}	back-transport velocity

Z	number of electrons

Greek symbols

ζ	zeta potential (mV)
α	collision efficiency
β	collision frequency
μ	fluid viscosity
ε	turbulent energy dissipation rate
υ	kinematic viscosity of fluid
ϕ	volume fraction of particles
θ	scattering angle
λ	in vacuo wavelength of beam
ξ	the validity limit
η	electrode overpotential (mV or V)
σ	distance between electrodes
ε	porosity
$\delta\chi$	thickness of membrane

Chapter 1- Introduction and Literature Review

One of the major challenges facing all countries today is to provide clean water to their expanding populations. Due to population growth, urbanization and climatic changes, even highly developed countries, such as the U.S, are realizing the importance of improving existing water supply networks by utilizing all potential water resources. These resources include recycled wastewater as well as raw water, which in the past might have been neglected due to its poor quality. There is, therefore, a need to develop innovative, more effective and less expensive techniques for treatment of water and wastewater. A wide range of water and wastewater treatment techniques are known which the application of varies depending on the quality of the raw water and the intended use of the treated water. Electroflocculation (EF) is gaining popularity and is becoming recognized as an alternative to conventional coagulation/flocculation processes. Despite treatment of wastewater by electrochemical processes for most of the 20^{th} century, even more so in recent years, limited scientific research has explored the efficiency of the technology as an alternative process for water treatment. No substantial research has been conducted on the mechanisms of coagulation and flocculation in the EF process which are directly affected by the unique conditions the process creates, caused by imposing an electrical current to produce the active coagulant species – and are yet to be understood.

1.1 Coagulation, definition and role in water treatment

One of the most effective unit operations of water purification is the coagulation of colloidal and otherwise finely divided particles prior to sedimentation and filtration. In essence, coagulation is preparation of unwanted suspensoids for phase separation. Coagulation basically refers to all reactions and mechanisms which result in the overall process of particle aggregation. These include in situ coagulant formation and chemical particle destabilization which lead to physical inter-particle contacts.

1.1.1 Colloid stability

Colloids are termed reversible or irreversible, depending on their stability (Kruyt, 1952). Reversible colloids are energetically or thermodynamically stable, whereas irreversible colloids are thermodynamically unstable. The latter include clays, metal oxides and microorganisms, which comprise all of the solid particles present in natural water. Irreversible colloids can be kinetically stable or unstable. Kinetically stable colloids coagulate at a slow rate whereas kinetically unstable colloids coagulate rapidly. The coagulation process is used to transform a stable colloidal suspension into an unstable one by increasing the rate or kinetics at which the particles aggregate.

1.1.2 Stabilization theory

Colloidal stability can arise from either electrostatic or steric interactions. Electrostatic stabilization is caused by the surface charge of the colloid. Most particles in water have a negative charge and attract positive ions, which accumulate in the interfacial region surrounding the particle. This rigid layer of counterions is called the Stern layer (fig. 1.1.2-1). The combination of both primary charge and counterion accumulation in the interfacial region result in an electrical double layer. The electrostatic attraction of ions of opposite charge to the particle counterions, and molecular diffusion that acts against the concentration gradients produced by the electrostatic effects, cause the formation of a cloud of ions around the particle known as the diffuse layer. When two similarly charged colloids approach one another, their diffuse layers overlap and interact. This electrostatic interaction results in a repulsive force between them. The repulsive potential energy increases as the distance between the particles decreases. Attractive forces also exist between particles, which arise from dipole-dipole interactions between the atoms comprising the particles and water. These are van der Waals forces and result in an attractive potential energy that decreases with increasing separating distance between two particles. In the most basic case, the net inter-particle force between colloidal particles is governed by the sum of the attractive van der

Waals and the repulsive electrical double layer forces, as defined by the DLVO theory (Derjaguin and Landau, 1941; Verwey and Overbeek, 1948).

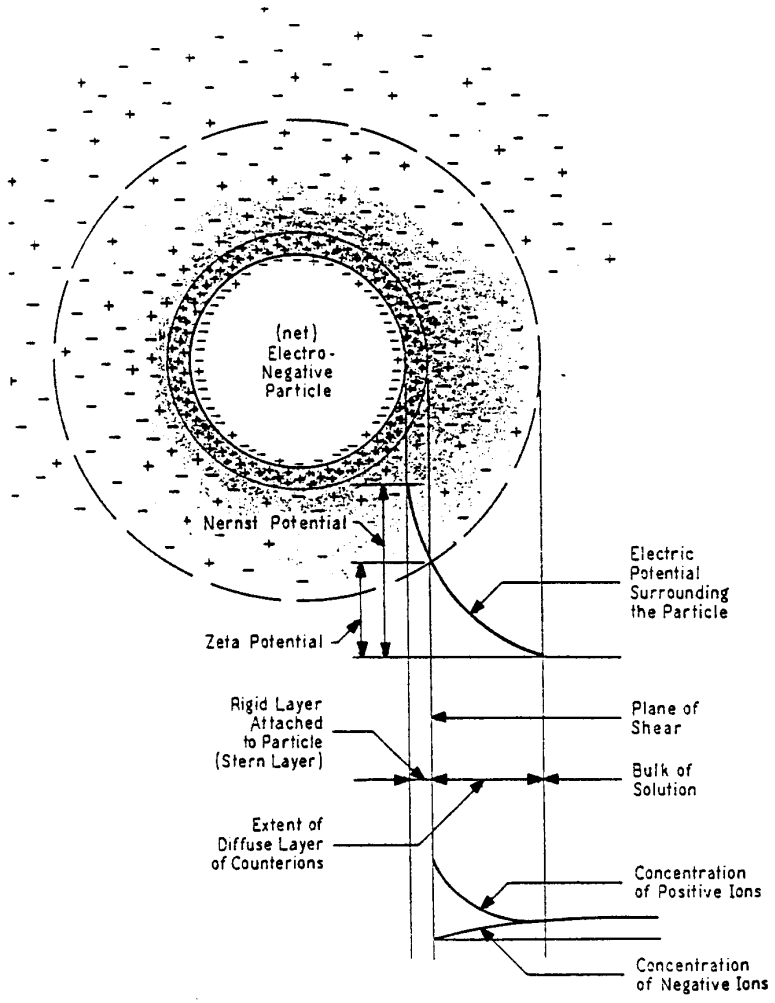

Figure 1.1.2-1 A negatively charged particle, the diffuse layer and location of the ζ potential.

1.1.3 ζ potential

The ζ potential is defined as the potential that causes the motion of particles associated with the plane of shear of fluid around the particles, which is located at the outer border of the Stern layer (Lyklema, 1978). The ζ potential depends on the potential at the surface of the particle and the composition of the Stern layer. It is an indirect measurement of the charge on particles, and its value determines the extent of the electrostatic forces of repulsion between charged particles, which indicates the extent of stability of the suspension. These forces

change with the addition of a coagulant, and the ζ potential serves as a destabilization indicator. The destabilization ability of a coagulant is comprised of coagulant-colloid, coagulant-solvent, and colloid-solvent interactions. The ζ potentials of particles in natural water are typically –20 to –40mV. Suspensions that are destabilized well due to charge neutralization can have ζ potentials close to 0mV.

1.1.4 Destabilization mechanisms

The destabilization of colloidal suspensions is achieved by addition of a chemical coagulant. There are four distinct destabilization mechanisms (Stumm and Morgan, 1962; Stumm and O'Melia, 1968; Amitharajah and O'Melia, 1990):

- compression of the double layer
- adsorption to produce charge neutralization
- enmeshment in a precipitate
- adsorption allowing interparticle bridging

1.1.4.1 Compression of the double layer

A high concentration of electrolyte in solution produces a correspondingly high concentration of counterions in the diffuse layer. The volume of the diffuse layer necessary to maintain electroneutrality is, therefore, decreased reducing the effective "thickness" of the diffuse layer. This decreases the repulsive interaction between the colloidal particles and van der Waals forces become dominant, eliminating electrostatic stabilization and allowing coagulation (Verwey and Overbeek, 1948). Both simple and complex salts can promote coagulation by double layer compression. Destabilization occurs in the presence of ions of opposite charge to the colloid (positive ions) the extent of which differs with different ionic charges. The effects of different salts on coagulation is summarized in the Shultz-Hardy law which states that the destabilization of a colloid by an electrolyte is caused by ions of opposite charge to the colloid, and that the coagulation effectiveness increases with ion charge.

1.1.4.2 Adsorption and charge neutralization

Often coagulant-colloid interactions have more impact than electrostatic effects (Tamamushi and Tamaki, 1959). This is due to relatively higher covalent chemical bond energies than those of electrostatic interactions. The destabilization ability of a coagulant is comprised of coagulant-colloid, coagulant-solvent, and colloid-solvent interactions. For coagulants commonly used in water treatment, such as hydrolyzed aluminum ions and cationic polyelectrolytes, specific adsorption is dominant and generally caused by coagulant-colloid interactions. They bind to specific sites on the colloid surface and by doing so neutralize the electrostatic surface charge of the colloid. When using coagulants that promote coagulation through adsorption and charge neutralization, smaller doses are required (than when using simple metal salts). At high doses charge reversal can occur (the net charge on the particles is reversed from negative to positive by adsorption of excess (positively charged) coagulant) which results in restabilization of the suspension (Matijevic et. al., 1964; Posselt et. al., 1968).

1.1.4.3 Enmeshment in a precipitate

When metal salts are used as coagulants in sufficient concentration, and at a favorable pH, precipitation of metal hydroxides occurs (e.g. $Fe(OH)_3$ and $Al(OH)_3$ precipitates). Colloidal particles can be enmeshed in these precipitates as they are formed and also collide with them afterwards (Packham, 1965). This type of coagulation is termed “sweep-floc” coagulation and combines destabilization and transport processes, resulting in considerably improved particle removal than when particles are destabilized by charge neutralization alone. Part of the reason is the greatly improved rate of aggregation, due to the increased solids concentration.

1.1.4.4 Adsorption and interparticle bridging

Destabilization by bridging is caused by polymer coagulants. Segments of a single polymer can absorb on more than one particle, thereby linking the particles together (Ruehrwein and Ward, 1952; Michaels, 1954; Laher and Healy, 1963). Effective bridging requires that absorbed polymers extend far enough from the particle surface to attach to other particles and

also that part of the surface is free for adsorption of the extended segments. Surface saturation can occur if excess polymer is used, which causes restabilization (by steric stabilization) of the suspension (Laher and Healy, 1963).

1.1.5 Metal salts as coagulants

Hydrolyzing metal salts, based on aluminum or iron, are very widely used as coagulants in water treatment. The most common additives are aluminum sulfate (generally known as "alum"), ferric chloride and ferric sulfate. Other products based on pre-hydrolyzed metals are also now widely used, including a range of materials known as polyaluminum chloride. Their mode of action depends on the specific hydrolysis products, while cationic monomeric or polymeric hydolysis products will lead to adsorption and charge neutralization (Matijevic et. al., 1961; Stumm and O'Melia, 1968) and amorphous hydroxide precipitate will induce "sweep flocculation".

1.1.5.1 Monomeric hydrolysis products

All metal cations are hydrated to some extent in water. The primary hydration shell comprises of water molecules which are in direct contact with the central metal ion. In the cases of Al^{+3} and Fe^{+3} it is known that the primary hydration shell consists of six water molecules in octahedral coordination (Richens, 1997). Due to the high charge on the metal ion, water molecules in the primary hydration shell are polarized, and this can lead to a loss of one or more protons, depending on the solution pH. In effect, the water molecules are being replaced by hydroxyl ions, giving a lower positive charge, according to the sequence:

$$Me^{+3} \rightarrow Me(OH)^{+2} \rightarrow Me(OH)_2^{+} \rightarrow Me(OH)_3 \rightarrow Me(OH)^{-4} \qquad (1.1.5.1\text{-}1)$$

This scheme is oversimplified, as dimeric, trimeric and polynuclear hydrolysis products of Al^{+3} and Fe^{+3} can form. However, these can often be ignored, especially in dilute solutions, and may not greatly affect the overall metal speciation (Duan and Gregory, 2003).

1.1.5.2. Aluminum

Dissolution of the aluminum cation (Al^{+3}) into a solution will result in the formation of various hydrolysis products in equilibrium with the amorphous hydroxide precipitate. The total amount of soluble species in equilibrium with the amorphous hydroxide is effectively the solubility boundary of aluminum, which reaches a minimum at 0.03mg/l, at pH 6.3 (fig. 1.1.5.2-1), with solubility increasing as the solution becomes either more acidic or alkaline (Stumm and Morgan, 1962; Stumm and O'Melia, 1968; Letterman et al., 1999; Duan and Gregory, 2003). Thermodynamics dictates the speciation of the stable aqueous species, and considering only mononuclear speciation, complexes are initially formed as described by equations (1.1.5.2-1)-(1.1.5.2-4):

$$Al^{+3}_{(aq)} + H_2O \rightarrow AlOH^{+2}_{(aq)} + H^{+}_{(aq)} \qquad (1.1.5.2\text{-}1)$$

$$AlOH^{+2}_{(aq)} + H_2O \rightarrow Al(OH)_2^{+}{}_{(aq)} + H^{+}_{(aq)} \qquad (1.1.5.2\text{-}2)$$

$$Al(OH)_2^{+}{}_{(aq)} + H_2O \rightarrow Al(OH)_{3(s)} + H^{+}_{(aq)} \qquad (1.1.5.2\text{-}3)$$

$$Al(OH)_{3(s)} + H_2O \rightarrow Al(OH)_4^{-}{}_{(aq)} + H^{+}_{(aq)} \qquad (1.1.5.2\text{-}4)$$

Although the speciation of aluminum systems has been well documented in the literature (O'Melia, 1972; Sposito, 1996; Duan and Gregory, 2003), little information is available on the kinetics which determines the rate at which thermodynamic equilibrium is attained. The complexity of the aqua-aluminum system is neither completely understood nor completely quantified (Letterman et al., 1999). Hence, it will be assumed that mononuclear hydrolyzed species adequately predict aluminum hydroxide precipitation.

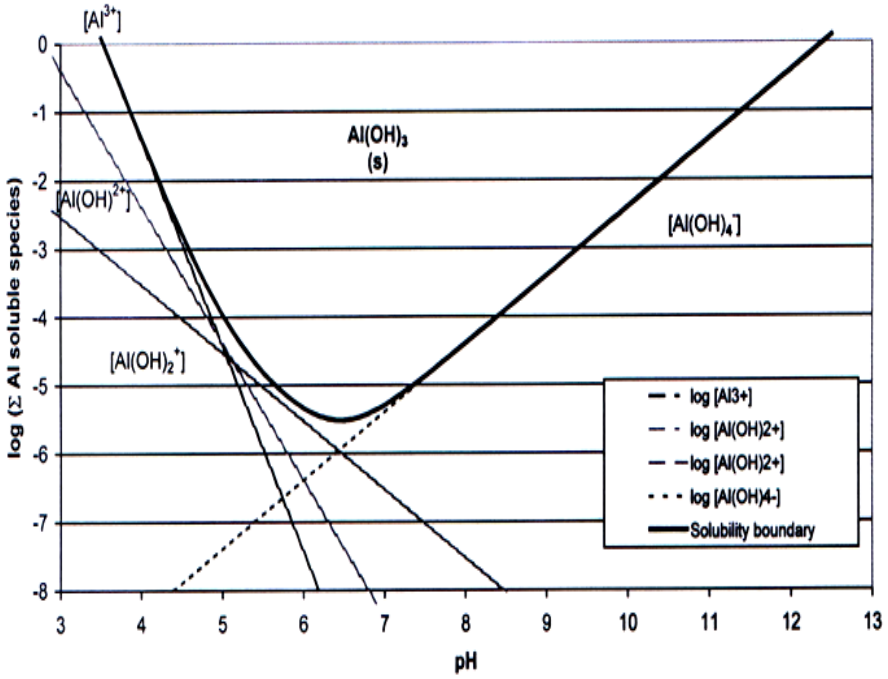

Figure 1.1.5.2-1 Solubility diagram of aluminum hydroxide ($Al(OH)_{3(s)}$) considering only mononuclear species (Holt et al., 2002).

1.1.5.2.1 Precipitation of amorphous aluminum hydroxide

Several models for aluminum hydroxide precipitation have been suggested (Bottero et al., 1987; Bradley et al., 1993), although detailed mechanisms are still not clear. The initially precipitated form undergoes rearrangement on ageing or heating and eventually attains long-range crystalline order. However, in the context of coagulation by hydrolyzing metal salts, it is the rapidly-formed amorphous precipitate which is of most interest.

The effect of mixing conditions on aluminum precipitation has been studied in some detail by Clark et al. (1993), whose work showed that there is competition between the formation of polynuclear hydrolysis products and the precipitated solid. With more intense mixing, the results indicated that precipitation would be favored.

The surface charge characteristics of the precipitated aluminum are of utmost importance in coagulation. Like oxides and other minerals, it exhibits an iso-electric point (i.e.p) at which the apparent (electrokinetic) surface charge is zero. At pH values below the i.e.p the precipitate is positively charged and at higher pH values it will have a negative charge. The

value of the i.e.p depends on the preparation details and on the specific solution composition, therefore there are discrepancies in values reported in the literature. The i.e.p of aluminum hydroxide has been found to be between pH 8-9, depending on sampling procedure (Sposito, 1996). The varying charge with pH will greatly affect precipitation and consequently the overall coagulation process, as towards the i.e.p, as stability decreases, the particles will be able to aggregate into large settleable flocs. Floc size and density is a crucial parameter in determining the effectiveness of the coagulation process. It should be noted that the i.e.p for aluminum hydroxide occurs at a pH value well above that of minimum solubility, so that the largest flocs do not correspond with the maximum amount of precipitate (Duan and Gregory, 2003).

1.2 Flocculation

The second stage of the overall process of coagulation is flocculation. In this stage destabilized suspended particles are aggregated into larger floc in two steps: transport and attachment. The rate of aggregation is determined by the rate at which interparticle collisions occur and the fraction of collisions which result in attachment. As the aggregates grow in size, hydrodynamic shearing forces can cause them to break up. These simultaneous processes lead to a steady-state distribution of aggregate sizes.

The transport step, bringing about the collision of two particles is caused by local variations in fluid/particle velocities. Several mechanisms that can induce the relative motion of particles in the fluid are identified as (Smoluchowski, 1917):

- Brownian diffusion, which is the random motion due to diffusion for small sub-micron particles in suspension (also termed *perikinetic flocculation*).
- Fluid shear from mixing. The spatial variations of the fluid velocity cause the particles to move with different velocities in the flow, and thus promote collisions (also termed *orthokinetic flocculation*).
- Differential settling due to different particle settling velocities.

Attachment depends upon short range forces between the particles (e.g. van der Waals forces) which are a function of particle surface properties (as discussed in section 1.1). These interactions determine whether or not the colliding particles would form a permanent attachment, and will influence the resulting strength of the aggregates. Moreover, these steps influence the frequency and efficiency of the particle-particle collisions which ultimately determine the rate of aggregation. The number of collisions – frequency – is affected by the mode of transport mechanisms, while the collision efficiency – the percentage of successful collisions resulting in bonding/aggregate formation – depends on colloidal interactions.

1.2.1 Flocculation modeling

The most basic model describing the rate of successful collision between two particle sizes, *i* and *j*, is given by:

$$\text{Rate of flocculation} = \alpha\beta(i,j)n_i n_j \qquad (1.2.1\text{-}1)$$

α= *collision efficiency*

$\beta(i,j)$= *collision frequency between particles of size i and j.*

ni,nj = the particle concentration for particles of size i and j, respectively.

The collision frequency, β, is a function of the mode of flocculation (*perikinetic, orthokinetic or differential settling*). The collision efficiency, α, has values between 0 and 1, and is a function of the degree of particle destabilization. In effect, β is a measure of the transport efficiency leading to collisions, whilst α represents the percentage of those collisions leading to attachment.

Nearly all flocculation models are based upon this one fundamental equation. The values of α and β are dependent upon a large number of factors ranging from the nature of the particles to the destabilization mechanism and mixing intensity during flocculation.

The first major attempt at modeling the flocculation process was made by Smoluchowski (1917). The model he developed has formed the core of almost all subsequent research into flocculation modeling.

The rate of change in the number concentration of particles of size k is given by:

$$dn_k/dt = \tfrac{1}{2} \Sigma \beta_{ij} n_i n_j - n_k \Sigma \beta_{ik} n_I \qquad (1.2.1\text{-}2)$$

Subscripts *i*, *j* and *k* represent discrete particle sizes. The first term on the right defines the increase in particles of size *k* by flocculation of two particles whose total volume is equal to the volume of a particle of size *k*. The second term describes the loss of particles of size k because of their aggregation with other particle sizes. By presenting an equation for each value of *k*, Smoluchowski constructed a series of differential equations that described the whole of the flocculation process. These equations are non-linear and their solution complex, therefore simplifying assumptions were made in order to create more "manageable" equations:

- The collision efficiency factor, α, is unity for all collisions.
- Fluid motion undergoes laminar shear.
- The particles are monodispersed (all of them are the same size).
- No breakage of flocs occurs.
- All particles are spherical in shape and remain so after collision.
- Collisions involve only two particles.

Based on these assumptions, Smoluchowski developed the following analytical expressions for both perikenitic and orthokinetic flocculation:

$$\beta_{perikentic} = (2KT/3\mu)(1/d_i + 1/d_j)(d_i + d_j) \qquad (1.2.1\text{-}3)$$

$$\beta_{orthokinetic} = (1/6)(du/dy)(d_i + d_j)^3 \qquad (1.2.1\text{-}4)$$

K = Boltzman's constant

T – absolute temperature of the fluid (^oK)

μ = fluid viscosity

du/dy = velocity gradient of the fluid

Smoluchowski produced solutions to the set of differential equations for both perikinetic and orthokinetic, the solution for the latter being:

$$N_T = N_0 \exp(4/\pi)\, du/dy\, \phi\, t \qquad (1.2.1\text{-}5)$$

N_t = total particle count at time t

N_0 = initial particle count

ϕ = volume fraction of the particles. Assumed to be constant and given by $(4/3)\pi a^3 N_0$ where a is the particle radius.

A treatment of flocculation in turbulent conditions was first carried out by Camp and Stein (1943). Their assumption was that the collision mechanism of colloidal particles in a turbulent flow is analogous to that in laminar shear flow. They used a "root mean square velocity gradient", G, to characterize the distribution of shear rates in a stirred tank.

$$G = (\varepsilon/\upsilon)^{1/2} \qquad (1.2.1\text{-}6)$$

Where ε is the turbulent energy dissipation rate and υ is the kinematic viscosity of the suspending fluid.

When replacing the shear rate in the coagulation kernel of laminar shear flow (*du/dy*) with *G,* the collision frequency is:

$$\beta = (G/6)(di + dj)^3 \qquad (1.2.1\text{-}7)$$

Harris et al. (1966) extended this development further and showed that the rate of particle aggregation becomes proportional to G:

$$dN_T/dt = -KG\phi N_T \qquad (1.2.1\text{-}8)$$

K is an empirical aggregation constant that depends on system chemistry, the heterogeneity of the suspensions and variations in the scale and intensity of turbulance.

Different integrated forms of this equation have been developed for different flow systems, for example the previous authors (Harris et al., 1966) showed that for a series of identical completely-mixed reactors:

$$n_1^o/n_1^m = (1 + K\phi GT/m)^m \qquad (1.2.1\text{-}9)$$

K= empirical aggregation constant

m = number of compartments

n_1^0, n_1^m *= number concentrations of primary particles (or coagules) in the unflocculated water and in the effluent of the* m_{th} *compartment*

1.2.2 Modern modeling approaches

One of the assumptions of the original Smoluchowski model is that flocs do not break once formed. Floc breakage cannot be neglected when flow conditions are turbulent. Early computer simulations identified the importance of this in modeling flocculation by exploring

the effect of different breakage assumptions on the predictions of flocculation models (Fair and Gemmell, 1964). Argaman and Kaufman (1970) developed the first model describing the net rate of disappearance of primary particles, taking into account that floc breakage occurs:

$$dn_1/dt = -K_A\, G\, n_1 + K_B\, G^{\delta} \qquad (1.2.2\text{-}1)$$

K_A = *the aggregation constant, incorporating K and* ϕ

K_B = *the floc breakup constant, dependant on the internal binding forces or floc strength of the aggregate, and* δ*, a constant that varies between 2-4 depending on hydraulic factors* (Parker et al., 1972).

Argaman and Kaufman applied their equation to a flocculator system and developed the following simplified equation, assuming a single flocculator compartment:

$$n_1^0/n_1^1 = 1 + K_A\, G\, T / 1 + K_B\, G^2\, T \qquad (1.2.2\text{-}2)$$

This model has served as a base for all "classic" flocculation models.

In more recent years developments in fractal mathematics (section 1.3.1) has enabled a more complex approach to flocculation modeling, which has created modernized expressions, incorporating the effects of hydrodynamic interactions (Adler, 1981; Han, 1989; Han and Lawler, 1991).

Early classical models are all based upon the assumption that interparticle interactions are negligible until the point of contact. However, in reality the hydrodynamic forces impact significantly upon colliding particles (Adler, 1981; Lawler, 1993). The motion of fluid created by the movement of particles towards one another causes them to rotate around each other, so that they deviate from the linear path assumed in the classical approach. In addition, flocs can be regarded as porous objects (and not complete spheres) which allow fluid to flow through

them, thus impacting floc movement during flocculation (Kusters et. al., 1997; Lee et. al., 2000). Consequently, the classical approach to flocculation modeling is known as the *rectilinear* approach, and the new, alternative is known as the *curvilinear* approach, whereby hydrodynamic forces cause rotational floc movement which leads to the disruption of a linear attachment route.

Adler (1981) was the first to apply the theory of hydrodynamic interactions to heterodispersed systems. The author indicated that the lack of consideration of hydrodynamic interactions had led to an overestimation of flocculation collision frequencies. Lawler (1993) calculated the collision efficiencies for various size ratios of colliding particles taking account of hydrodynamic forces. The results showed that compared to the rectilinear model, the curvilinear model predicted orders of magnitude of collision frequencies less, even more so for orthokinetic flocculation. Numerical expressions approximating the correction factors for converting the rectilinear model to the curvilinear model are presented by Han and Lawler (1992).

Later developments in the modeling of hydrodynamic forces between colliding particles focused on two areas: drag upon the aggregates and aggregation paths. In the former, Veerapaneni and Weisner (1996) calculated the flow and associated drag on a sphere with nonuniform porosity, and Li and Logan (1997) modified the permeability expression of Brinkman (1947). In the latter, Kusters et al. (1997) used results from Adler (1981) to calculate the collision efficiency between uniformly porous aggregates. He found that large porosities led to enhanced collision efficiencies. However, successful application of these models is largely limited to idealized, artificial systems – such as suspensions of uniform latex spheres – due to constraints imposed by the requirement for surface homogeneity.

More recent research has been directed at macroscopic parameters pertaining to floc growth, and in particular the transient fractal dimension (section 1.3.1) (Sato et al., 2004). This parameter can at present only be determined empirically through fairly sophisticated modern techniques for particle characterization, but it ultimately permits the characterization of any system with reference to a single parameter. The current level of understanding of the factors

affecting fractal dimension in real flocculation systems is low, although the area is developing rapidly (Thomas et al., 1999).

1.3 Floc structure in flocculation

Several phases of floc growth occur during flocculation. Initially, particle growth is dominant, in which particles combine by coagulation and their size increases rapidly. As flocculation continues the flocs form large, porous and open structures that are more susceptible to fragmentation by fluid shear (Tambo, 1991). After a characteristic time, a steady state is reached between aggregation and fragmentation, characterized by an aggregate size distribution that does not change with time and is unique to each system (Spicer and Pratsinis, 1996). Aggregate structure has been found to impact the kinetics of the flocculation process. The rate of aggregation of colloidal particles has been observed to exert a significant influence over the apparent fractal dimension of the resulting aggregate, and models have been developed connecting the collision frequency and the fractal dimension of the aggregates (Jiang and Logan, 1991). Due to the large porosities these aggregates attain, the fluid flow is able to penetrate them, resulting in enhanced collision efficiencies (Schmidt-Ott et al., 1990; Kusters et al., 1997). Moreover, porous aggregates are fragmented by fluid shear stresses more rapidly than compact mass equivalent particles (Potanin, 1991; Flesch et al., 1999). Aggregate restructuring can also occur, by re-aggregation of fragments or by shear interactions that rearrange the structure (Oles, 1992; Selomulya et al., 2003).

1.3.1 Fractal dimension

Research of aggregate structure became possible with the development of methods enabling analysis of the complex structure of particle aggregates, the most significant being fractal geometry which emerged with the publication of Mandelbrot's work (Mandelbrot, 1987). Fractal mathematics enabled the representation of the apparently wild, complex structures of aggregates by simple parameters known as fractal dimensions. Fractal geometry uses

dilational symmetry (or scale invariance) as a measure to characterize structures: this consists of covering the object with a minimum number of overlapping spheres of a given diameter, l, then repeating this operation with spheres of decreasing diameter, while studying how the minimal number of spheres, N_l, varies with the diameter, l, when $l \rightarrow 0$. An object can be defined as fractal, with a fractal dimension, D, if N_l asymptotically grows as l^{-D} when $l \rightarrow 0$. Therefore, the expression which describes the whole concept of fractal structure is:

$$N_l \alpha l^{-D} \qquad (1.3.1\text{-}1)$$

N_l = *number of particles*

l = *diameter of sphere*

D = *(number) fractal dimension*

For linear, planar and three dimensionally compact objects, the exponent D, will have maximum values of 1, 2, and 3 respectively, while for porous aggregates (colloidal assemblages), D may take a fractional value. In such cases the exponent is known as the "fractal dimension" which typically exhibits values in the range 1.7-2.5 (or higher if restructuring occurs), for three dimensional objects (Jullien and Botet, 1997).

The first experiments that investigated the fractal nature of particle aggregates were reported in 1979 by Forrest and Witten, using image analysis techniques to determine the mass fractal dimension of metallic oxide smoke particles. Later experiments (Tambo and Watanabe, 1979; Klimpel and Hogg, 1986; Oles, 1992) have shown that the aggregates formed by shear coagulation are usually "fractal-like". However, these aggregates are not really fractal in the strict sense of the word, since their scaling is only observed over a finite range of length scales. The concept of a fractal dimension can only be properly defined when using an asymptotic limit to infinitely small lengths. Practically, when considering real physical objects, there always exists a lower limiting characteristic length below which the object

cannot be described as fractal. Therefore, aggregates are not true fractals but can be referred to as natural fractals (Mandelbrot, 1987).

Much of the fractal work in the literature has considered the aggregation of colloidal particles in the presence of electrolyte. Two limiting regimes, namely diffusion limited cluster aggregation (DLCA) and reaction limited cluster aggregation (RLCA) have been investigated. Under RLCA conditions (repulsion barrier present, low salt concentration), particles must collide many times before sticking together and, as such, a large number of sites on the clusters may be sampled. Under DLCA conditions (no repulsion barrier, high salt concentration), particles readily "stick" to each other at the extremities. Experiments have shown that different colloidal systems (gold, silica, polystyrene) produced the same fractal dimension in each of the limiting regimes, while their formation kinetics were also similar (Lin et al., 1989). This led to the assumption that aggregation behavior was independent of the detailed chemical nature of the colloid system and it has become generally accepted that, in perikinetic coagulation processes, the aggregate mass fractal dimension (D_3) ranges from 1.75 (DLCA) to 2.1 (RLCA) (Bushell et al., 2002). The lower fractal dimension of the DLCA aggregates reflects the loose, open nature of the aggregates formed. Nevertheless, certain colloid systems have been found to deviate from this universality, depending on the way the aggregation was induced – charge neutralization as opposed to charge screening (Zhang and Buffle, 1996).

1.3.1.1 Fractal analysis techniques

A number of techniques have appeared in the literature to determine the fractal dimension of aggregates of fine particles. The most common techniques are scattering (light, X-ray, or neutron), settling and image analysis (Bushell et al., 2002).

1.3.1.1.1 Image Analysis

The major advantage of image analysis over other techniques is that it provides information regarding particle morphology. The disadvantage is that its measurement statistics are less

good than other techniques which measure an ensemble of particles. Conventional image analysis is limited to characterization of the surface mass fractal dimension of the floc which can be no larger than 2. There are several methods to obtain the fractal dimension of images: box counting, sand box technique (Forrest and Witten, 1979; Tence et al., 1986), and confocal scanning laser microscopy. This research will use the box counting method to analyze the images. The box counting method covers the object being analyzed with tiles having the same dimensionality as the containing space. Since images are two dimensional, the image is covered with squares of a certain size using the minimum number of squares to just completely cover the image of the object. Then, the process is repeated with smaller squares. The fractal dimension measured by this technique is:

$$D = \lim_{L \to 0} - \log(N)/\log(L) \qquad (1.3.1.1.1\text{-}1)$$

N is the number of squares required to cover the object, and L is the resolution or size of the square. Plotting the number of squares against the resolution on a log-log plot returns the fractal dimension of the aggregate. Only part of the spectrum is used for this type of analysis, because at the large L end of the spectrum the resolution is courser than the image itself, and the object behaves dimensionally as a point. So, at a very low resolution (large L), the slope will be zero (N will be 1). As the resolution improves there is a transition where there are effects from gross aggregate shape and at high resolution the fractal dimension (texture) is eventually apparent. When dealing with images from microscopes preprocessing of the image is required to prepare it for box counting. One image (one aggregate) is used for each analysis, and it is important to distinguish between aggregate and background.

1.3.1.1.2 Static light scattering

The basic principle of scattering techniques is that particles, when illuminated by a radiation source, will scatter secondary radiation in all directions due to reflection, refraction and diffraction. The scattering patterns are specific for different particle sizes, and they are

influenced by the shape, homogeneity, the relative refractive index of particles to medium, and by the wavelength of the incoming radiation. These scattering intensities can be detected by a specific detector array and are translated into a measure of the particle size, according to available approximations that were developed for particles of different sizes and optical properties (Sorensen, 1997). The scattering patterns are related to the scattering angle in a way which can also be used to obtain information on the structure of the aggregates. The magnitude of the wave number or the momentum transfer, q, in relation to the scattering angle, θ, is (Sorensen, 1997):

$$q = (4\pi n/\lambda)\sin(\theta/2) \qquad (1.3.1.1.2\text{-}1)$$

where θ is the scattering angle, λ is the *in vacuo* wavelength of the incident beam, and n is the refractive index of the medium. The inverse of this variable (q^{-1}) indicates the length scale of the scattering experiment.

The angular scattering intensity, $I(q)$, of a fractal aggregate with no multiple scattering is the product of the form factor, $P(q)$, which represents the scattered intensity function from a single primary particle, and the structure factor, $S(q)$, that describes additional scattered intensity due to the spatial correlation between the particles in the aggregate:

$$I(q) \propto S(q)P(q) \qquad (1.3.1.1.2\text{-}2)$$

The form factor, $P(q)$, is constant at small q, so that $I(q)$ solely depends on the aggregate structure at large length scales ($q^{-1} >> r_s$, primary particle/scatterer radius). The structure factor, $S(q)$, is constant at large q, and therefore $I(q)$ depends on the primary particles at the low length scale of the aggregate.

In the range of fractal geometry, $S(q)$ is a power law function of the form (Thill et al., 2000):

$$S(q) \propto q^{-Df} \qquad (1.3.1.1.2\text{-}3)$$

For: $r_s << q^{-1} << \xi$, where r_s is the scatterer radius and ξ is the distance above which the mass distribution inside the aggregate cannot be considered fractal.

The above equation can be used for structural measurements if applying the Raleigh-Gans-Debye (RGD) approximation, which assumes that elementary units (primary particles) within the scattering body (aggregate) all scatter independently. The approximation is valid for non-absorbing particles in the limit that both:

$$|m-1| << 1 \qquad (1.3.1.1.2\text{-}4a)$$

$$(4\pi n/\lambda)L|m-1| << 1 \qquad (1.3.1.1.2\text{-}4b)$$

where m is the relative refractive index of the scatterers (primary particles) and L is the length of the scattering body (the diameter of the primary particles).

The measure of D_f assuming RGD approximation is acquired from the slope of the logarithmic plot of $I(q)$ versus q. However, in reality the measured scattering intensity is in fact contributed to by all the aggregates in the scattering volume, and not only a single aggregate composed of equal sized particles as approximated by the scattering theories. Albeit in a dispersion all aggregates contribute differently to $S(q)$ due to variation in their sizes (and therefore also in the validity limit ξ), and therefore the global slope of the structure factor is not strictly the fractal dimension. In light of this, the absolute slope of the logarithmic plot of $I(q)$ versus q will be referred to as the scattering exponent (*SE*), as it may not necessarily represent the real mass fractal dimension of the aggregates. The *SE*, however, does still portray structural properties, and higher *SE* values will indicate more compact aggregates – and vice versa (Guan et al., 1998; Waite, 1999).

The system presented in this study represents a complex water system, thus the light scattering results presented for a mixture of aluminum hydroxide and kaolin should be interpreted with caution. However, for relatively narrow distributions, polydispersity effects are expected to be insignificant (Lawler, 1997; Bushell and Amal, 1998).

1.4 Electroflocculation (EF)

Electroflocculation (EF) is a coagulation/flocculation process in which the coagulant is generated in situ by electrolytic oxidation of an appropriate anode material, thus differing from the conventional process in which chemical coagulants such as metal salts or polymers and polyelectrolytes are used for destabilizing emulsions and colloidal suspensions. In this process, as in standard coagulation, colloidal solids, metals and soluble inorganic pollutants can be removed from water and wastewater by destabilization mechanisms (section 1.1.4) followed by flocculation and subsequent solid-liquid separation processes such as sedimentation or filtration. The principles of electrochemical dissolution are those associated with basic electrochemistry, whereby, applying an electrical current to an electrolytic cell promotes an anodic and cathodic reaction.

1.4.1 Electrochemical processes in water and wastewater treatment

Electrolytic processes to treat wastewater by generation of chlorine for deodorizing and disinfecting were patented as early as 1887. A sewage treatment plant using these methods was built in London in 1889 and operated for 10 years. Electrochemical techniques for separating oil in wastewater were already being used in 1903. The process was used to treat condensed water from steam engines, to remove oil, before it entered the steam boiler as feedwater. Electrolytic sludge treatment plants were in operation as early as 1911 in Santa Monica, California and Oklahoma. Steel electrodes alternatively connected to the positive and negative terminals of a dc power supply were used to treat sewage in demonstration plants and all were praised for their high quality effluent and lack of odor. In the Soviet Union

electrochemical water purification with a soluble iron anode was first used at a power station in 1925. Stuart introduced the same process in the U.S.A in 1946 to remove color from drinking water using aluminium electrodes (Stuart et al., 1946). Foyn used electrolytic treatment of wastewater using magnesium salts and alkalization in order to remove phosphorous at high pH (Foyn et al., 1963).

Combined electrochemical processes were also developed combining EF with electroflotation or electroprecipitation. One of the first experiments with electroflotation was conducted in 1911, treating domestic sewage in the U.S.A. Electroflotation was introduced into the mining and metal-processing industries in the early 1900's and soon gained popularity. In 1946 Rivkin obtained a patent for the electroflotation of ore, although the method was not taken into commercial use by the industry (Mallikarjuan and Venkatachalam, 1984). Today electroflotation processes are used extensively in the mining industry.

Despite the above, electrochemical treatment of water and wastewater was only ever marginally practiced. However, awareness has grown, mainly over the past decade, as to the advantages of using such techniques, although in general, technological developments have focused on commercialization of the process by minimizing electrical power consumption and maximizing effluent throughput rates.

1.4.1.1 EF - Research and technology

Limited scientific research has explored the fundamental mechanisms of the technology as an alternative process for water treatment, although a wide range of applications have been reported: to treat urban wastewater (Pouet and Grasmick, 1995; Mills, 2000; Adin and Vescan, 2002), wastewater from the paper and pulp industries, mining and metal-processing industries (Alexandrova et al., 1994), to treat water containing foodstuff wastes (Chen et al., 2000), oil suspensions (Clemens, 1981; Balmer and Foulds, 1986; Ogutveren and Koparal, 1997; Carmona et al., 2006), dyes (Ogutveren and Koparal, 1992; Do and Chen, 1994; Lin and Peng, 1994; Ciardelli and Ranieri, 2001; Mollah et al., 2004), fluoride (Mameri et al., 1998; Huang and Liu, 1999; Mameri et al., 2000, Shen et al., 2003), arsenic (Kumar et al.,

2004), sulfide, sulfate and sulfite (Murugananthan et al., 2004), phosphate (Dobolyi et al., 1978), suspended particles (Vik et al., 1984; Matteson et al., 1995; Abuzaid et al., 1998; Holt et al., 2002; Larue et al., 2003), chemical and mechanical polishing waste (Lin and Lin, 1998; Belongia et al., 1999). Lately, more research has been conducted into the efficiency of EF for removal of TOC and humic substances using various cell configurations (Jiang et al., 2002), and as pretreatment for enhanced virus removal using microfiltration (Zhu et al., 2005). Still, research has focused on efficiency and removal rates rather than on the fundamental chemical and physical mechanisms of the EF process. Understanding these mechanisms will enable a deeper understanding of the process, which will lead to improved system design and process control.

1.4.1.2 Description of EF technology

In its simplest form, an EF reactor may be made up of an electrolytic cell containing one anode and one cathode. When connected to an external power source, an oxidation reaction occurs at the anode and a reduction reaction at the cathode. This basic arrangement is not suitable for full scale water/wastewater treatment, because the rate of metal dissolution is not rapid enough to achieve adequate dosing, and electrodes with a large surface area are required. To overcome this, electrode design can be varied, and reported configurations are numerous – including aluminum pellets in a fluidized bed reactor (Barkley et al., 1993), bipolar aluminum electrodes (Mameri et al., 1998), mesh electrodes (Matteson et al., 1995), bipolar steel raschig rings (Ogutveren and Koparal, 1992), and simple plate electrodes (Vik et al., 1984; Mameri et al., 1998; Holt et al., 2002). The electrode material depends on the type of coagulant required in the system. The cathode material is of less importance, although, due to competing redox reactions, by-products are formed which can affect the cathode surface if highly reactive metals are used. Hydrolysis occurs in which oxygen gas is formed at the anode. The oxygen oxidizes the surface of the cathode thus forming a passivation layer. This increases the resistance within the cell, causing a drop in voltage across the cell, which, in turn, decreases the metal dissolution at the anode. In addition, cathodic dissolution can occur,

due to a highly basic local environment caused by hydroxl ion formation at the cathode (Picard et al., 1999). Using cathodes made from inert metals, or metals that oxidize slowly, or using an ac generator, can overcome this problem (Ivanishvili et al., 1987).

1.4.2 Electrochemical cells and potentials

Any oxidation-reduction equilibrium is studied by measuring the potential of an electrochemical cell in which the two half-reactions making up the equilibrium are participants. The potential difference that develops between the cathode and the anode of the cell is a measure of the tendency for the reaction to proceed from a nonequilibrium condition to an equilibrium state. The potential of cells is the difference between two half-cell, or single-electrode potentials, one associated with the half-reaction at the cathode (E_c), and the other associated with the half-reaction at the anode (E_a). Absolute half-cell electrode potentials cannot be determined because all voltage measuring devices measure only differences in potential, therefore, *relative* half-cell potentials are measured. Relative half-cell potentials can be combined to give cell potentials and are widely applicable in chemical calculations, provided that they are all measured against a common reference half-cell. The *standard hydrogen electrode* (SHE) is the conventional reference half-cell against which all others are compared. The half-cell reaction responsible for the potential that develops at this electrode is:

$$2H^+_{(aq)} + 2e^- \rightarrow H_{2(g)} \qquad E^0 = 0V \qquad (1.4.2\text{-}1)$$

The hydrogen electrode is reversible and acts either as an anode or as a cathode, depending upon the half-cell with which it is coupled. The potential of a hydrogen electrode depends upon temperature and upon the activities of hydrogen ion and molecular hydrogen in the solution. For the SHE, the activity of hydrogen ions is specified as unity and the partial pressure of the gas (which determines the activity of molecular hydrogen in the solution) as

one atmosphere. *By convention, the potential of the standard hydrogen electrode is fixed at zero at all temperatures.*

Operational reaction potentials will vary according to both the electrode material used and the aqueous environment. The Nernst equation (eq. 1.4.2-2) is used to calculate the equilibrium potential for any half reaction. Assuming ideality (γ_i=1), concentrations (c_i) can be used in place of activities (Bard and Faulkner, 2001).

$$E = -\Delta G^0/nF - RT/nF \Sigma v_i \ln c_i \qquad (1.4.2\text{-}2)$$

The electrode overpotential (η) is the extra energy required in addition to the reduction potential in order for a reaction to proceed. It reflects a kinetic barrier to the reaction and it a measure of the degree of polarization – deviation from the electrode's equilibrium value (E_0).

$$\eta = E - E_0 \qquad (1.4.2\text{-}3)$$

The overall potential for a reactor is thus calculated as the sum of the anodic (E_a), cathodic (E_c), solution (E_s) and loss (E_l) potentials (eq.1.4.2-5). The solution potential (E_s) is a function of its conductivity (σ), the distance between electrodes (Δb), and the current density (i_c) (eq. 1.4.2-4). E_s is included to account for potential losses which can be due to the *IR drop of the cell*, while E_l can be attributed to *concentration polarization and kinetic polarization*. The IR drop of a cell, or *ohmic resistance*, is its resistance to the flow of charge. Concentration polarization occurs when a reactant species do not arrive at the cathode surface or product species do not leave the anode surface fast enough to maintain the desired current. This causes the current to be less than the value predicted. In kinetic polarization, the magnitude of the current is limited by the rate of electron transfer between reactants and electrodes. This is most common for electrode processes that form gaseous products and is often negligible for reactions that involve the deposition or solution of a metal.

Hence, a reactor's real potential is dictated, in addition to anodic and cathodic potential requirement, by solution characteristics, electrode geometry and the way in which the reactor is operated.

$$E_l = \Delta b i_c / \sigma \qquad (1.4.2\text{-}4)$$

$$E_{cell} = E_c - E_a - E_s - E_l \qquad (1.4.2\text{-}5)$$

In order to maintain a desired current, a potential greater than the theoretical potential must be applied to the cell, which takes into account the overpotential requirements.

However, measures can be taken to reduce the magnitude of the overpotential: decreasing the distance between the electrodes and increasing the active surface area of the anodes, and the specific conductivity of the solution, will reduce the ohmic resistance of the cell. Moreover, increasing the transport of metal ions from the anode surface to the bulk solution, by intensifying the mixing conditions within the cell can reduce the mass transfer overpotential.

1.4.3 Electrochemical dissolution

Anodic dissolution can be calculated using *Faraday's law* (eq. 1.4.3-1), which describes the relationship between current intensity and the amount of metal dissolved. This equation is used to calculate the coagulant dosage in EF:

$$m = (I\ t\ MW) / (Z\ F) \qquad (1.4.3\text{-}1)$$

m = metal dissolving (gr)

I = current intensity (A)

t = time (s)

MW = molecular weight of metal (gr/mol)

Z = number of electrons involved in the oxidation/reduction reaction

F = Faraday's constant (96,485 coloumbs/mol)

1.4.3.1 Aluminum dissolution

Aluminum is the most commonly used anode material reported in the literature. Equation 1.4.3.1-1 presents aluminum's anodic dissolution:

$$Al^{+3}_{(aq)} + 3e^{-}_{(aq)} \rightarrow Al_{(s)} \qquad E^{0}_{A} = -1.66V \qquad (1.4.3.1\text{-}1)$$

Oxygen evolution occurs also at the anode:

$$4OH^{-}_{(aq)} \rightarrow O_{2(g)} + 2H_2O + 4e\text{-} \qquad E^{0}_{A} = -0.40V \qquad (1.4.3.1\text{-}2)$$

Simultaneously, an associated cathodic reaction, the evolution of hydrogen occurs:

$$2H_2O + 2e^{-} \rightarrow 2OH^{-}_{(aq)} + H_{2(g)} \qquad E^{0}_{c} = -0.83V \qquad (1.4.3.1\text{-}3)$$

Under acidic conditions, hydrogen evolution will occur according to:

$$2H^{+}_{(aq)} + 2e^{-} \rightarrow H_{2(g)} \qquad E^{0}_{c} = 0V \qquad (1.4.3.1\text{-}4)$$

The complexity of electrochemical reactions increases with multi-transfer step and multi-electron processes. Numerous interactions may occur before, during and after electron transfer (including chemical reactions – e.g. protonation, dimerisation or other surface reactions such as adsorption or desorption). Any of these processes could prove to be a rate limiting step for a given EF reactor (Bard and Faulker, 2001).

1.4.4 EF as an alternative to conventional flocculation (CF)

When considering EF as an alternative to conventional flocculation (CF), the differences between the two processes should be considered. The use of electrolysis creates a unique coagulation and flocculation environment as the dosing regime is additive over time, negative counter-ions are not introduced, and competing redox reactions occur simultaneously – the first and foremost being hydrolysis. Moreover, in EF the dosing regime is an additive process over time in which negative counter-ions are not introduced. Negative counter-ions can influence the metal hydrolyzed species, which are coordinated with hydroxyl ions, because

they can replace the hydroxyl, thereby changing the charge of the active species (Duan and Gregory, 2003). The absence of these counter-ions can affect the coagulation mechanism which depends on the types of species present in solution. The hydrolysis produces, in addition to hydroxyl ions at the cathode, hydrogen gas at the cathode and oxygen gas at the anode which form micro-bubbles and could affect aggregate growth. It is also possible that the electrical field imposed could affect ion and particle transport.

1.5 Membrane Processes

Micorofiltration (MF) and ultrafiltration (UF) are the most commonly used membrane processes in water and wastewater treatment as they can be used to remove all, or portions of, typical contaminants found in water (suspended particles, dissolved inorganic salts, dissolved organic material, microorganisms), with the exception of dissolved organic salts (Schafer et al., 2000). These types of membranes act as physical filters, and when applying both processes to remove suspended particles or microorganisms, there is little difference between them. Both UF and MF are pressure-driven membrane processes and operate at relatively low feed pressures (5-30 psi), thus achieving higher flux rates than nanofiltration (NF) or reverse osmosis (RO). This makes them very cost-effective when treating water that does not require reduction of hardness or removal of other soluble inorganic ions.

1.5.1 MF and UF membranes - Chemistry and Structure

MF and UF membranes are typically made of either organic polymers or inorganic materials (Cheryan, 1998). Cellulosic organic polymer membranes are constructed using cellulose acetate (CA), CA blends, or cellulose triacetate. Other materials such as polysulfone, polyvinylchloride copolymer, polypropylene and polyethersulfone are also used. Inorganic membranes are constructed using metal oxides of silver, titania, zirconia and alumina.

1.5.2 Mode of operation

There are two ways to operate filtration equipment: dead-end or cross flow. In the dead-end mode, the feed is pumped directly towards the filter, resulting in only one stream entering the filter module and only one stream (permeate) leaving the filter. However, most MF and UF modules are operated in the cross-flow mode, in which the feed is pumped across or tangentially to the membrane surface (Hong et al., 1997). In this mode of operation, there is one stream entering the module and two streams leaving the module (retentate and permeate). If the feed contains relatively high solids and/or the solids need to be recovered easily, cross-flow is preferred, because it limits the buildup of solids on the membrane surface, which in operational terms means a higher flux average.

1.5.3 Flux

With UF and MF membranes there is a fairly good correlation between pore size and experimental water flux. The flux is the flow rate of permeate through the membrane and is given in terms of velocity (cm/sec). There are four major operating parameters that affect the flux: pressure, feed concentration, temperature and turbulence in the feed channel. In an ideal situation, e.g., with uniformly distributed and evenly sized pores in the membrane, with no fouling, negligible concentration polarization, the best description of fluid flow through microporous membranes is given by the Hagen-Poiseuille model for streamline (laminar) flow through channels (Cheryan, 1998):

$$J = (\varepsilon d_p^2 P_T)/32\delta\chi\mu \qquad (1.5.3\text{-}1)$$

J = *flux*

ε = *porosity*

d_p = *pore diameter*

P_T = *applied pressure*

μ = *viscosity of solvent*

$\delta\chi$ = *thickness of the membrane*

1.5.3.1 Flux decline and fouling mechanisms

Deviations from the linear flux-pressure relationship of equation 1.5.3-1 will occur due to a decreased driving force and/or increased resistance. These are caused by the accumulation of materials near or onto the membrane surface which precipitate or form a layer that resists the flow of permeate (cake formation), internal blocking by materials entering the membrane pores, adsorption of materials onto the membrane surface, or changes in the membrane structure (Carroll et al., 2000, Cho et al., 2000, Jones and O'Melia, 2001).

Models have been developed to predict the flux under different conditions, such as the *mass transfer ("film theory") model*, which is used for modeling flux in pressure-independent, mass transfer-controlled systems, and the *resistance model*. According to the *resistance model*, the flux J_p can be described by:

$$J_p = \Delta P/\mu\Sigma R_i = \Delta P/\mu(R_m + R_a + R_p + R_{cp} + R_c) \qquad (1.5.3.1\text{-}1)$$

ΔP = *pressure gradient*

μ = *viscosity of solvent*

R_m = *initial membrane resistance*

R_a = *adsorption inside the membrane pores*

R_p = *blocking of the membrane pores*

R_{cp} = *concentration of foulants near the membrane surface (concentration polarization)*

R_c = *deposition on the membrane surface forming a cake layer*

Most mathematical models of fouling relate the flux to the time or to volume permeated, and generally show an exponential relationship (Song, 1998).

Extensive research has been carried out on factors affecting the fouling behavior of membranes. The major factors referring to membrane properties are:

- Hydrophilicity: With aqueous feedstreams, the ideal membrane should be hydrophilic (water-attracting). If the material is hydrophobic, it will adsorb components that are hydrophobic or amphoteric, resulting in fouling. When treating water containing organic matter (natural organic matter or synthetic organic chemicals), adsorption (using activated carbon), can be used in conjunction with the membrane system to remove the organic material, thus decreasing fouling and improving the membrane performance (Lin et al., 2000).
- Surface topography: The roughness of the membrane surface affects its fouling properties. Atomic force microscopy (AFM) produces topographical images of the membrane surface, which can give information about surface morphology, surface pore size distributions and surface porosity (Bowen et al., 2000). Most membrane surfaces are composed of "peaks" and "valleys". Adhesion of materials to the membrane surface tends to be greater in the valleys, therefore, choosing membranes with "smoother" surfaces could reduce fouling.
- Charge on the membrane: Most membranes have a negative (net) charge, under usual process conditions. The charge on the membrane is of importance when the feed contains charged particles, such as colloids. The electrostatic interactions between charged particles and the membrane surface affect the fouling behavior of the membrane. The particle characteristics can be changed by changing the solute properties (e.g., pH and salt concentration), which influences directly the permeate flux (Hoogland et al, 1990). Studies addressing the charge effect of particles on membrane performance, using cross-flow UF, have shown that an increase in the particle charge increased the permeate flux (McDonogh et al, 1989).
- Pore size: Larger pore membranes will initially have higher flux than tighter membranes, but will eventually (sometimes rapidly), have lower flux. This is most

common with MF applications, and is most likely due to internal blocking of the larger pores (Bowen et. al., 1995). Fouling is really the result of specific interactions between the membrane and various solutes in the feedstream, therefore, solute properties are also of great importance. The major solute properties affecting fouling are: salt concentration, pH and temperature. The solubility, surface charge and structure of specific materials within the solution are directly affected by changes in these. For example, the solubility of a protein is generally lowest at its isoelectric point. Changing the pH can increase the solubility of the protein, and thereby increase the flux (Jones and O'Melia, 2001).

1.5.3.2 Colloid ultrafiltration

The rate at which a colloid is convected to the membrane will be determined by the balance of forces on the colloid in the direction perpendicular to the membrane (Altman and Ripperger, 1997):

$$V_{p,y} = (1/C_D)(F_{BT} + F_y) = J + v_{BT} \qquad (1.5.3.2\text{-}1)$$

Where F_{BT} and F_y are the back-transport and filtrate flow drag forces, respectively. C_D is the drag coefficient of the particle, and v_{BT} is the flow away from the membrane (back-transport velocity, less than zero).

The rate of particle convection to the membrane decreases as the rate of back transport approaches the rate of permeation drag. When the flux equals the magnitude of the back-transport velocity (v_{BT}), no convection of particles to the membrane will occur. In these conditions the flux can be referred to as the *critical flux*, below which there cannot be no particle deposition.

The effect of particle diameter and hydrodynamics on the net rate of particle convection to the membrane has been studied (Cohen and Probstein, 1986; Weisner et al., 1989). For particles

smaller than 0.3μm, Brownian diffusion controls back transport and shear effects are negligible, while for larger particles (1-2μm), inertial lift forces begin to dominate (Cohen and Probstein, 1986). Hence, fouling can be reduced by increasing particle sizes, specifically using coagulation/flocculation in the pre-treatment stages.

1.5.3.2.1 Flux enhancement

Enhancing the flux of the membrane can either be done mechanically or by chemically pre-treating the feed. Mechanical flux enhancement can be achieved by using turbulence promoters, such as inserts or baffles, placed in the feed channels of membrane modules (Drogui et al., 2001). In addition, back-flushing, pulsing and shocking can be used (Bourgeous and Darby, 2001). Pre-treatment of the feed, using coagulation/flocculation methods, has proven effective in reducing the fouling behavior of the membrane (Kim et al., 2001). Particularly in water and wastewater treatment, where the feed contains colloidal particles, pre-coagulation/flocculation has shown good results in removing turbidity and TOC, and in decreasing the colloidal fouling of the membrane (Lahoussine-Turcaud et al., 1990; Peuchot and Ben Aim, 1992; Abdessemed et al., 1998; Lee et al., 2000; Soffer et al., 2000, Judd and Hillis, 2001).

1.6 Research Objectives

The aim of this research is to gain a better understanding of the EF process, primarily on a theoretical level, but also to evaluate the applicability of the process as a viable alternative to conventional coagulation. As such, the specific objectives are:

- Elucidate the mechanisms of coagulation and flocculation in EF while connecting changes in suspension characteristics and floc evolution and floc morphology to operational parameters.
- Compare EF with conventional flocculation (CF) with regard to destabilization mechanisms and floc structural evolution.
- Examine the applicability of the process as a viable alternative pretreatment to membrane ultrafiltration.

Chapter 2 - Materials and Methods

Different experimental procedures were used for research sections. Thus the methods are specified according to research section.

2.1 Characterizing solution changes and floc morphology

Colloidal suspension

0.3gr of kaolin ($AlSi_2O_5(OH)_4$, *Aldrich Chemical Company Inc. USA*) was suspended in 20 liters of distilled water (15mg/l final concentration) and homogenized using an *Ultraturax 2000, Ganke and Kunkel, GMBH*. 1.66gr of $NaHCO_3$ (*BDH Laboratory Suppliers, England*) was added (final concentration 83mg/l), the pH was corrected to 5 and 6.5 with NaOH or H_2SO_4, and conductivity was increased with $NaNO_3$ (*Riedel-Dehaen*, *GMBH*)**.**

EF unit

An EF unit which can be operated as a batch or continuous unit was designed (fig. 2.1-1). It consisted of a cylindrical plexyglass shell, with a volume dimension of 77.64cm^3 (H=6.5cm, D=3.9cm) and two concentric electrodes, inserted one inside the other, creating a space into which water could flow to be treated. The outer electrode (H=6.5cm, D=3.8cm) was stainless steel and served as the cathode. The inner electrode was aluminum, which was the anode (H=6.5cm, D=1.8cm). The anode was perforated with 28 holes, each with a diameter of 0.5cm, leaving an effective anode area of 31.27cm^2. Through the anode a baffle was fitted, which was connected to a motor, powered by an external power source. Adequate mixing conditions were created within the cell due to the holes perforated through the anode. The electrodes were connected to a DC external power source .The cell was used in all experiments as a batch cell.

Particle size analysis

Particle size distribution (PSD) measurements were performed over a range of 2μm-300μm, using a *HIAC Royco Liquid Particle Counting System*.

Aggregate morphology/fractal dimension

The aggregates resulting from the process were photographed using an *Olympus digital camera DP70* (12.0 mega pixel resolution) which was mounted on a *Reichart* microscope. Morphological characterization of suspended aggregates is a microscopic technique which is complementary to macroscopic methods for characterizing flocculated suspensions. Microscopy allows individual particles to be viewed, scrutinized and analyzed at high magnification, however sample extraction and preparation should be conducted with utmost care, so to not disrupt the structure. In this case, a drop of the sample was put onto a microscopic slide, *without* using a cover slip. Image analysis was used to morphologically characterize the resulting aggregates (i.e primary kaolin particles vs. aluminum hydroxide floc) and for quantifying their structure using a two-dimensional fractal dimension (D_2). To calculate D_2, the images were processed using standard software (photoshop), and then were analyzed using NIH-Image software which uses the box counting method. The fractal dimension measured by this technique is:

$$D = \lim_{L \to 0} - \log(N)/\log(L) \qquad (2.1\text{-}1)$$

N is the number of squares required to cover the object, and L is the resolution or size of the square. Plotting the number of squares against the resolution on a log-log plot returns the fractal dimension of the aggregate. One image (one aggregate) was used for each analysis, following application of thresholding. Several images were acquired for each measurement and the fractal dimensions obtained are based on an average of 7-8 aggregates.

ζ potential

The ζ potential of the post electroflocculated suspension was measured using a *Malvern Zetamaster S*. Each result was an average of three readings.

Experimental procedure

The cell was filled with the kaolin suspension, a velocity gradient (G) was set ($0sec^{-1}$, $10sec^{-1}$ or $30sec^{-1}$), and a current was applied for 1min. The G values were chosen according to typical values used for slow mixing in lab apparatus and larger scale systems.

The suspension underwent an additional 5 min mixing, after which a sample of the effluent was taken for analysis. The mixing time was set so floc size obtained would be adequate for microscopic analysis. The cell was operated in galvanostatic mode: the current was set and the potential found its own value dependent on the system's overall resistance. This ensured coagulant production at a predetermined rate, defined by Faraday's law. The currents used for the experiments were 0.05A, 0.1A, 0.2A, 0.3A producing $1.6mA/cm^2$, $3.2mA/cm^2$, $6.4mA/cm^2$, $9.6mA/cm^2$ respectively. The current densities are in good accordance with figures reported in the literature (Mameri et al, 1998; Holt et al, 2002). The respective aluminum doses obtained were: 4mg/l, 8mg/l, 16mg/l, 24mg/l, for a dosing time of 1 min. Some experiments explored the effect of current density on the resulting aggregates, and these were carried out using 1/2 the current densities, and a dosing time of 2 min.

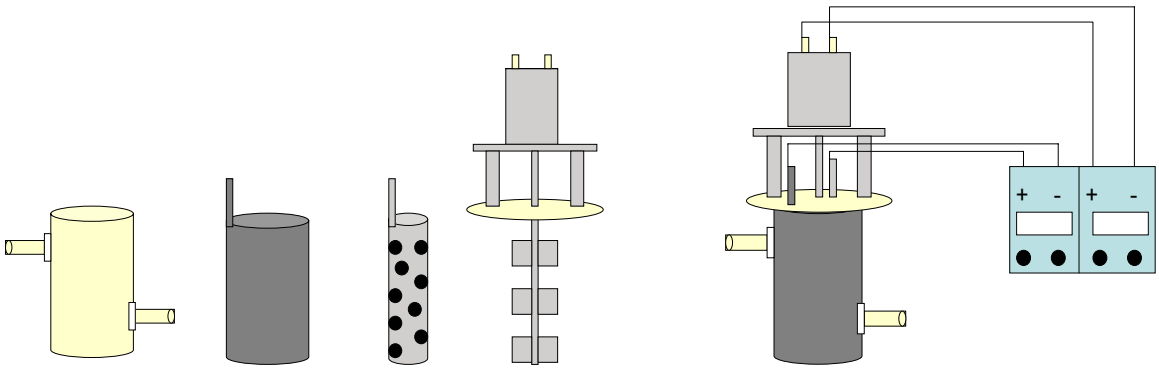

Figure 2.1-1 Left: EF cell components: (from left to right) outer cell, outer electrode (stainless steel cathode), inner electrode (aluminum anode, perforated), mechanical baffle. Right: Components combined into EF cell and connected to DC power supply.

2.2 Monitoring size and structural evolution of flocs in EF and CF using static light scattering

Colloidal suspension

1.2gr of kaolin ($AlSi_2O_5(OH)_4$, *Aldrich Chemical Company Inc. USA*) was suspended in 20 liters of distilled water (60mg/l final concentration) and homogenized using an *Ultraturax 2000, Ganke and Kunkel, GMBH*. 1.66gr of $NaHCO_3$ (*BDH Laboratory Suppliers, England*) was added (final concentration 83mg/l), the pH was corrected to 5, 6.5 and 8 with NaOH or H_2SO_4, and conductivity was increased to 1mS/cm with $NaNO_3$ (*Riedel-Dehaen, GMBH*).

EF unit

An EF batch unit was designed (fig. 2.2-1). It consisted of a plexyglass cap, which could be fitted onto a 1 L chemical glass and to which the electrodes were attached. The inner electrode, the cathode, was made from stainless steel and concentric in form (H=10cm, D=2.5cm). It was fitted onto the arm of a magnetic stirrer, and stationary throughout all the experiments. The outer electrode, the anode, was made from aluminum and could be used in two sizes, for applying different current densities: a concentric electrode (H=10cm, D=9.5cm) and two separate electrodes, with a total effective area of 1/4 of the former electrode. The electrodes were connected to a DC external power source. Mixing conditions within the cell were achieved with the magnetic stirrer and a constant mixing speed of 145 rpm was used for all experiments.

Floc size and structure analysis

Size distributions and structural information of kaolin-$Al(OH)_3$ flocs were determined as a function of time using a *Malvern Mastersizer Microplus*, which ascertains size by analysis of forward scattered light. The size distribution data given by the instrument covers the size range of 50nm to 500μm.A He-Ne laser light (λ = 633nm) was passed through a 2.0mm-width measurement cell in which the sample flowed. The beam was converged by a 300mm focusing lens and 42 detectors enabling the collection of light scattered from 0.03^o to 46.4^o. The plane of polarization of the laser beam is parallel to the detector axis (vertical). Size

distribution information was obtained using supplied software which uses Mie theory to develop a scattering pattern that matches the scattering pattern of the sample being measured. Information on distribution size is presented in this study as the volume mean diameter:

$$D(V, 0.5) = \Sigma_i (V_i d_i)/\Sigma_i V_i \qquad (2.2\text{-}1)$$

Where V_i is the relative volume in size class i with mean class diameter d_i.

Information on floc structure was obtained by measuring the intensity of light (I) at all detectors and plotting log I versus log q (eq. 1.3.1.1.2-1). Information regarding the angles of the detectors and intensity correction data, based on the geometric configuration of the detectors, was supplied by Malvern Instruments.

Image analysis

Image analysis was used in conjunction with scattering measurements as a complementary analysis to ascertain floc properties over time. The aggregates resulting from the process were photographed using an *Olympus digital camera DP11* (3.0 mega pixel resolution) which was mounted on an *Olympus Stereoscope SZX12*. All photographs were taken at magnification x 50. The images here were not used for structure quantification by fractal analysis due to the relatively low resolution of the images obtained, as in this case particles may be incorrectly sized due to a blurred boundary between the particles and background (Chakraborti, et al., 2003).

ζ potential

As specified in section 2.1.

Experimental procedure

The EF apparatus was fixed onto a 1L chemical glass containing 800ml of kaolin suspension, the electrodes submerged in the suspension. A current was applied for various time intervals (3, 6 and 10 minutes) at the end of which samples were analyzed (for pH, size distribution, ζ potential and image analysis). The complete dose of aluminum was achieved at 10 minutes,

for each applied current, after which additional aluminum was not introduced into solution. At this stage samples underwent continuous mixing and measurements were taken at two more time intervals: 15 and 20 minutes. For all size distribution measurements, the Malvern Microplus was operated at a gentle pump speed of 400, so to minimize disruption of floc structure. The EF cell was operated in galvanostatic mode: the current was set and the potential found its own value dependent on the system's overall resistance. This ensured coagulant production at a predetermined rate, defined by Faraday's law. The currents used for the experiments were 0.042A, 0.11A and 0.22A, yielding aluminum doses of 2.43mg/l, 6.48mg/l and 12.96mg/l respectively. These doses are equivalent to aluminum content in 30mg/l, 80 mg/l and 160 mg/l commercial alum (8.1% of the total molecule). Current densities were altered by using different anode sizes. These are summarized in table 2.2-1.

Current applied	Current density (full anode)	Current density (1/4 anode)
0.042A	0.197mA/cm^{2}a	0.788mA/cm^2
0.11A	0.516mA/cm^2	2.062mA/cm^2
0.22A	1.031mA/cm^2	4.125mA/cm^2

Table 2.2-1 Current densities used for experiments.

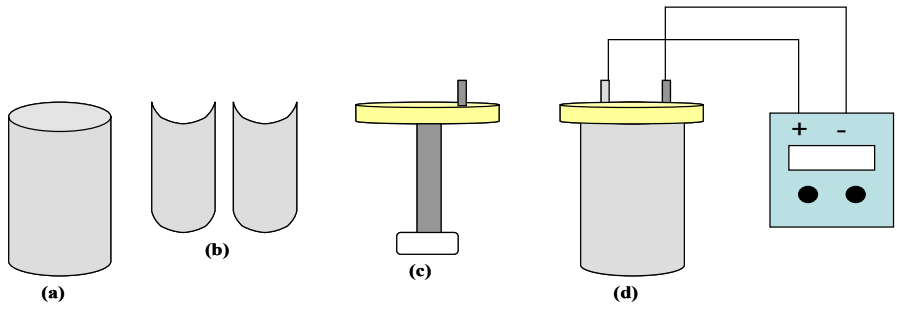

Figure 2.2-1 Components of the EF batch cell: a. Full aluminum anode (213.3cm^2) b. 2 aluminum anodes, 1/4 total area of full anode (53.33cm^2) c. Stainless steel cathode fitted onto magnetic stirrer arm and attached to plexyglass cap d. Complete EF apparatus fixed onto a 1L chemical glass and connected to DC power supply.

Alum dosing

To create conditions in which alum dosing could be compared to the dosing regime in EF, alum was added to the suspension for identical time intervals as current operation in the EF unit (3, 6 and 10 minutes) at the end of which samples were analyzed (for pH, size distribution, ζ potential and image analysis). The complete alum dose was achieved at 10 minutes, and from this stage onwards samples underwent continuous mixing and measurements were taken at two more time intervals: 15 and 20 minutes.

A stock solution of 10,000ppm commercial alum ($Al_2(SO_4)_3 18H_2O$) was prepared, and additive dosing was performed using a syringe pump (*74900 series, Cole- Parmer*). The preset dosing rates used were 0.24ml/min, 0.64ml/min and 1.28ml/min to achieve final doses of 30mg/l, 80mg/l and 160mg/l respectively.

2.3 EF as pretreatment to membrane ultrafiltration

Colloidal suspension

0.3gr of kaolin ($AlSi_2O_5(OH)_4$, *Aldrich Chemical Company Inc. USA*) was suspended in 20 liters of distilled water (15mg/l final concentration) and homogenized using an *Ultraturax 2000, Ganke and Kunkel, GMBH*. 1.66gr of $NaHCO_3$ (*BDH Laboratory Suppliers, England*) was added (final concentration 83mg/l), the pH was corrected to 5, 6.5 and 8, with NaOH or H_2SO_4, and conductivity was increased to 1mS/cm with $NaNO_3$ (*Riedel-Dehaen*, *GMBH*).

EF unit

The EF unit was a batch cell comprised of two flat sheet electrodes (an aluminum anode and stainless steel cathode), with an active area of $9cm^2$, which were immersed in the treated suspension, and connected to an external DC power supply. The cell was run at constant current (range used was 0.06A-0.2A), for a fixed 7 minutes dosing period, and the doses were equivalent to 2.43mg/l, 6.48mg/l and 12.96mg/l aluminum, respectively.

Membranes

The ultrafiltration membranes used in this study were hydrophilic Polyethersulfone flat sheet membranes manufactured by *Microdyn-Nadir* (Germany), with a nominal molecular weight cut-off of 50kDa, and pure water flux > 250l/m^{2}h. Prior to use the membranes were soaked for 12 hours in distilled water purified with reverse osmosis.

Ultrafiltration test unit

A schematic diagram of the laboratory-scale membrane test unit is shown in figure 2.3-1

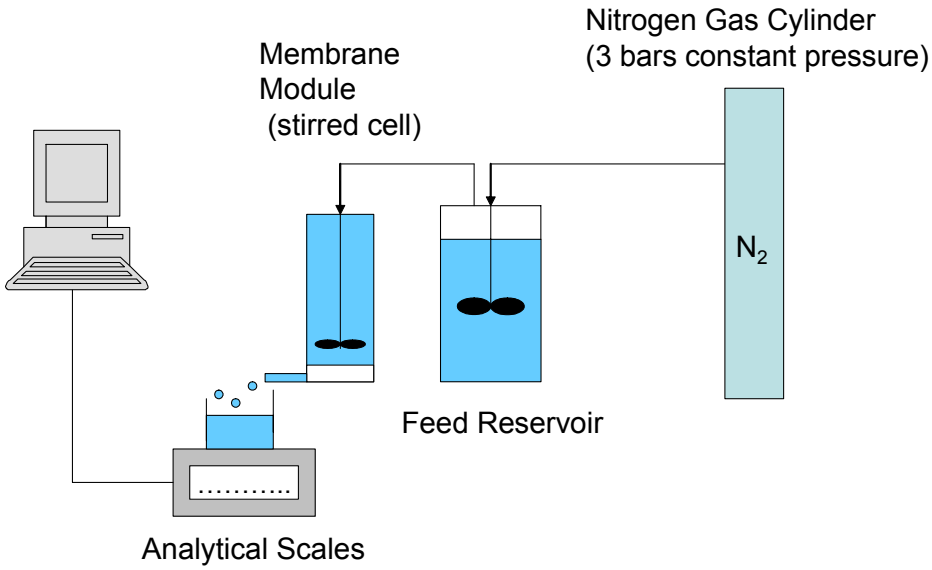

Figure 2.3-1 Schematic diagram of the membrane test unit

The membrane filtration unit was comprised of a nitrogen gas cylinder, which maintained a constant pressure of 3 bars throughout the unit. A polypropylene feed reservoir, with a volume of 1250ml, held the colloidal suspension prior to the membrane module. The membrane module, made from polypropylene, was operated as a stirred cell. It contained an internal magnetic stirrer bar suspended close to the upper surface of the membrane with motion induced by a magnetic stirrer table placed beneath it. A flat disc membrane with an area of 11.3cm^2 was held in place with an O-ring. The permeate was collected in a chemical glass mounted onto an electronic balance (*Sartorius max 3100gr*), which was connected to a

computer containing software that calculated the permeate flux from permeate weight accumulation.

Particle size analysis

As specified in section 2.1.

ζ potential

As specified in section 2.1.

Cake characterization

Membranes exhibiting cake formation were dried (at room temperature) and photographed using scanning electronic microscopy (*SEM, Joel-JSM-5600*).

Aluminum measurements

Residual aluminum in the permeate was measured using ICP (*Inductively Coupled Plasma, Cole-Parmer).*

Experimental procedure

1 liter of the kaolin suspension underwent electroflocculation for 7 minutes, in a rapid mix regime (using magnetic stirrer at 120 rpm), and then was transferred to a jar test apparatus (*Phipps and Bird, USA*) for an additional 20 minutes slow mixing (30 rpm). Samples were taken from the flocculated suspension for particle characterization (particle size distribution and ζ potential), before filtering through the membrane unit. The flux was measured through the membrane, at room temperature (~20^{o}C) at constant pressure (3 bars) over a 25 minute time span.

Chapter 3 - Results and Discussion

3.1 Characteristics of an electroflocculated kaolin suspension

3.1.1 Changes in ζ potential and pH

The current applied in the EF process has a double effect, by both generating the coagulant species and by causing hydrolysis in which excess hydroxyl ions are formed at the cathode, resulting in an increase in pH. In these dynamic conditions, coagulation mechanisms shift, depending on the current applied. The shift in pH and consequent shifting speciation of aluminum mononuclear complexes, causes the ζ potential of the electroflocculated suspensions to change. Figure 3.1.1-1 shows the change in ζ potential and pH as a function of applied current for a 15mg/l kaolin suspension at two different initial pH values: 5 and 6.5. The ζ potentials of the kaolin suspensions, without applying any current, were: -17.9mV and -21.7mV for pH 5 and 6.5 respectively.

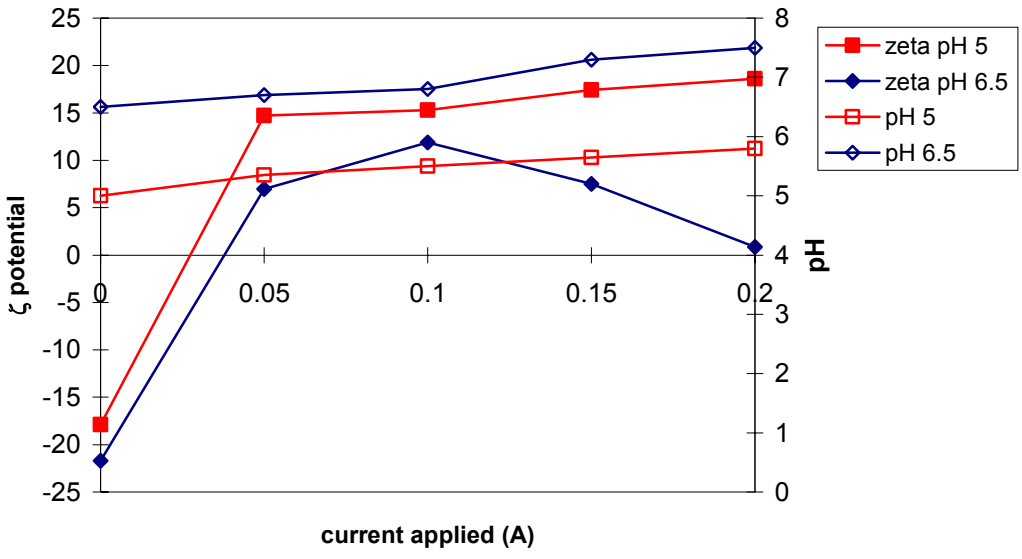

Figure 3.1.1-1 Change in ζ potential vs. applied current for initial pH 5 and 6.5. C_{kaolin}=15mg/l, conductivity=1mS/cm, $t_{dosing+mixing}$=6min, G=30sec^{-1}

The ζ potential depends on the potential at the surface of the particle and the composition of the Stern layer. It is an indirect measurement of the charge on particles, and its value determines the extent of the electrostatic forces of repulsion between charged particles. For coagulants such as hydrolyzed aluminum ions, as in this case, specific adsorption is dominant and generally caused by coagulant-colloid interactions. They bind to specific sites on the colloid surface and by doing so neutralize the electrostatic surface charge of the colloid.

At pH 5 the governing aluminum mononuclear species in solution are Al^{+3} and $Al(OH)^{2+}$ (Duan and Gregory, 2003), and it is assumed that dominant coagulation mechanism is adsorption and charge neutralization. Therefore, the ζ potential of the suspension under these conditions becomes more positive as a function if the applied current, until stabilizing at +17mV, for an applied current of 0.1A and above (within the measured range). At 0.1A, the pH rises to 5.7 and conditions become favorable for aluminum hydroxide precipitation (transition *into* "sweep-floc"). Aluminum hydroxide is charged positively below its i.e.p (between pH 8-9), and therefore in the precipitation zone, the ζ potential stabilizes at a positive value. Increased aluminum hydroxide precipitation stabilizes the pH due to the removal of the excess hydroxyl ions from solution. This coagulation mechanism combines both destabilization and transport processes.

At pH 6.5 the governing coagulation mechanism is "sweep-floc", as at this pH formation of amorphous aluminum hydroxide is considered optimal. At this pH other positive mononuclear species, Al^{+3} and $Al(OH)^{2+}$, are also present, although in reduced amounts. These contribute to the charge neutralization and ultimately charge reversal, indicated by the change in ζ potential towards more positive values, reaching a maximum of +12mV, at 0.1A (fig. 3.1.1-1). At currents higher than 0.1A, a drop in the ζ potential occurs, and its value becomes less positive. At 0.2A, at a final pH of 7.5, the ζ potential reaches an iso-electric point (i.e.p), due to the presence of negative mononuclear species which counteract the effect of the positive species in solution. At 0.1A, the pH is 6.8. At currents above this the pH

increases even more and speciation shifts towards the aluminate ion, $Al(OH)_4^-$ - indicated by the less positive ζ potential.

3.1.2 Effect of mixing conditions in EF process

Adequate mixing conditions are required for optimal aggregation: to disperse the coagulant homogenously and to create collisions between particles. If the particles are submicron in size Brownian motion is appreciable, however as the particles grow into larger aggregates, other transport mechanisms become dominant. The applied velocity gradient (G) plays a major role in flocculation mechanisms, as it represents the shear rate in a mechanically agitated system. In the EF process the applied velocity gradient also affects the coagulation mechanisms, as it helps control the pH of the treated suspension and ultimately aluminum hydroxide precipitation. Experiments were conducted at pH 5, without applying a velocity gradient ($G=0sec^{-1}$) and these produced suspensions with a higher final pH, than those treated applying a velocity gradient (fig. 3.1.2-1).

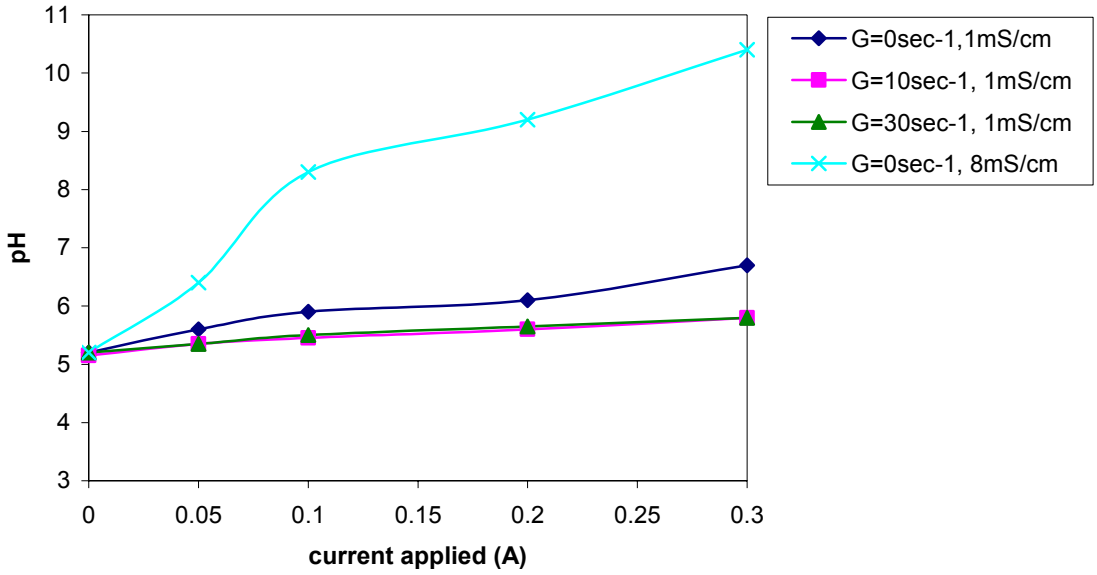

Figure 3.1.2-1 Change in pH vs. applied current, for varying velocity gradients.

C_{kaolin}=15mg/l, conductivity=1mS/cm, 8mS/cm, $t_{dosing+mixing}$=6min, initial pH 5.

For conductivity values of 1mS/cm, and velocity gradients of both $10sec^{-1}$ and $30sec^{-1}$ a similar result is obtained, the final pH not exceeding 6, for the maximum current used, 0.3A.

However, the pH rises to 6.6, when a velocity gradient is not applied ($G=0sec^{-1}$). For experiments conducted with suspensions with high conductivity values (8mS/cm), the rise in pH was even more substantial for $G=0sec^{-1}$ (fig. 3.1.2-1), reaching 10.1 at 0.3A, for a suspension at initial pH 5. Applying a velocity gradient ($G=10sec^{-1}$ and $G=30sec^{-1}$) did lower the pH to similar values shown in fig. 3.1.2-1 for 1mS/cm suspensions. The significant increase in pH for high conductivity suspensions, when mixing conditions aren't imposed, is most likely due to a screening affect other charged particles produce when in high concentration in solution. The transport of ions, when mixing is not induced, is via diffusion. If other ions are present in large concentrations, the aluminum produced at the anode and the hydroxyl ions produced at the cathode won't be able to come in contact efficiently, because a dense barrier of other ions exists between them. Mixing "breaks" this barrier and enables efficient contact, thus resulting in aluminum hydroxide precipitation and a lower final pH.

The application of a velocity gradient does not only affect primary kaolin particle collisions, but also collisions between Al^{+3} and hydroxyl ions which result in aluminum hydroxide precipitation as colloidal matter - this is a key factor in maintaining a relatively stable pH throughout the EF process. Moreover, enhanced precipitation induces sweep floc coagulation which generally gives considerably improved particle removal as opposed to aggregation via charge neutralization alone. This can be explained by the greatly improved rate of aggregation, due to the increased solids concentration. The effect of mixing conditions on aluminum hydroxide precipitation has been studied in some detail by Clark et al. (1993) who showed that there is a competition between the formation of aluminum hydrolysis products and precipitated solid. With more intense mixing, the results indicated that precipitation would be favored.

3.1.3 Aggregates formed in EF

Morphological characterization of suspended aggregates is a microscopic technique which is complementary to macroscopic methods for characterizing flocculated suspensions. Image analysis was used to morphologically characterize the resulting aggregates (i.e primary kaolin

particles vs. aluminum hydroxide floc) and for quantifying their structure using a two-dimensional fractal dimension (D_2).

3.1.3.1 Morphology

Figure 3.1.3.1-1 shows types of aggregates and flocs obtained after EF (magnification x10).

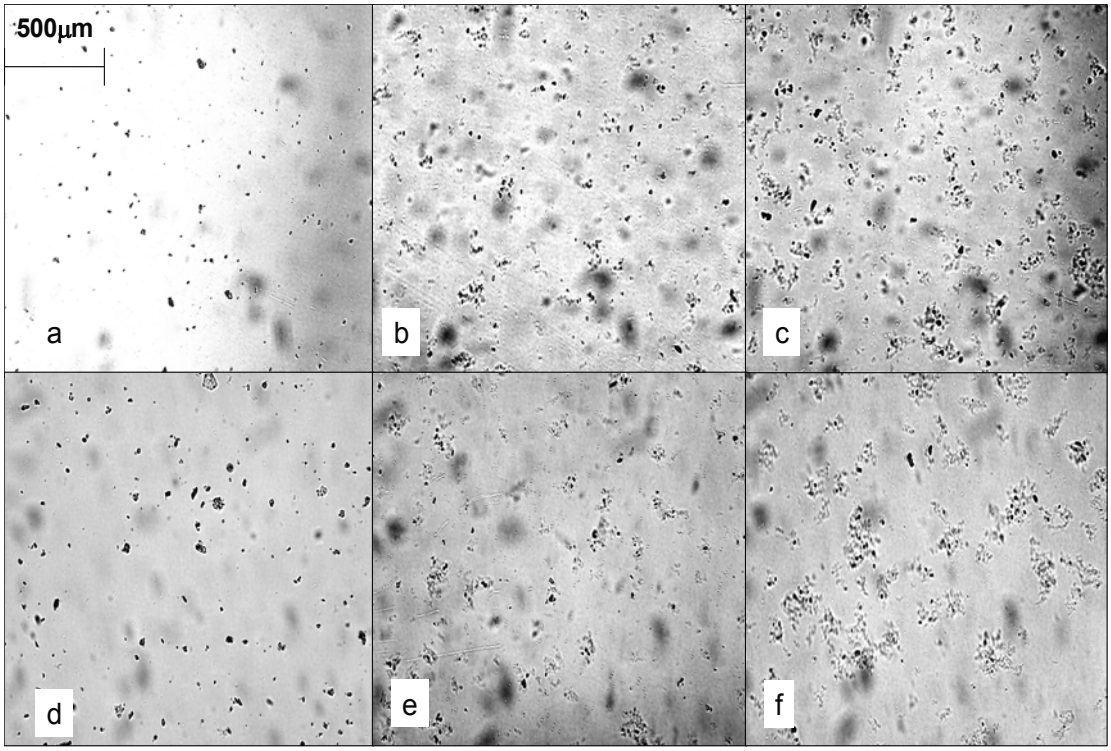

Figure 3.1.3.1-1 C_{kaolin}=15mg/l, $t_{dosing+mixing}$=6min **a.** pH 5, 1mS/cm, 0A, G=0sec^{-1} **b.** pH 5, 1mS/cm, 0.05A, G=30sec^{-1} **c.** pH 5, 1mS/cm, 0.1A, G=30sec^{-1} **d.** pH 5, 8mS/cm, 0.1A, G=0sec^{-1} **e.** pH 5, 8mS/cm, 0.1A, G=10sec^{-1} **f.** pH 5, 8mS/cm, 0.3A, G=10sec^{-1}

The visible data shows distinct differences between aggregates, both in morphology and in size, obtained under different EF conditions. In general, a difference is evident between kaolin aggregates and aluminum hydroxide flocs. The former has a dense, compact structure, and the latter a more open, loose structure. Under control conditions, without applying current or velocity gradient (a.), the primary kaolin particles appear dispersed. Some minor aggregation of primary kaolin particles has occurred (indicated by larger black clusters). This can probably be explained by a degree of Brownian diffusion occurring, coupled with double

layer compression (Verwey and Overbeek, 1948) promoted by the addition of electrolyte ($NaNO_3$) to achieve adequate conductivity values (minimum 1mS/cm) for operation of the EF cell. Applying a current and velocity gradient induces flocculation which results in precipitation of aluminum hydroxide and formation of flocs which enmesh the primary kaolin particles. These flocs increase in size as the current increases (b. and c.). At initial pH 5 (as shown in fig. 3.1.3.1-1), raising the current shifts the coagulation mechanism from adsorption and charge neutralization more towards sweep-floc, because the pH shifts to values which favor precipitation. Under these conditions, a higher current will increase precipitation and consequently larger flocs will form. For higher conductivity values (8mS/cm), significant kaolin aggregation occurs, and no aluminum hydroxide precipitation is observed, when a current is applied alone (d.), without applying a velocity gradient. The high level of electrolyte in solution, coupled with the aluminum dose has most likely lowered the repulsion barrier between primary particles, and enabled aggregation. Some aggregates observed are large in size (up to 50μm), and considering the time span of the experiments, it is unlikely Brownian diffusion is the primary transport mechanism. This raises questions regarding the effect of the electric field on particle transport in the EF process, which could explain the enhanced kaolin aggregation without applying a velocity gradient. For high conductivity values, when both current and velocity gradient are applied, similar results to those at lower conductivity values are obtained, and increased precipitation is observed (e. and f.). At pH 6.5, for all currents, with application of a velocity gradient, precipitation was observed. Moreover, floc size increased with current increase. At pH 6.5, the dominant coagulation mechanism is sweep-floc, for all currents applied. Although speciation shifts towards negative mononuclear species at the higher currents (0.2A, 0.3A produce a final pH of 7.3 and 7.5 respectively), increased precipitation occurs at the beginning of the process, due to the large amount of Al^{+3} introduced into solution. Despite the existence of negative mononuclear species at the end of the process, their effect on coagulation is negligible, because aluminum hydroxide flocs have already formed extensively.

3.1.3.2 Fractal dimension

The fractal dimension of aggregates/flocs in the experiments was based on imaging, and therefore is two-dimensional and is referred to as D_2.

Current (A)	Al^{+3} Dose (mg/l)	Current Density (mA/cm^2)	G (sec^{-1})	Conduct. (mS/cm)	T_{dose} (min)	pH	Ave. Fractal Dimension (D_2)	Standard Deviation
0	0	0	0	1	1	5	1.68	0.04
			10				1.70	0.07
			30				1.62	0.09
0.05	4	1.6	0	1	1	5	1.68	0.09
			10				1.46	0.05
			30				1.52	0.08
0.1	8	3.2	0	1	1	5	1.68	0.08
			10				1.51	0.06
			30				1.48	0.04
0.2	16	6.4	0	1	1	5	1.67	0.05
			10				1.48	0.07
			30				1.39	0.01
0.3	24	9.6	0	1	1	5	1.60	0.06
			10				1.52	0.07
			30				1.45	0.08
0	0	0	0	1	1	6.5	1.64	0.07
			10				1.64	0.05
			30				1.63	0.07
0.05	4	1.6	0	1	1	6.5	1.65	0.11
			10				1.57	0.09
			30				1.48	0.03
0.1	8	3.2	0	1	1	6.5	1.67	0.07
			10				1.49	0.04
			30				1.48	0.05
0.2	16	6.4	0	1	1	6.5	1.68	0.04
			10				1.51	0.05
			30				1.45	0.04
0.3	24	9.6	0	1	1	6.5	1.50	0.04
			10				1.48	0.06
			30				1.51	0.04
0.025	4	0.8	10	1	2	5	1.51	0.04
			30				1.50	0.06
0.05	8	1.6	10	1	2	5	1.48	0.07
			30				1.46	0.05
0.1	16	3.2	10	1	2	5	1.47	0.05
			30				1.44	0.04
0.15	24	4.8	10	1	2	5	1.43	0.06
			30				1.41	0.05
0	0	0	0	8	1	5	1.66	0.09
			10				1.59	0.07
			30				1.67	0.05
0.05	4	1.6	0	8	1	5	1.70	0.08
			10				1.50	0.06
			30				1.51	0.05
0.1	8	3.2	0	8	1	5	1.65	0.04
			10				1.47	0.07
			30				1.46	0.05
0.2	16	6.4	0	8	1	5	1.61	0.08
			10				1.46	0.04
			30				1.43	0.07
0.3	24	9.6	0	8	1	5	1.65	0.06
			10				1.48	0.03
			30				1.42	0.1

Table 3.1.3.2-1 Average two-dimensional (D_2) fractal dimensions obtained for different operational parameters.

The fractal dimension was used to quantify aggregate/floc structure, and subsequently served as a mathematical parameter for tracking differences between aggregates formed in different experiments, resulting from varying operational parameters, such as applied current (Al^{+3} dose), current density, pH, conductivity and G. Table 3.1.3.2-1 summarizes the results.

The values obtained without applying a velocity are similar for most experiments, and are between 1.60±0.06 and 1.70±0.08. These are representative of kaolin aggregation, in a dilute electrolyte, as in these conditions aluminum hydroxide precipitation is limited as no mixing is induced. However, at pH 6.5 and 0.3A, the D_2 calculated is low compared to these values – 1.50±0.04. This can be explained by the fact that the high Al^{+3} dosage and pH have created some degree of precipitation, despite absent mixing conditions. This is probably via diffusion, as large amounts of Al^{+3} and OH^- ions are created in these conditions. The more open and loose structure which characterize aluminum hydroxide flocs, as opposed to kaolin aggregates, is the reason for the lower average D_2. In general, a trend is observed in which D_2 decreases as the current increases, when a velocity gradient is applied, although differences obtained from 0.05A and above are not significant.

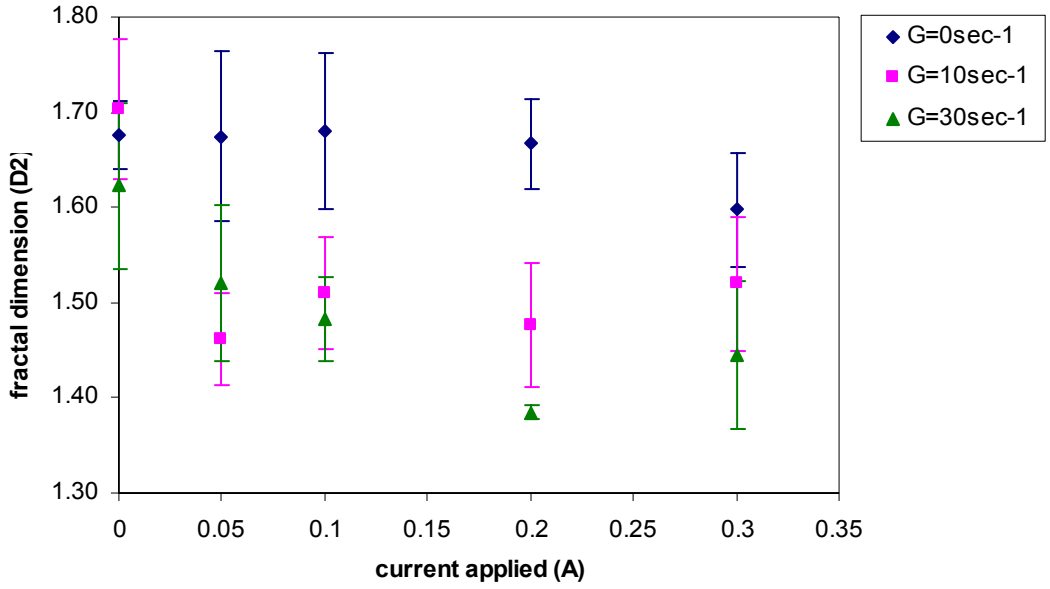

Figure 3.1.3.2-1 Fractal dimension, D_2, vs. current intensity, for different G values, C_{kaolin}=15mg/l, $t_{dosing+mixing}$=6min, pH 5, conductivity=1mS/cm. Error bars represent one standard deviation.

Moreover, t-tests comparing D_2 values obtained for different currents between sets (i.e. different currents at same G), both at pH 5 and 6.5, indicated that these differences are indeed not appreciable ($P>0.05$). Figure 3.1.3.2-1 shows the differences in D_2 obtained at pH 5, as a function of applied current and velocity gradient.

D_2 for all currents applied, in the absence of mixing conditions, does not significantly change, and is between 1.60 ± 0.06 and 1.68 ± 0.09. Application of a velocity gradient does lower the resulting average D_2, because mixing induces aluminum hydroxide precipitation and floc formation. There is not an appreciable difference (based on t-tests) between D_2 values, when applying a velocity gradient, for all currents. Therefore, the resulting D_2 values for $G=10sec^{-1}$ or $G=30sec^{-1}$ are considered similar. For a doubled dosing period (2 min), there appears to be a more distinct difference between D_2 values obtained for different currents. For currents of 0.025A and 0.15A, and $G=10sec^{-1}$, the resulting D_2 values were 1.51 ± 0.04 and 1.43 ± 0.06, respectively. Therefore, for an increased dosing period (2 min), lower currents produced higher D_2 values, than for higher currents. When comparing current densities, for 1min and 2 min dosing, no significant differences are observed. For different current densities and identical doses, a trend is observed, at higher dosage levels: lower current densities produced lower D_2 values. To achieve equivalent doses using half current densities, a doubled dosing period was required. In these conditions, despite the lowered dissolution rate of Al^{+3} ions (mg/sec), the ions first dissolved have a longer effective time to react in solution. This could lead to better growth and consequently larger flocs exhibiting lower D_2 values.

When comparing D_2 values obtained from suspensions with different conductivities (1mS/cm vs. 8mS/cm), some differences are observed for 0.1A and 0.2A, when a velocity gradient was not applied ($G=0sec^{-1}$). Figure 3.1.3.2-2. shows the shows the differences in D_2 obtained at pH 5, for different conductivities, as a function of applied current, with and without applying a velocity gradient.

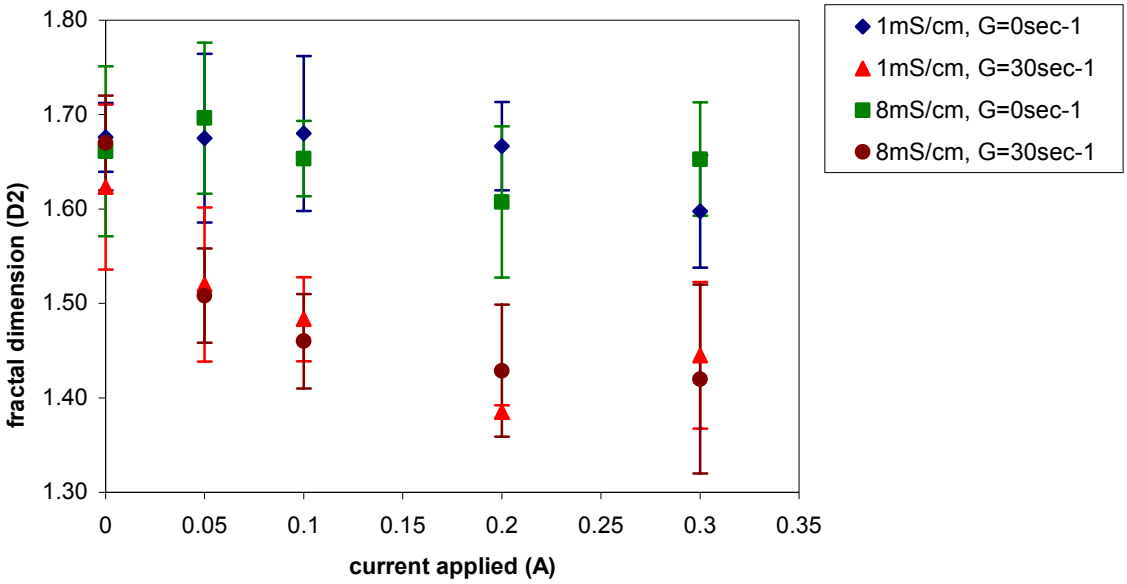

Figure 3.1.3.2-2 Fractal dimension, D_2, vs. current intensity, for G=0sec^{-1} and 30sec^{-1}, C_{kaolin}=15mg/l, $t_{dosing+mixing}$=6min, pH 5, 1mS/cm and 8mS/cm. Error bars represent one standard deviation.

The differences in D_2, between 1mS/cm and 8mS/cm, obtained for G=0sec^{-1} and currents of 0.1A and 0.2A are directly related to the morphology of the kaolin aggregates, which do form even though a velocity gradient was not applied. The average D_2 obtained under these conditions is lower for 8mS/cm than for 1mS/cm. T-tests, comparing D_2 values obtained for same currents between sets (i.e. comparing 0.1A at 1mS/cm and 8mS/cm, at constant G), yielded probability values which indicated that differences could not be significant. However, one cannot ignore the images obtained under these conditions which show distinct differences in kaolin aggregation, as a function of conductivity. This underlines the advantage of using image analysis techniques as a complementary technique to other macro techniques, for verifying the true nature of aggregates and flocs formed. Figure 3.1.3.2-3 shows the differences between images obtained after EF of suspensions with different conductivities (magnification x10).

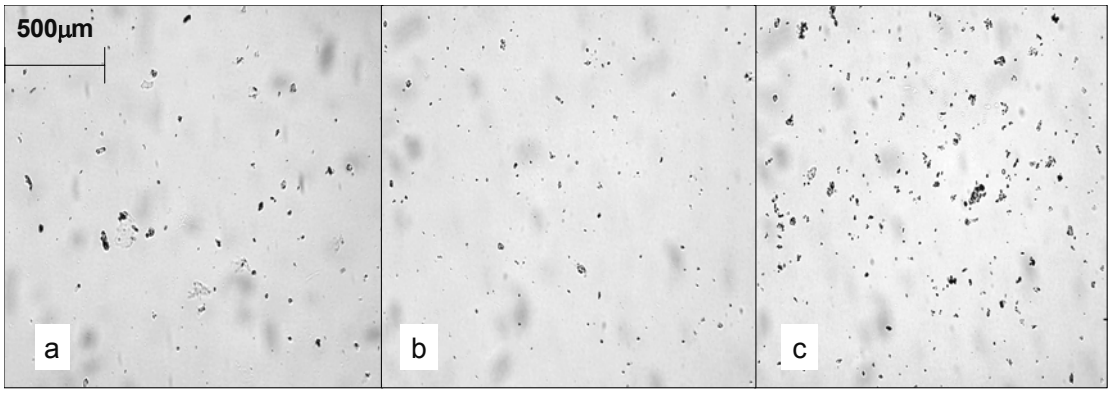

Figure 3.1.3.2-3 C_{kaolin}=15mg/l, $t_{dosing+mixing}$=6min **a.** pH 5, 1mS/cm, 0.1A, G=0sec^{-1} **b.** pH 5, 8mS/cm, 0.05A, G=0sec^{-1} **c.** pH 5, 8mS/cm, 0.1A, G=0sec^{-1}

The images indicate that for higher conductivity values (8mS/cm), significant kaolin aggregation occurs, when a current is applied alone, without inducing mixing conditions. Minor aluminum hydroxide precipitation is observed, but evidently not sufficient to promote growth of flocs. The high level of electrolyte in solution, at 8mS/cm, coupled with an adequate aluminum dose (0.1A) has promoted flocculation via double layer compression and/or adsorption and charge neutralization. However, the size of the resulting aggregates (some up to 50μm) and the relatively short time span of the experiments (6 minutes total), pose questions regarding the primary transport mechanism which has enabled aggregation in these conditions – without inducing mixing conditions. Brownian diffusion exists, but it is unlikely it serves as the sole transport mechanism, enabling aggregation into large aggregates, within a short period of time. In EF, an electric field is induced, while the current passes through the cell. This could enhance particle transport, although in addition bubble formation could also serve as a supplementary mixing mechanism which would explain the enhanced kaolin aggregation occurring without application of a velocity gradient. For 8mS/cm, when both current and velocity gradient are applied, transport via diffusion becomes negligible and similar D_2 results to those at lower conductivity values are obtained as increased precipitation is observed.

Little literature exists on D_2 values of resulting aggregates/flocs in flocculation processes using alum; none exists on aggregates/flocs formed in EF. Gorczyca and Ganczarczyk (1996) reported D_2 values for alum flocs formed in inorganic clay and mineral suspensions to be between 1.71 and 1.97 ($\pm$0.05). Li and Ganczarczyk (1989) calculated fractal dimensions of alum flocs to be between 1.59 and 1.97, from measurements conducted by Tambo and Watanabe (1979). Chakraborti et al. (2003) found the D_2 values of flocs formed by flocculation of latex particles with alum to be between 1.94$\pm$0.18 and 1.48$\pm$0.08, depending on alum dose, shear rate, and observation times. Although some D_2 values of aggregates/flocs formed in the EF process fall within the ranges reported by authors, in general the values obtained after EF are within the lower range. The unique physical-chemical conditions in EF, which differ from those created in conventional flocculation, affect coagulation/flocculation mechanisms and consequently the morphology of the resulting aggregates/flocs.

3.1.3.3 Particle size distribution

Particle size distribution analysis was carried out as a complementary procedure to image analysis, to maximize data on aggregate/floc formation in the EF process, and examine a connection between the fractal dimensions calculated and floc/aggregate size. From particle distribution measurements, a correlation can be observed between the D_2 and size. Figure 3.1.3.3-1 shows the undersize frequency % of sizes obtained at different currents (and densities) and dosing times.

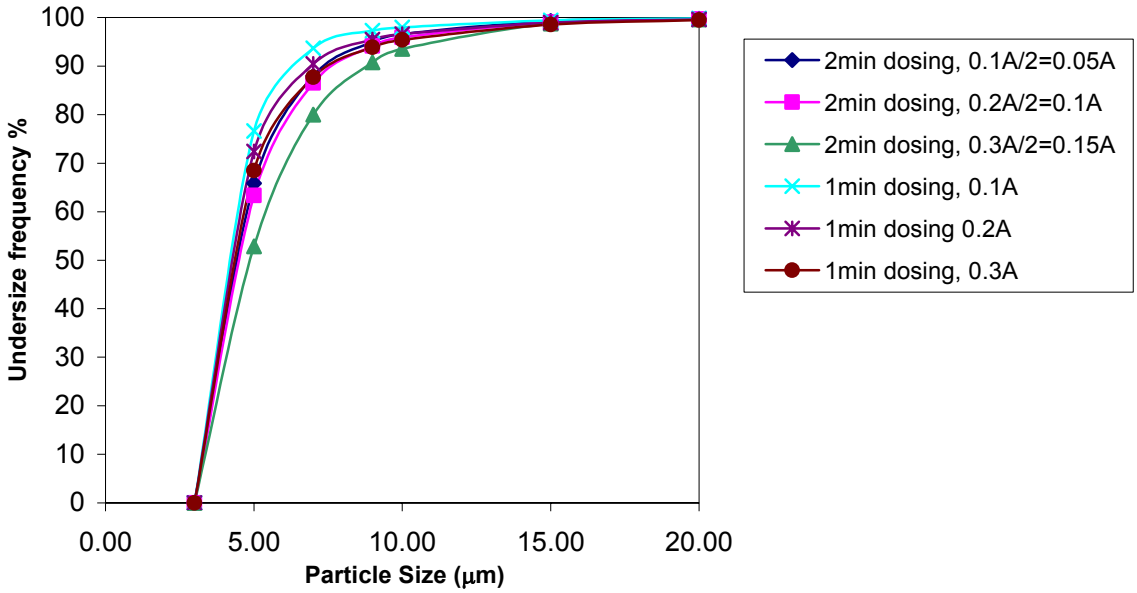

Figure 3.1.3.3-1 Undersize frequency %, C_{kaolin}=15mg/l, pH 5, 1mS/cm, G=30sec^{-1}, varying currents (densities) and dosing times.

For 0.05A and 0.15A, a dosing period of 2 minutes, and G=30sec^{-1}, D_2 values were 1.46±0.05 and 1.41±0.05, respectively, although these differences are not considered significant. Particle size distributions show that for 0.15A, larger particles are obtained than for 0.05A. Thus, a trend can be detected in which lower D_2 values correspond to larger particle sizes. When comparing current densities, for equal total doses, a similar trend is observed. For a current density of 1.6mA/cm^2, 2 minutes dosing, the resulting D_2 value is 1.46±0.05. For 3.2mA/cm^2, 1 minute dosing, the average D_2 is 1.48±0.04. Particle counts show that higher current densities (shorter dosing periods) produce smaller sizes, which correspond to higher D_2 values.

When observing particles counts conducted on suspensions with different conductivities, without the application of a velocity gradient, the same trend is observed: larger particles produce smaller D_2 values. Figure 3.1.3.3-2 shows the undersize frequency % of sizes obtained at different currents for suspensions with different conductivities.

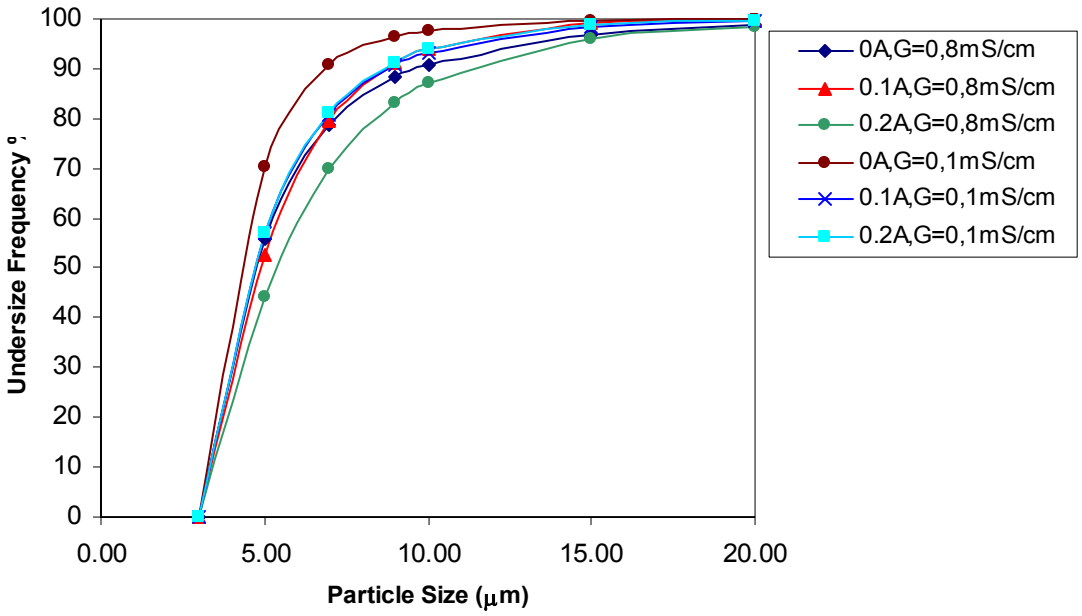

Figure 3.1.3.3-2 Undersize frequency %, C_{kaolin}=15mg/l, $t_{dosing+mixing}$=6min, pH 5, conductivity=1mS/cm and 8mS/cm, G=0sec^{-1}

For 0.2A, larger particles are observed at 8mS/cm than at 1mS/cm. In these conditions, the corresponding D_2 values were 1.61$\pm$0.08 and 1.67$\pm$0.05, respectively. Although the differences in average D_2 obtained for different conductivities are not considered significant, a correlation is observed, which also corresponds to image analysis results.

The connection between floc size and fractal dimension is typical of forming aggregates (Spicer and Pratsinis 1996; Kusters et al., 1997; Chakraborti 2003). Aggregation models, which have been used to calculate theoretical fractal dimensions of aggregates are based on the assumption that primary particles are solid and have a fractal dimension of Euclidean value (i.e. D_2=2). In this case, as clusters begin to form, and aggregates grow, the fractal dimension will decrease as size increases, until a point where the aggregates are sufficiently large in comparison to the primary particles that comprise it (Meakin, 1988). At this point, any other addition of particles will not have an affect on structure, and the fractal dimension will not change. However, in real water systems, primary particles are not necessarily solid and in orthokinetic flocculation shear forces must be acknowledged as a limiting growth

factor which can also affect the final structure, due to fragmentation and restructuring (Clark and Flora, 1991; Selmoulya, 2003).

3.2 Size and structure evolution of kaolin-$Al(OH)_3$ flocs in EF

3.2.1 Size distributions and solution changes over time

The initial stages of floc growth in the EF process were examined. Unlike conventional flocculation, in EF the aluminum dosing is additive over time (until the current is stopped) while simultaneously generating hydroxyl ions. Aluminum super-saturation leading to aluminum hydroxide precipitation depends primarily on aluminum dose and pH (Sposito, 1996) and therefore in the initial stages of EF, mass is continuously being added to the system, as dosing continues and the pH rises. The employed initial pH values were chosen to cover the pH range in which aluminum hydroxide precipitation would occur and floc evolution could be measurable. At pH 8 no significant floc formation was observed, hence results refer to pH 5 and 6.5. Figure 3.2.1-1 shows the evolution of size distributions over time for currents of 0.042A and 0.22A (maximum anode area), at initial pH 5 and 6.5. The size distribution graphs show the evolution of size over time, with modal diameters at the end of the process reaching above 200μm, with the spread reaching the upper detection limit of the instrument. For 0.042A, the growth appears similar for the initial 3 minutes of the process, for both pH values, while after 6 minutes, at pH 6.5 it is accelerated, resulting in a wider distribution spread. This behavior is also evident for 0.22A - the initial 3 minutes show similar size distributions after which at pH 6.5 an accelerated growth rate is observed. The initial 3 minutes appear to be an induction period, in which the aluminum hydroxide precursor particles are developing into sizes which will lead to enhanced aggregation as the process progresses. This period is considerably shorter for 0.22A and pH 6.5, as after only 3 minutes sizes as large as 100μm are already observed. The size distributions indicate that while growth into larger floc is occurring, smaller particles are simultaneously being formed, and thus a wider distribution spread. For 0.042A and pH 5 the size distribution narrows after

15 minutes, whereas at pH 6.5 after 10 minutes. For 0.22A, this occurs at pH 5 and 6.5, after 10 and 6 minutes respectively. Although colloidal particles of aluminum hydroxide are continuously being formed until the current is stopped, at 10 minutes, their presence in solution, as colloidal matter, depends on contact opportunities. A higher number of particles would increase the number of collisions, leading to formation of larger particles and providing additional contact opportunities for the submicron particles (Chowdhury et al., 1991). At pH 6.5 precipitation of aluminum hydroxide is considered optimal, therefore larger

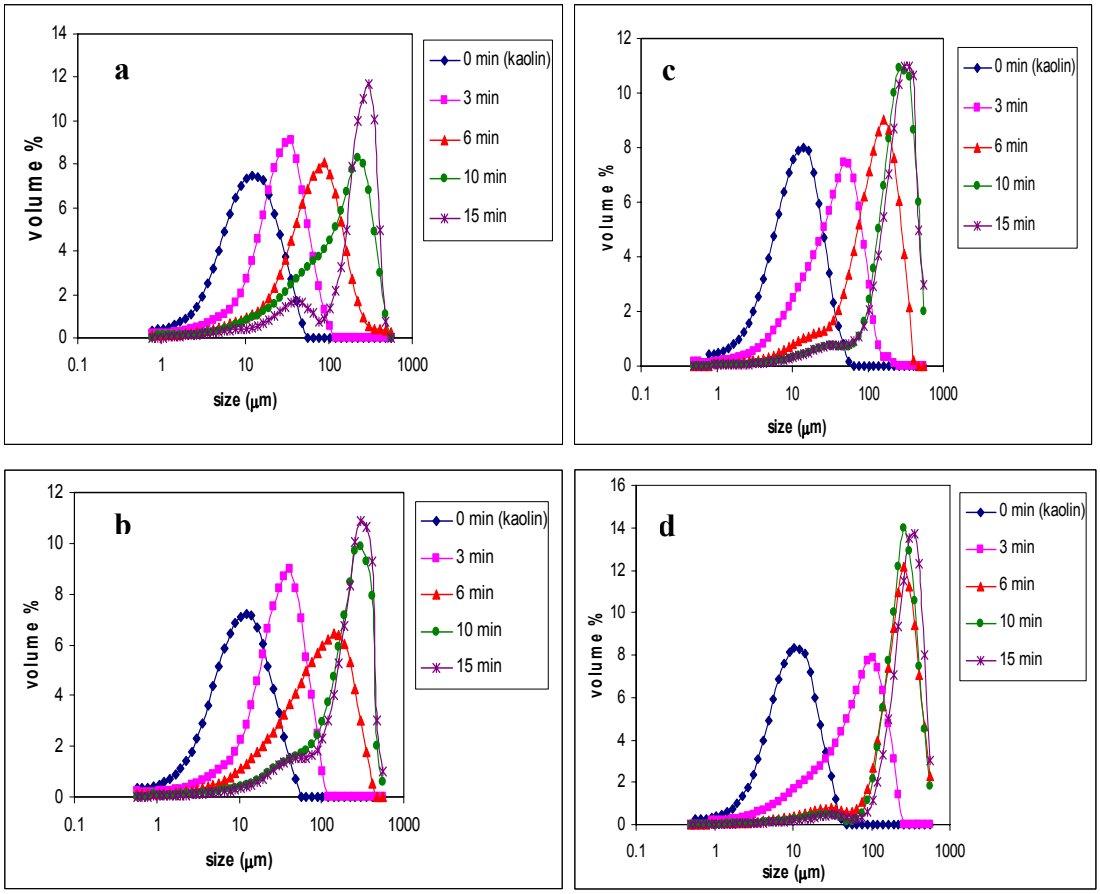

Figure 3.2.1-1 C_{kaolin}=60mg/l **a.** 0.042A, pH 5 **b.** 0.042A, pH 6.5 **c.** 0.22A, pH 5 **d.** 0.22A, pH 6.5.

amounts of precursor particles are formed and for both currents, at this pH a more rapid growth rate is observed. For higher currents (0.22A) a significantly shorter induction period is observed. The higher growth rate observed for 0.22A, is due to increased dosage of

aluminum, which will increase at this pH the precipitation of aluminum hydroxide, resulting in larger amounts of aluminum hydroxide precursor particles.

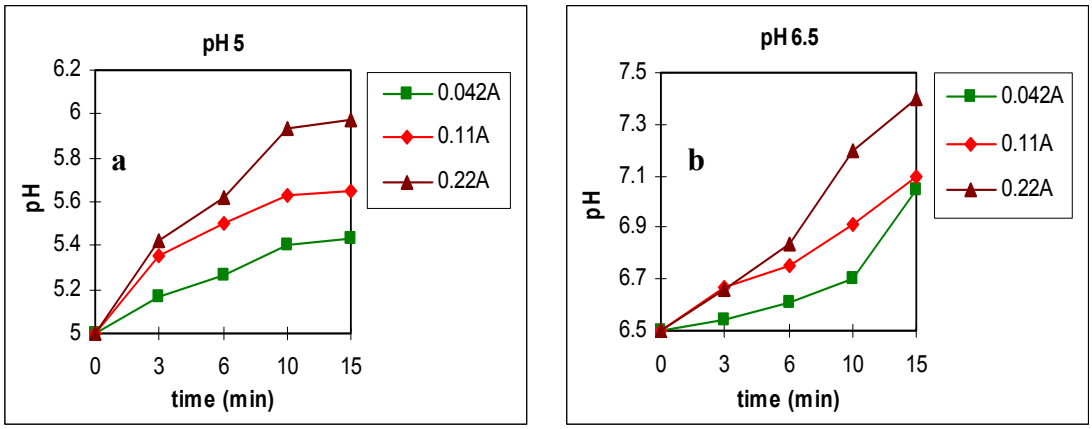

Figure 3.2.1-2 Change in pH for each time interval. **a.** initial pH 5 **b.** initial pH 6.5.

Although pH 5 is not considered an optimal sweep floc regime (Amirtharajah and O'Melia, 1990), the addition of hydroxyl ions into the solution coupled with the continuous aluminum dosing pushes the equilibrium towards enhanced aluminum hydroxide precipitation and substantial growth is observed – even so, at a reduced rate compared to pH 6.5. At pH 5 the positive soluble aluminum mononuclear species govern the solution (Duan and Gregory, 2003), although as the process progresses, the pH rises and conditions become favorable for aluminum hydroxide precipitation (transition *into* sweep-floc regime), which stabilizes the pH after 10 minutes (fig. 3.2.1-2) due to the removal of the excess hydroxyl ions from solution. However, at pH 6.5, the pH increases rapidly at end of process compared to the beginning, due to the move *out* of sweep floc regime as speciation shifts towards soluble negative mononuclear species. Under these conditions removal of the excess hydroxyl ions is limited, as aluminum hydroxide precipitation is no longer favorable, hence the sharper rise in pH. Despite the increase in pH and shift away from optimal precipitation conditions at the end of the process, the growth at pH 6.5 is more rapid than at pH 5.

Growth of particles into larger flocs is not only dependent on particle precursor numbers, but also on their ability to form stable bonds. Surface charge also plays a role in determining floc evolution (Nowostawska et al., 2005) which is measured here in the form of ζ potential -

indicating electrostatic repulsive forces in the suspension (fig. 3.2.1-3). The initial values of the kaolin suspension are -30 and -34 mV, which are the ζ potentials of the kaolin suspension at initial pH 5 and 6.5 respectively.

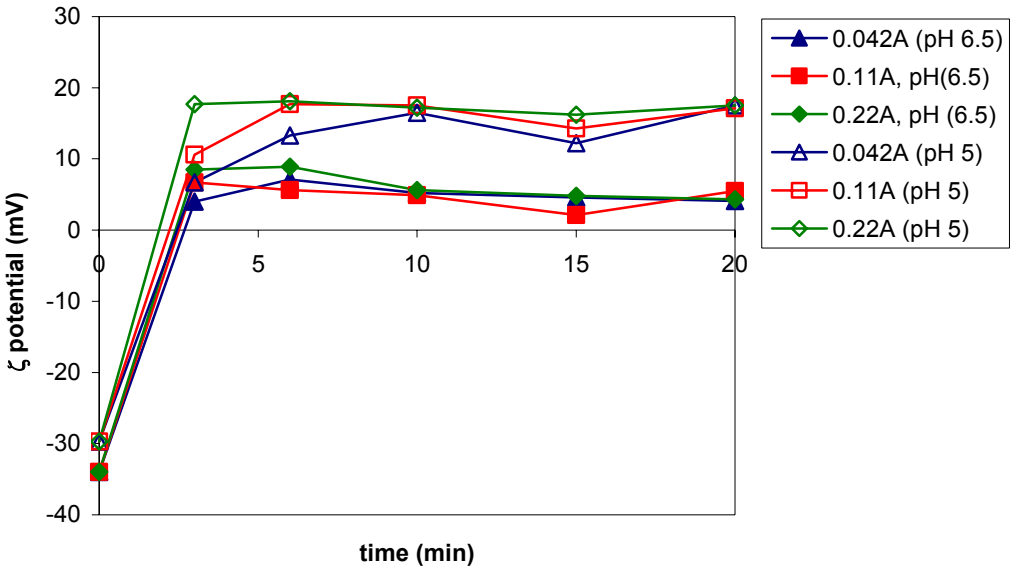

Figure 3.2.1-3 ζ potential changes over time for C_{kaolin}=60mg/l, pH 5 and 6.5, 0.042A, 0.11A, 0.22A

Within 3 minutes of EF, for both pH values, the ζ potential "jumps" to positive values which is indicative of the positive aluminum ions generated in solution, and the hydrolyzed species subsequently formed. In the initial stages, at pH 5, positive soluble aluminum mononuclear species in solution are dominant, and the ζ potential of the suspension in these conditions becomes more positive compared to pH 6.5. Stabilization occurs at 3, 6 and 10 minutes for 0.22A, 0.11A and 0.042A respectively - as conditions become favorable for aluminum hydroxide precipitation. For the pH values reached from initial pH 5, for each current, the aluminum hydroxide will be charged positively, as its iso-electric point (i.e.p) is between pH 8-9 (Sposito, 1996). At initial pH 6.5 the process commences from optimal sweep floc conditions while shifting the speciation towards negative soluble aluminum mononuclear species as it progresses. The ζ potential in these conditions is less positive than at pH 5, as less positive mononuclear species are present throughout the (initial) stages. The aluminum

hydroxide surface charge is still positive, but nearer its i.e.p. A slight drop in the ζ potential, towards less positive values, is measured for all currents after 6 minutes, where speciation towards the negative mononuclear species begins to impact (also indicated by a sharper rise in pH (fig. 3.2.1-2), as less hydroxyl ion is removed from solution in the form of aluminum hydroxide precipitate).

3.2.2 Floc growth stages

Several stages of floc growth occur during flocculation. Initially, precursor particle growth is dominant, after which particles combine and their size increases rapidly. As flocculation continues, the flocs form large, porous and open structures that are more susceptible to fragmentation by fluid shear (Tambo, 1991). As a result, the final floc size distribution is a balance between particle growth and breakage (Spicer and Pratsinis, 1996). Figure 3.2.2-1 shows the evolution of the volume mean diameter with time, for 0.042A and 0.22A with different current densities and pH values.

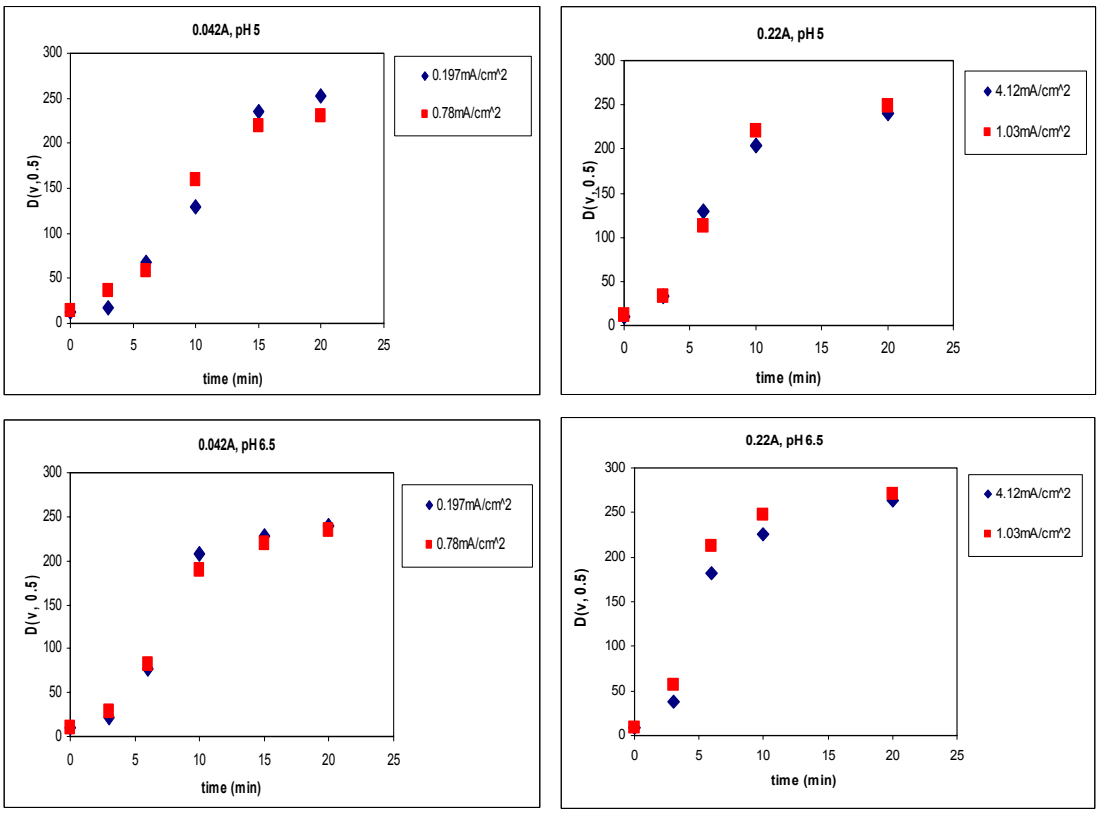

Figure 3.2.2-1 Evolution of the volume mean diameter for various current densities and pH values, C_{kaolin}=60mg/l.

The graphs show that the current density does not affect the growth pattern of the flocs, within the ranges used in this experiment. Hence, all results now will refer to experimental data obtained using full anode area. Within the experimental conditions, the total dose of aluminum dictates the growth pattern, and factors such as current density and voltage (which is dependant on current density) do not impact floc development. All graphs exhibit sigmoidal behaviour and three development stages. The first stage is the induction of aluminum hydroxide precursor particles, and limited growth due to primary collisions between those particles. Stage two exhibits enhanced growth of an exponential type, and in stage three the flocculation rate diminishes because of aggregate break up. These stages have been observed elsewhere (Kusters et al., 1997; Flesch et al., 1999). For both currents stage two commences at similar times (after 3 minutes), after which enhanced growth rates are observed for 0.22A, more so at pH 6.5. The transition to steady state (stage three) occurs when the flocs have reached a volume mean diameter of approximately 200μm, a size where disruption is caused by hydrodynamic stresses and fragmentation begins to dominate. The time of transition depends on the growth rate. For 0.042A and pH 5, this transition occurs at 15 minutes, while at pH 6.5 at an earlier time of 10 minutes. For 0.22A, pH 5 and 6.5 these times are 10 and 6 minutes respectively. In addition, for 0.22A and pH 6.5, the floc size obtained at steady state is larger than for all other conditions (above 250 μm). The increased aluminum dosing with this current, at an initial pH where aluminum hydroxide precipitation is optimal, increases the floc growth rate and apparently the strength of linkage between the particles comprising the floc, making it more resistant to breakage. This is in agreement with other studies (Francois, 1988), which found an increase both in floc growth rate and the collision efficiency with increased alum concentration during kaolin flocculation. Although at initial pH 5, the aluminum equilibrium shifts into sweep floc regime as the process progresses, this has less impact on the growth rates, than when starting out in optimal sweep floc regime, where initial nucleation and growth are maximized.

In the growth stages (induction and exponential), before transition to a steady state due to fragmentation, the relationship between the volume mean diameter and time can be written as:

$$D(V,0.5) = Ke^{bt} \qquad (3.2.2\text{-}1)$$

where K is a fitting parameter and b is the growth factor, dependent on the unique flocculation conditions.

By fitting the initial growth curves with a simple exponential regression, b can be calculated. Table 3.2.2-1 summarizes the various growth factors obtained for various currents and pH values.

Initial pH	b (0.042A)	R^2	b (0.11A)	R^2	b (0.22A)	R^2
5.0	0.236	0.98	0.303	0.92	0.381	0.99
6.5	0.297	0.98	0.329	0.94	0.528	0.99

Table 3.2.2-1 Growth factors calculated from initial growth curves.

Figure 3.2.2-2 shows the connection between growth factor and current, for each initial pH. A good degree of linearity is observed between the growth factor and applied current, within the current range used, higher currents producing higher growth factors. pH 6.5 yields not only higher growth factors, but also a higher growth dependency on current - which is larger by approximately 1.7 than that obtained at pH 5. These differences are most likely related to the generation of mass into the system in the primary stages of the process, where at initial pH 6.5 aluminum hydroxide early precipitation is increased more with increase in current, relatively to initial pH 5. However, the primary mass generated is not necessarily the sole

reason for the differences observed, as surface forces also play a role in particle coagulation enabling growth into larger floc. Floc structure has also been found to affect the growth profile as a larger collision profile (a more open structure), enhances the collision frequency (Kusters et al., 1997; Flesch et al., 1999). Different alum doses have been shown to generate different floc structures (Tambo and Watanabe, 1979), thus the current applied in EF should also have a similar effect. However, in EF, the current does not only control the coagulant dosage, but it also creates a dynamic physical/chemical environment in which speciation shifts as the pH rises, while micro-bubbles are being simultaneously formed as gaseous hydrolysis products are generated at the electrodes. All these are likely to have a profound effect on the evolving floc as floc structure is a crucial factor in understanding size evolution.

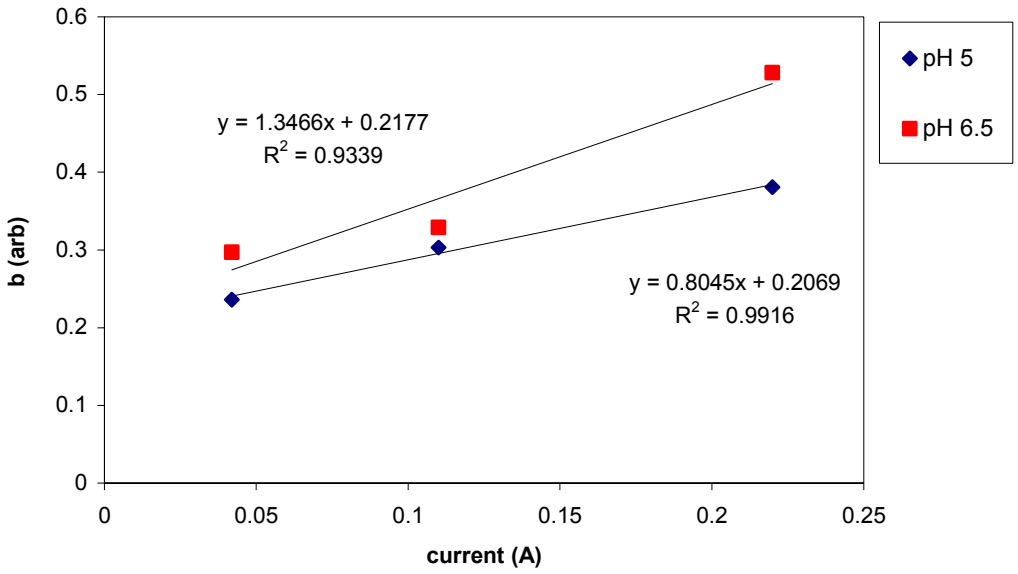

Figure 3.2.2-2 Dependency of growth factor on current at different pH values.

3.2.3 Structural evolution

Flocs undergo a series of processes including aggregation, fragmentation and, in some cases, structural rearrangement. The evolution of floc structure throughout the flocculation process depends on various factors such as floc size, formation and break-up rates, bonding forces and hydrodynamic forces (Selomulya et al., 2003). The change in floc structure can be quantified by monitoring the variation in the fractal dimension, or the scattering exponent

(SE). As mentioned in the introduction, the SE will be used in this research to define the structural properties of the flocs.

To interpret scattering plots to obtain structural data on the flocs, the question whether the primary particles maintain independent scattering must be raised beforehand, that is if the RGD approximation is valid (eq. 1.3.1.1.2-4a and 1.3.1.1.2-4b). Precipitation of aluminum hydroxide precursor particles and their growth has been studied (Li et al., 2005). It has been shown that detectable precursors/nuclei appear in the range of 100nm. Due to the uncertainty of the aluminum hydroxide precursor particles nucleating, a refractive index of 1.59 can be used as an approximation, based on the refractive index range of other aluminum hydroxide crystals (Li et al., 2005). In this case, the limitations for assuming RGD approximation for structural interpretation of scattering plots of aluminum hydroxide flocs are fulfilled:

$m = n_{Al(OH)3}/n_{water} = 1.59/1.33 = 1.195.$ $|m-1| = 0.195$ and

$(4\pi n_{water}/\lambda_{laser})L|m-1| = (4\pi 1.33/633)*100*0.195 = 0.5$

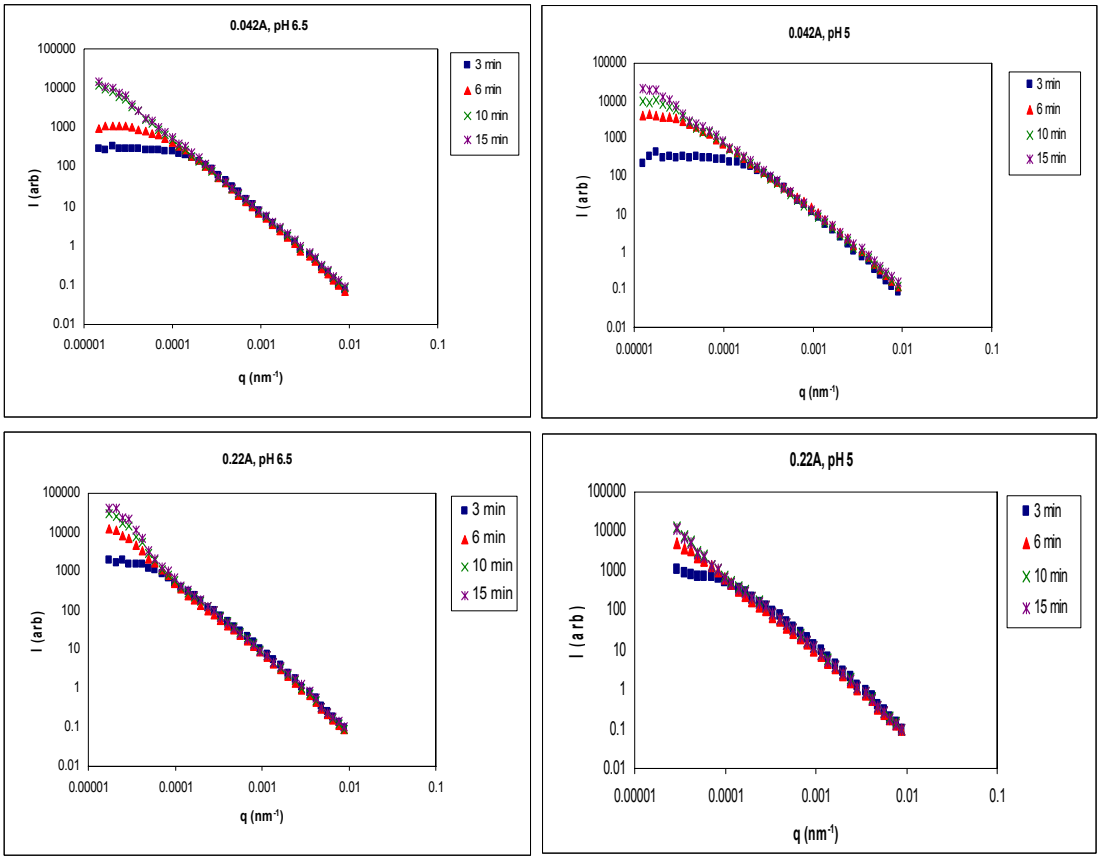

Figure 3.2.3-1 Conventional static light scattering plots (log(I) vs. log(q)) for flocs forming as a function of time.

Fig.3.2.3-1 shows typical scattering graphs of flocs at different time intervals. The graphs obtained for 0.22A, at both pH values, show that transition into an angle independent scattering region at low q is hardly apparent. A mild transition does occur at the beginning of the process, at 3 minutes, after which the graphs exhibit a dependency on q, even in the low range. This is presumably a result of the large size of the flocs obtained for 0.22, after 6 minutes and above, for both pH values. For 0.042A, the transition is more apparent, and occurs for most time intervals, at both pH values, except at pH 6.5 after 10 and 15 minutes, again due to the size of the flocs. For all graphs, one decade of linearity is observed for: $1.4*10^{-4}<q<1.6*10^{-3}$. This region will be used to calculate the SE, from the slope of the scattering plots.

Time (min)	**SE**, pH 6.5			**SE**, pH 5		
	0.042A	0.11A	0.22A	0.042A	0.11A	0.22A
3	1.83±0.04	1.78±0.02	1.77±0.02	1.75±0.06	1.86±0.02	1.78±0.03
6	1.93±0.01	1.95±0.01	1.78±0.01	1.78±0.02	1.81±0.02	1.84±0.02
10	1.89±0.01	1.88±0.02	1.81±0.02	1.88±0.01	1.90±0.01	1.87±0.02
15	1.93±0.01	1.93±0.01	1.86±0.01	1.87±0.01	1.87±0.01	1.87±0.02

Table 3.2.3-1 Scattering exponents obtained for various currents and pH values.

The results show that for all currents and pH values compaction occurs during the process, resulting in a final SE, at 15 minutes, which is higher than that obtained during the initial 3 minutes. In some conditions, fluctuations in the structural evolution are observed. This indicates the extreme fragile nature of the flocs.

For 0.042A, the flocs formed at pH 6.5 are more compact than those at pH 5. However, for 0.22A, the differences between the two pH values are not as distinct. From comparing 0.22A to 0.042A, at pH 6.5 it is evident that the higher current (aluminum dose) produced less

compact flocs, throughout all stages of the process. This also impacts the growth rate which has been observed to be higher at 0.22A, as the collision profile of the flocs forming is larger. Although for 0.22A, fragmentation starts at an earlier stage than for 0.042A (fig. 3.2.2-1) the flocs still maintain a more open structure, and reach a larger size by 15 minutes, thus indicating stronger linkage between particles comprising the floc.

This could be a result of the extent of transition out of favorable precipitation conditions. For 0.22A, compared to 0.042A, this transition is sharper, with the final pH reaching 7.4 as opposed to 7.0 for 0.042A. This affects the surface charge of the particles, as a higher pH will reduce the surface charge of the aluminum hydroxide precipitate shifting it towards its iso-electric point. A lower surface charge would decrease electrostatic repulsive forces, resulting in a higher collision efficiency and a stronger floc (stronger bonds). Moreover, at 0.22A, the generation of hydrogen gas is increased and therefore more micro-bubbles are present. These can be incorporated in the floc, thus creating a more porous structure. Figure 3.2.3-2 illustrates these differences visually.

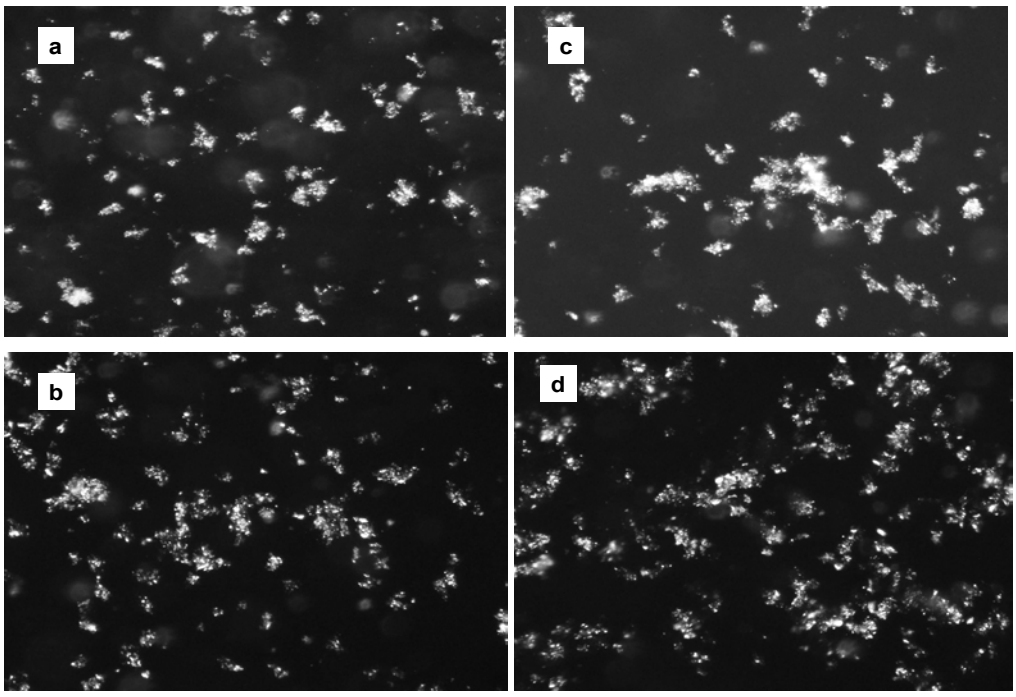

Figure 3.2.3-2 Floc structures obtained at pH 6.5 for **a.** 0.042A, t=6min **b.** 0.22A, t=6min **c.** 0.042A, t=10min **d.** 0.22A, t=10min

For 0.042A and pH 6.5, the flocs are well defined, and compact in structure, whereas 0.22A yields structures which are extremely tenuous displaying a porosity which seems even transparent in some regions. For pH 5, differences in the SE for flocs obtained at different currents are not appreciable, which indicate a rather open structure, as shown in figure 3.2.3-3. At this pH, the transition into more favorable aluminum hydroxide precipitation conditions occurs at the later stages of the process (as the pH and aluminum dose rise), thus the mass introduced into the system is less than at pH 6.5. In this case, incorporation of the micro-bubbles into flocs containing less mass would probably result in a more open structure. The flocs also exhibit less strength, and despite their large collision profile do not reach the size obtained at pH 6.5 for 0.22A. At pH 5, the surface charge of the aluminum hydroxide precipitating is more positive (further from the i.e.p) than at pH 6.5, indicating that repulsive electrostatic forces are stronger.

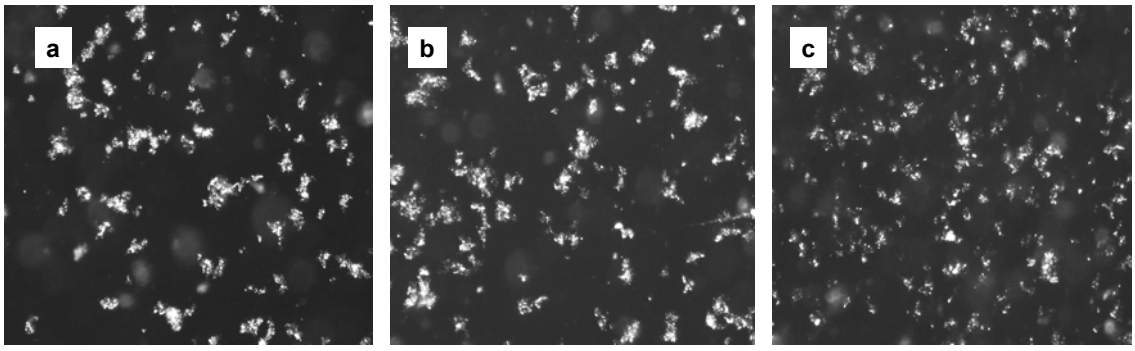

Figure 3.2.3-3 Floc structures obtained at pH 5, and 10 min for **a.** 0.042A **b.** 0.11A **c.** 0.22A

The above data shows that size and structure evolution of flocs in EF of a colloidal suspension stems from a delicate balance between mass introduced (particle numbers) at the initial stages of the process and the amount of gaseous products (in the form of microbubbles) in solution – both are current dependent. The initial particle numbers are also a function of pH, which creates, in conjunction with the current, conditions favorable for aluminum hydroxide supersaturation and precipitation. However, these also affect the surface charge of the flocs forming, which in turn affects the strength of the bonds between the precursor particles and ultimately the collision frequency and size of the floc. All these parameters,

which are intertwined, are summarized in a conceptual model (fig. 3.2.3-4) which predicts floc structure and size, with reference to the specific conditions studied here (EF of a model kaolin suspension).

At pH 5 less mass is generated as floc sweep regime is not optimal, and the repulsive surface forces at this pH are stronger for all currents, therefore the collision efficiency (α) is lower. The floc structure depends on the ratio of microbubbles/mass, as more open structures evolve, as the ratio increases. For lower currents this ratio is maintained (a low current results both in low mass and less microbubbles), but the reduced mass will result in flocs exhibiting a smaller collision frequency (β) that evolve slowly – but still portray a porous structure. For higher currents, the collision frequency is larger as more mass is generated along with hydrolysis products, resulting in a more rapidly evolving porous structure.

At pH 6.5 more mass is generated as the conditions are optimal for aluminum hydroxide precipitation. The repulsive surface forces are weaker, indicated by a ζ potential which is nearer to the i.e.p of aluminum hydroxide – hence, the collision efficiency is higher. For lower currents, the microbubble/mass ratio is smaller, and coupled with the reduced mass will result in a more compact floc which evolves slowly. For higher currents, microbubble generation is increased, resulting in a more open structure, but exhibiting strength. These flocs have both a large collision frequency and large collision efficiency – hence, the increased growth dependency on current and increased growth rate.

Figure 3.2.3-4 Conceptual model predicting floc evolution – rate and structure.

3.3 Evaluating EF as an alternative to CF

A comparative study between EF and CF was carried out, using aluminum as EF coagulant and alum as CF coagulant. A direct comparison between EF and CF is problematic, as both systems do not operate on an equivalent basis. In EF the coagulant addition is a function of current and time, whereas in CF it is a discrete (shot-fed) process. However, fundamental differences between these two processes do exist, and are manifested in the resulting solution and aggregate/floc characteristics. These differences should not be overlooked, as it is necessary to evaluate EF as a viable alternative process to CF. To create conditions, on which a theoretical comparison could be based, alum dosing was performed additively over time, and final dosing was set at 10 minutes for both processes.

3.3.1 pH 5 and 8

For pH 5 and 8 minimal floc formation was observed, except for pH 8 and 160mg/l alum, where sufficient growth occurs. Figure 3.3.1-1 summarizes size distributions over time for various alum doses and initial pH values.

The graphs show that floc evolution is limited for pH 5, as opposed to EF, where at this pH sufficient floc growth was observed for all currents applied. At pH 8, floc evolution is observed for 160mg/l whereas in EF, at this pH no formation was evident, for all currents applied. The growth at pH 8 and 160mg/l alum is limited compared to EF, with modal diameters not reaching above 200μm. However, the induction period, appears to be short, and within 3 minutes modal diameters have reached above 100μm. This was observed for high currents at optimal precipitation conditions in EF. Most likely the high alum dose and alkaline conditions have accelerated aluminum hydroxide precursor formation and thus the faster growth pattern. Despite fast initial growth stages the flocs do not reach the sizes obtained in EF, which could be a function of repulsive electrostatic forces. Figure 3.3.1-2 shows the changes in ζ potential over time for initial pH values of 5 and 8, and alum dosing.

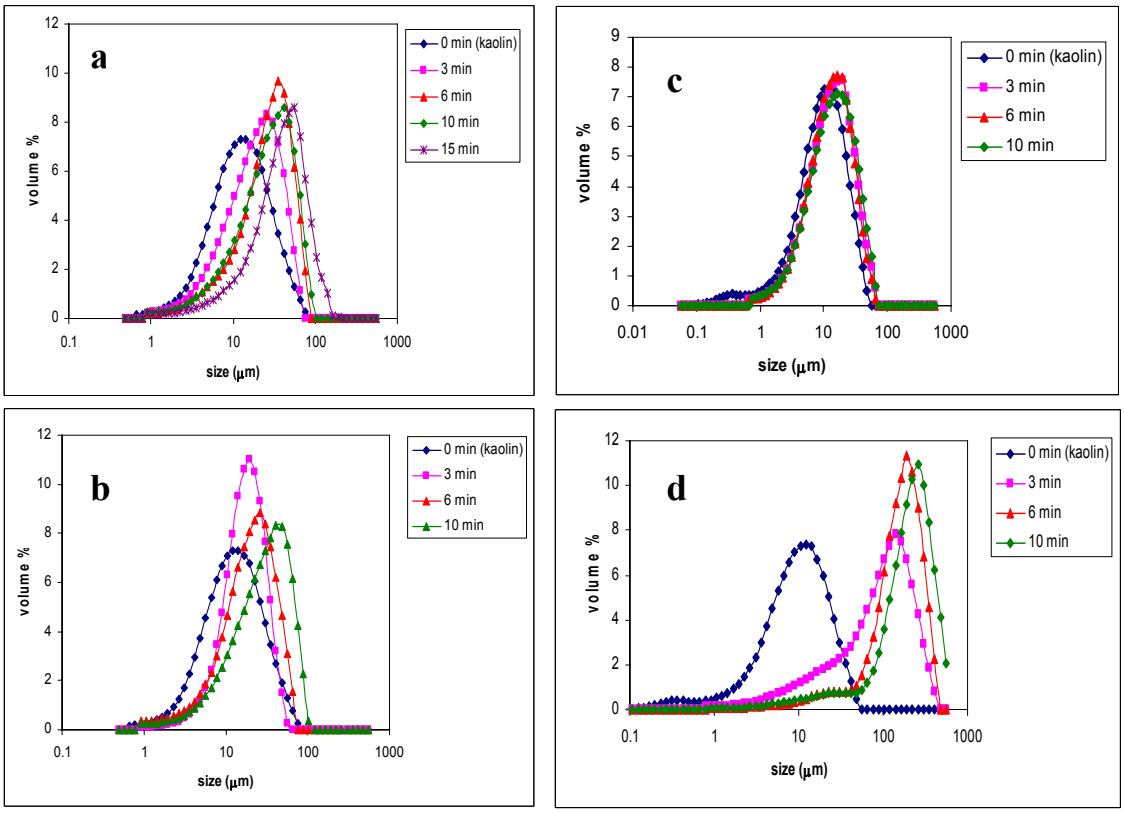

Figure 3.3.1-1 C_{kaolin}=60mg/l **a.** 30mg/l alum, pH 5 **b.** 160mg/l alum, pH 5 **c.** 30mg/l alum, pH 8 **d.** 160mg/l alum, pH 8.

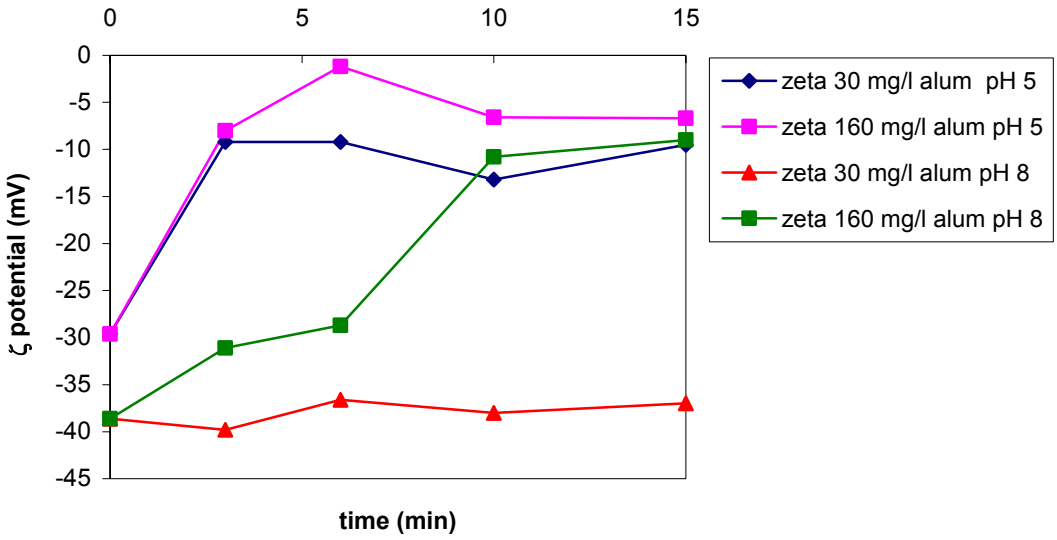

Figure 3.3.1-2 ζ potential as function of time for alum dosing, C_{kaolin}=60mg/l, initial pH 5 and 8.

The graph shows that for 160mg/l at pH 8, the ζ potential becomes less negative over time, as more alum is introduced into the system. Although at 6 minutes dosing the pH has dropped within optimal precipitation conditions (figure 3.3.1-3), the ζ potential is still quite negative (-10mV), indicating that indeed repulsive forces are a limiting growth factor. At pH 5 the pH values drop over time, thus the ζ potential is more positive, as positive soluble aluminum mononuclear species govern the solution.

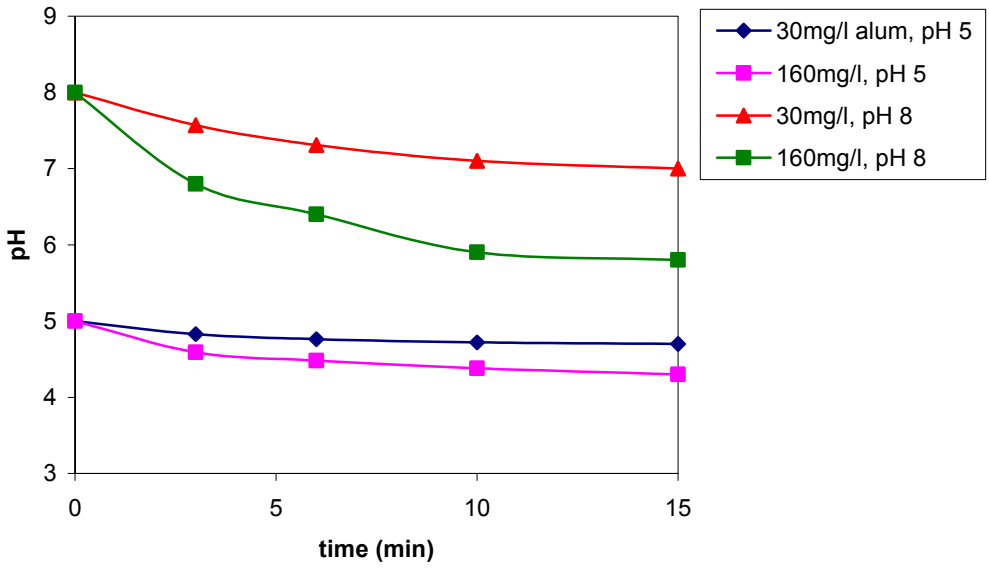

Figure 3.3.1-3 Change in pH for alum doses, C_{kaolin}=60mg/l, pH 5 and 8.

Electrostatic repulsive forces are decreased but generation of precursor particles which relies on aluminum hydroxide precipitation is the limiting factor - and therefore limited growth is observed.

3.3.2 pH 6.5

At pH 6.5, optimal aluminum hydroxide precipitation conditions, growth is observed for all alum doses. Figure 3.3.2-1 shows evolution of size distributions over time for alum dosing at pH 6.5. Increased growth is observed for 30mg/l alum and 80mg/l alum with modal diameters at the end of the process reaching above 200μm and above 150mm, respectively, with the

spread reaching the upper detection limit of the instrument. For 160mg/l the growth is less pronounced as final modal diameters are smaller than those achieved with the lower alum concentrations. As in EF, an induction period is observed, in which precursor particles are formed, over the initial 3 minutes, although for 30mg/l this is significantly shorter, as within this period sizes as large as 100μm are already observed.

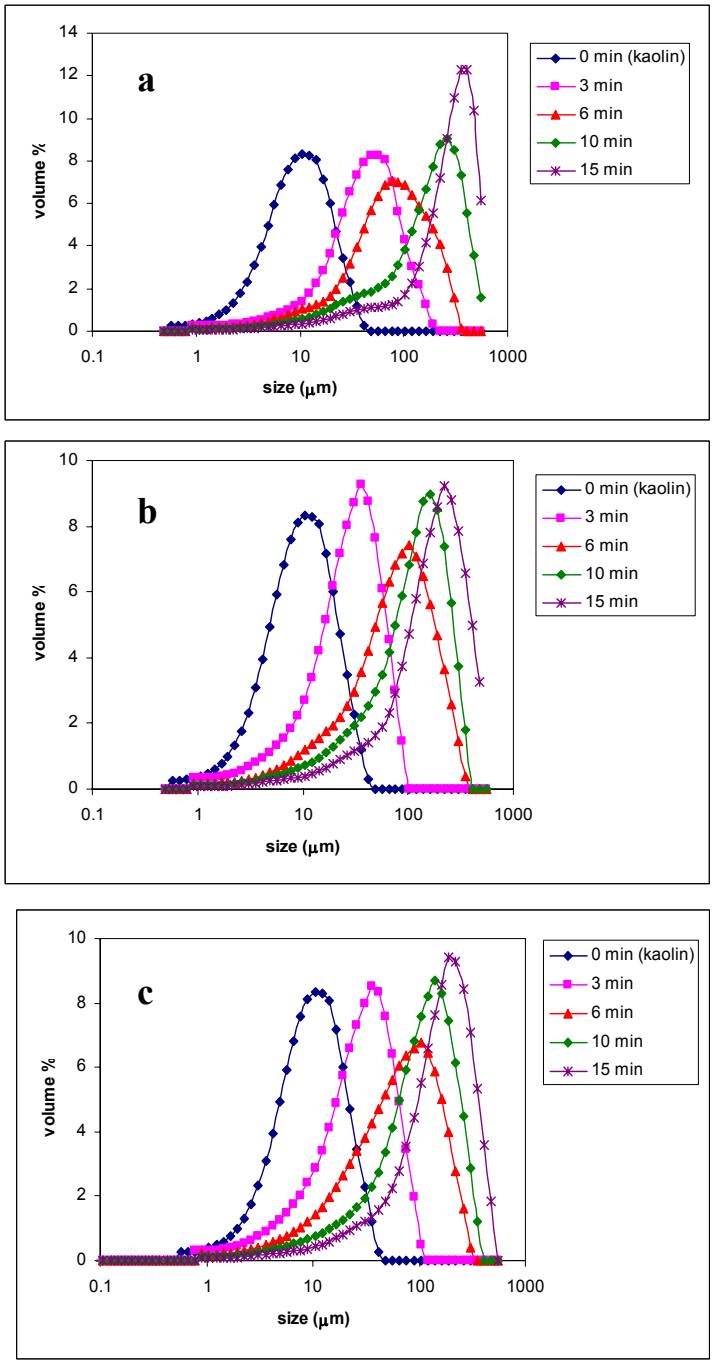

Figure 3.3.2-1 C_{kaolin}=60mg/l **a.** 30mg/l alum, pH 6.5 **b.** 80mg/l alum, pH 6.5 **c.** 160mg/l, pH 6.5

All the size distribution exhibit wide spreads, as like EF, the dosing is additive, resulting in simultaneous aluminum hydroxide precursor particle formation and flocculation into larger floc. However, higher growth rates are observed for EF. The unique conditions EF creates lowers the mass generation limitation due to continuous hydroxyl ion formation with pushes the equilibrium, according to Le Chatelier's principle, towards enhanced aluminum hydroxide precipitation for all currents applied. The changes in pH are distinctly different between the two processes with pH increase observed in EF, as opposed to pH decrease in CF (fig. 3.3.2-2).

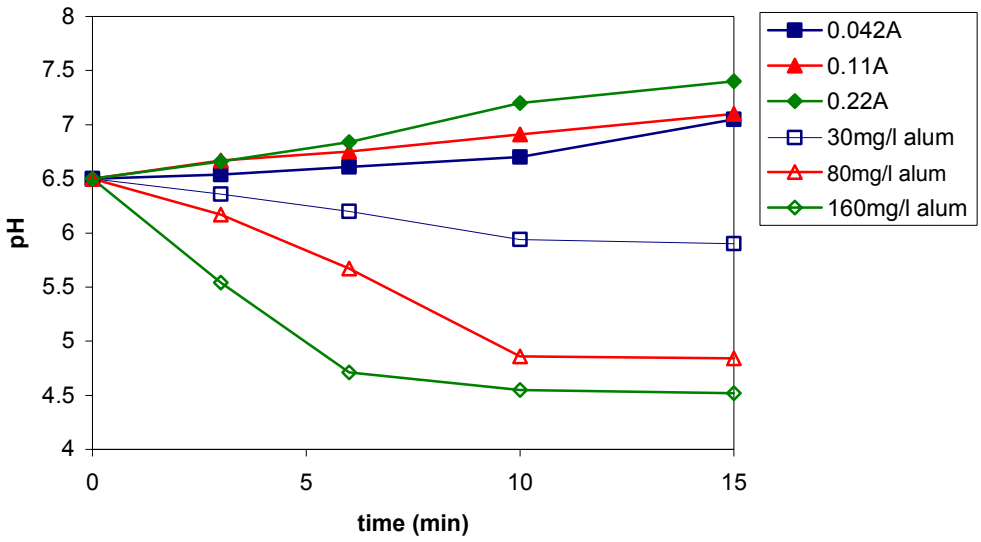

Figure 3.3.2-2 Changes in pH over time in EF and CF, C_{kaolin}=60mg/l, for various alum or aluminum doses.

The pH for 80mg/l and 160mg/l alum rapidly decreases at 6 minutes dosing, reaching pH values below 5, by the end of the process. Dosing with 30mg/l alum, however, decreases the pH marginally, which stabilizes at 6 during the final stages of the process. 30mg/l alum generates a larger number of precursor particles, as all stages of the process are within sweep floc regime, hence the increased growth rate and larger final sizes. For the other doses, transition out of sweep floc regime towards positive mononuclear speciation is pronounced,

which limits the amount of mass generated throughout the process which in turn limits floc growth. The growth exhibited with these doses stems from the initial stages, where aluminum hydroxide precipitation is optimal.

As specified previously, the growth of particles into larger flocs is not only dependent on particle precursor numbers, but also on their ability to form stable bonds. As such, surface charge impacts floc evolution. Figure 3.3.2-3 shows the differences in ζ potential between EF and CF at pH 6.5.

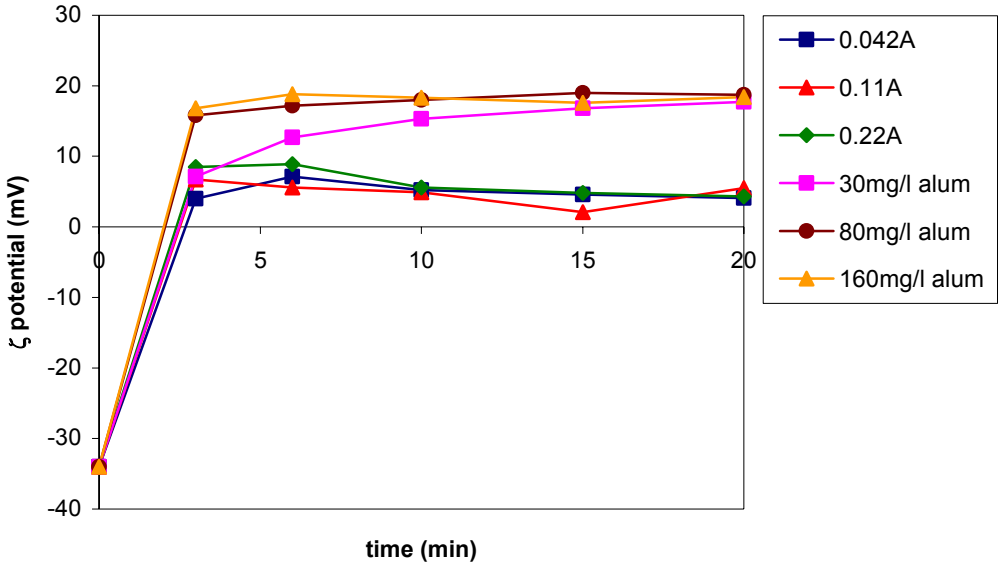

Figure 3.3.2-3 ζ potentials of suspensions over time, C_{kaolin}=60mg/l, for EF and CF, initial pH 6.5

The graph shows that for EF the ζ potential is less positive, therefore electrostatic repulsive forces are decreased - hence the enhanced growth rates compared to alum dosing. Although both processes commence from identical pH value, within optimal precipitation conditions, the ζ potentials are different, due to the differences in solution chemistry, primarily the pH.

EF generates hydroxyl ions thus reducing the positive ζ potential of the precursor particles towards an i.e.p, and reducing electrostatic repulsive forces between precursor particles. CF,

on the other hand, removes hydroxyl ions from solution, thus maintaining stronger repulsive forces between precursor particles manifested in a more positive ζ potential in solution. Unlike CF, EF creates conditions in which both mass generation limitations and surface charge limitations are reduced, which can explain enhanced growth profiles compared to the conventional process. Figure 3.3.2-4 shows the growth stages of flocs for initial pH 6.5, for EF and CF.

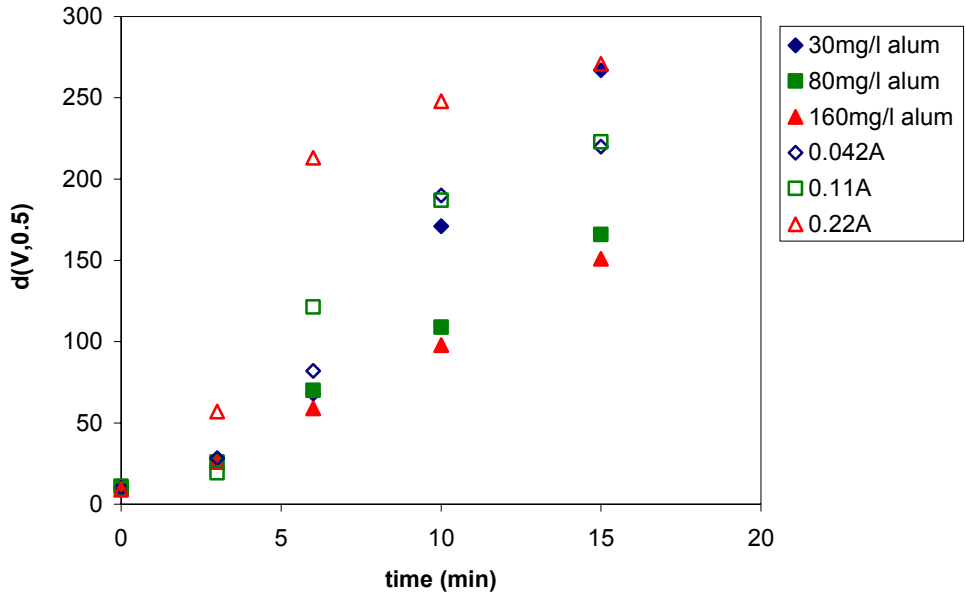

Figure 3.3.2-4 Evolution of volume mean diameter for various currents and alum doses, initial pH 6.5.

The graph shows that the growth rate of flocs formed in EF, for all applied currents, is faster than that using CF. For 30mg/l alum the final sizes are similar to those attained for 0.22A, but the path is different. While for 0.22A fragmentation is observed at 6 minutes, for 30mg/l this begins at 15 minutes, indicating a lower flocculation frequency and smaller growth profile. For 80mg/l and 160mg/l alum the growth patterns are devoid of sigmoidal behavior, as the sizes attained are not large enough to undergo fragmentation. As opposed to EF, there is no correlation between dose and growth factor in CF, as floc evolution depends on a delicate balance between optimal precipitation conditions and surface properties (i.e. electrostatic

repulsion forces). Because the former limitation is reduced in EF, floc formation is observed over a wider range of pH values and aluminum doses compared to CF in which floc formation is restricted to a far narrower pH/dosing range.

3.3.2.1 Structural properties

Growth kinetics can impact structural properties. In EF fast growth profiles have shown to produce flocs prone to fragmentation as larger sizes are attained more quickly, and these are more susceptible to shear forces and can undergo compaction and restructuring. In CF, the growth profiles of flocs formed with higher alum doses do not exhibit a diminished flocculation rate indicating a dominant fragmentation stage. However, for 30mg/l alum, this stage is observed after 15 minutes. At this lower dosage the flocs do exhibit final sizes equivalent to those measured for 0.22A, although the growth path indicates a slower growth rate. Slower growth rates, and reduced exposure to hydrodynamic forces should affect the structural properties of the flocs.

Scattering plots were used to obtain the structural data. Figure 3.3.2.1-1 shows typical scattering plots of flocs formed with alum dosing at different time intervals.

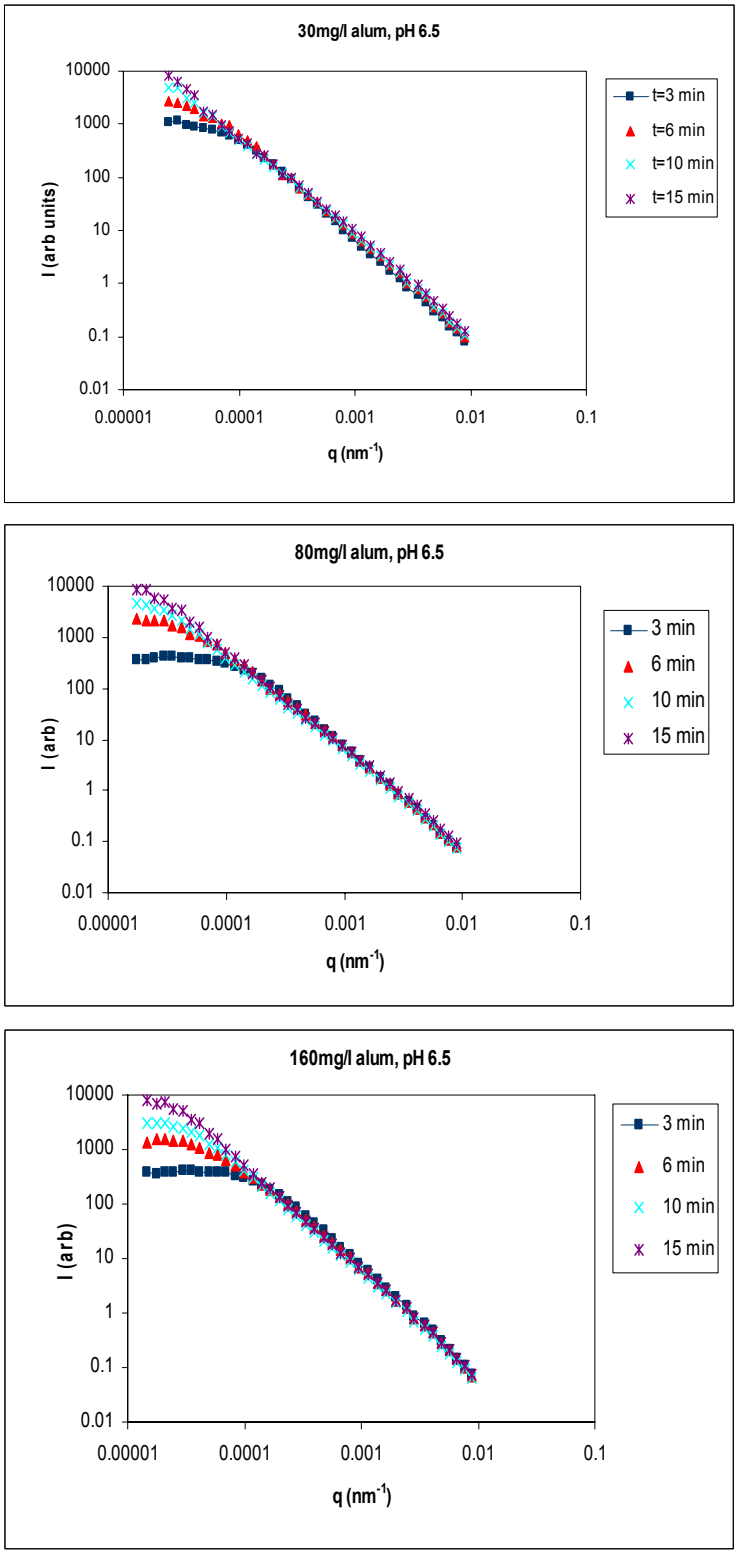

Figure 3.3.2.1-1 Conventional static light scattering plots (log(I) vs. log (q)) for flocs forming as a function of time for alum dosing.

The graph obtained for 30mg/l alum shows that transition into an angle independent scattering region at low q is hardly apparent for flocculation times above 3 minutes. A mild transition occurs within 3 minutes after which the graph exhibits a dependency on q, even in the low range. This is due to the large size of the flocs obtained for 30mg/l. The other graphs, for 80mg/l and 160mg/l alum, show a stronger transition into a q independent range for most times, although for 15 minutes flocculation this is less apparent due to the larger sizes obtained at this time. For all the graphs, one decade of linearity is observed for: $1.4*10^{-4}<q<1.6*10^{-3}$. This region will be used to calculate the SE, from the slope of the scattering plots.

Time (min)	SE		
	30mg/l alum	80 mg/l alum	160 mg/l alum
3	1.99±0.03	1.87±0.02	1.81±0.03
6	1.91±0.02	1.89±0.01	1.84±0.01
10	1.83±0.01	1.82±0.01	1.84±0.01
15	1.78±0.02	1.84±0.01	1.86±0.01

Table 3.3.2.1-1 Scattering exponents obtained for various alum doses at pH 6.5

The results show that the flocs are less prone to compaction. The SE for the higher doses changes marginally throughout the process, maintaining generally a stable value. For these doses floc growth has been shown to be limited, and no substantial difference between values is observed over time. For 30mg/l alum, the SE decreases with time, indicating growth into a more porous structure. In this case, both precipitation conditions and surface forces enabled growth into larger floc exhibiting a stability which was not observed for equivalent sized flocs obtained in EF. Images of types of flocs formed by alum dosing are shown in figure 3.3.2.1-2. The lower dose formed flocs which appear well defined with clear structures evolving, whereas the flocs obtained at higher doses appear "fluffy", exhibiting a transparency which is

not observed at the lower dose. As discussed previously, in EF the flocs undergo compaction and restructuring which is indicative of their fragile nature. Moreover, their enhanced growth rates render them susceptible to hydrodynamic shear forces for longer periods of time, as larger sizes are attained more rapidly. A comparison of SE values obtained in CF to the values obtained in EF (Table 3.2.3-1) demonstrates that structural evolution of the flocs obtained in CF is different. For adequate flocculation conditions (i.e. sufficient growth) in CF, flocs evolve from a more compact structure into a more porous structure, whereas in EF evolution is generally from a less compact structure into a more compact one, although fluctuations have also been observed. This behavior sheds some light on the flocculation mechanisms occurring in EF as opposed to CF. In EF electrostatic repulsive forces are weaker, resulting in a higher flocculation efficiency and more successful collisions. The gaseous products formed in the process could also play a role in the adhesion of precursor particles together, acting as additional "glue". The combination of these would enable a diffusion limited type of reaction, resulting in a fragile floc, exhibiting porosity in early stages

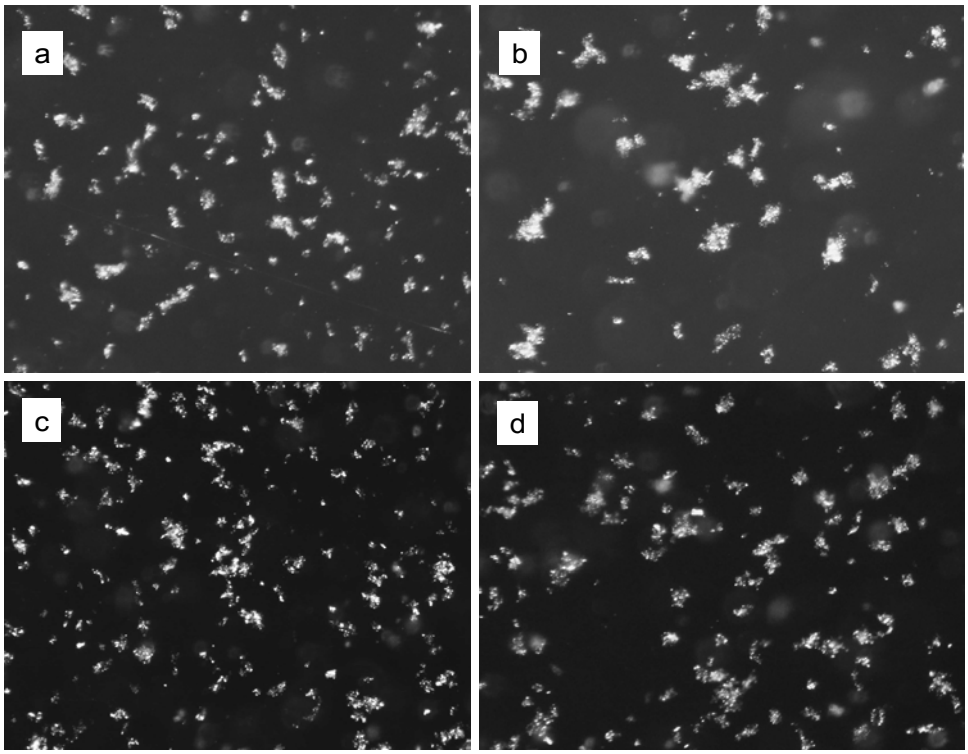

Figure 3.3.2.1-2 Floc structures obtained at pH 6.5 for **a.** 30mg/l alum, t=6min, **b.** 30mg/l alum, t=10 min **c.** 80mg/l alum, t=6min **d.** 80mg/l alum, t=10min.

of growth, but more easily disrupted by shear forces, thus undergoing restructuring and compaction. In CF electrostatic repulsive forces are stronger, resulting in a reaction limited type of reaction which exhibits slower growth rates (lower flocculation efficiency) and produces flocs which are more compact in the early stages of growth. These are able to develop into more porous structures, because they are less affected by shear forces, due to their relatively tighter structure compared to the very loose structure obtained in EF. However, the final structure will be limited to shear forces within the system.

3.4 EF as pretreatment to colloidal ultrafiltration

3.4.1 Characteristics of the kaolin suspension undergoing ultrafiltration

As discussed previously, the current applied in the EF process has a double effect, by both generating the coagulant species and by causing hydrolysis in which excess hydroxyl ions are formed at the cathode, resulting in an increase in pH. This impacts the ζ potential which serves as an indicator for coagulation efficiency. Figure 3.4.1-1 shows the change in pH and ζ potential as a function of applied current for a 15mg/l kaolin suspension at different initial pH values. The ζ potential of the kaolin suspensions, without applying any current:

-17.9mV, -21.7mV and -23.7mV for pH 5, 6.5 and 8 respectively.

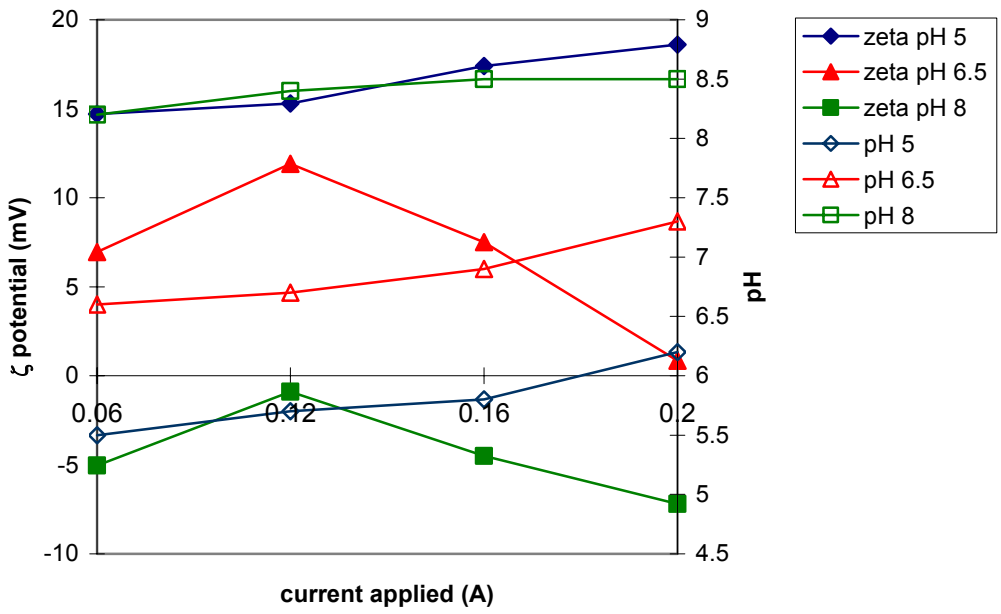

Figure 3.4.1-1 Change in pH and ζ potential vs. applied current for pH 5, 6.5 and 8. C_{kaolin}=15mg/l, t=7min.

3.4.2 Membrane ultrafiltration

The permeate flux was measured for suspensions, that had undergone electroflocculation using aluminum as the anode material. The aluminum doses were controlled by the applied current, which was kept constant during each run. The results show that pre-EF enhances the

permeate flux at pH 5 and 6.5, but only marginal enhancement is observed at pH 8. When treating relatively dilute suspensions, the concentration layer, if formed, contributes negligible resistance to the actual cake resistance (Waite, 1999), thus the assumption is that the primary fouling factor is cake formation. However, all flux curves show a degree of pore blocking for all pH values. The residual aluminum in permeate was also measured. These are shown in figure 3.4.2-1.

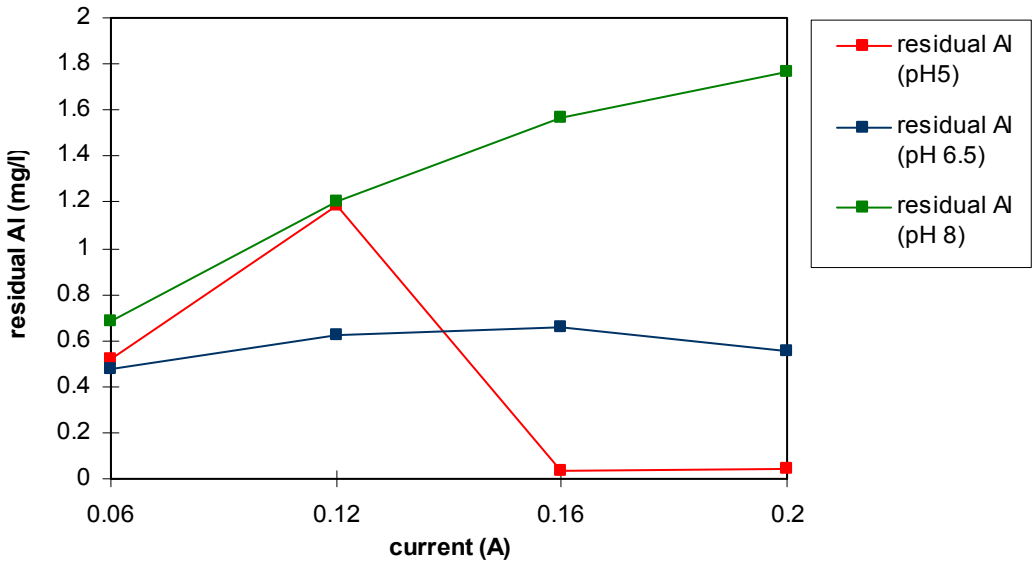

Figure 3.4.2-1 Residual aluminum concentration in permeate for various pH values and currents.

3.4.2.1 pH 5

At initial pH 5 filtration of kaolin causes significant flux decline, and by the end of the run it has reached 40% of the initial flux (fig. 3.4.2.1-1). Pre-EF of the suspension improves the filtration, and at all currents flux enhancement is observed. At 0.06A the maximum flux enhancement occurs, by which the flux has improved by 15%, reaching a critical flux at 55% of the initial flux. At 0.12A, 0.16A and 0.2A similar behavior is observed, by which the permeate flux reaches critical flux at 60% of the initial flux. The difference in membrane behavior obtained after EF at 0.06A relatively to the other applied currents can be explained

by the transition to a different coagulation mechanism, which occurs at higher doses of aluminum.

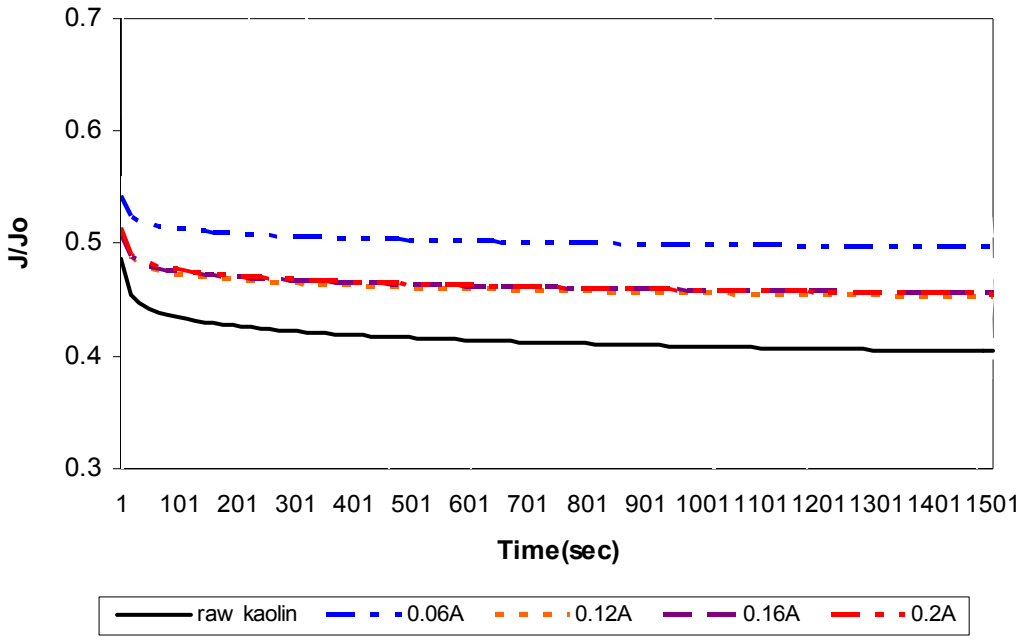

Figure 3.4.2.1-1 Permeate flux (J) as a fraction of initial flux (Jo) over the course of ultrafiltration of an electroflocculated kaolin suspension, C_{kaolin}=15mg/l, initial pH 5, at various applied currents.

At pH 5 the governing aluminum species in solution are Al^{+3} and $Al(OH)^{2+}$, and therefore it can be assumed that at this initial pH the dominant coagulation mechanism is adsorption and charge neutralization, although some aluminum hydroxide does precipitate in these conditions. In this case it appears that at the minimum applied current, 0.06A, adsorption and charge neutralization is the dominant coagulation mechanism, thus producing aggregates that form a more stable cake on the membrane surface, which has a higher porosity than the dense, compact cake formed by filtration of kaolin (fig. 3.4.2.4-1a). At the higher currents, 0.12A, 0.16A and 0.2A we observe improved membrane behavior due to increased formation of aluminum hydroxide in solution, which catches the smaller particles (by "sweep floc" mechanism) thereby enhancing the permeate flux. However, the decline in flux relative to the flux obtained at 0.06A, is due to increased cake formation of gelatinous aluminum hydroxide

on the membrane surface. From SEM analysis, aluminum hydroxide seems to form a "blanket" on the membrane surface, and exhibits different characteristics than the cake formed from filtration of raw kaolin, which appears to be very dense and tightly packed (fig. 3.4.2.4-1). In addition, aluminum hydroxide flocs, unlike kaolin particles (which have an average size of 1μm), are large enough to be sheared from the membrane surface (Weisner et al., 1989). Particle size distribution measurements of the electroflocculated suspension show an increase in particle counts for particles between 5μm-10μm for the higher applied currents. Since permeability of the filter cake and back transport by hydrodynamic forces both increases with increasing particle size (Fu and Dempsey, 1998), this can also explain the flux enhancement. This, however, may not be the sole factor that causes this difference between the two types of suspensions – density and morphology may also play an important role here. Previous results have shown that at pH 5, for all currents EF produces flocs with a similar porosity (exhibited by lower scattering exponent or fractal dimension), although very fragile and undergo compaction. In light of this, increase in membrane performance can be connected not only to floc size, but also to floc stability and structure, which impacts the porosity of the cake formed on the membrane surface.

The residual aluminum measured in the permeate at the higher currents was 0.030mg/l and 0.039mg/l (for 0.16A and 0.2A respectively) (fig. 3.4.2-1), indicating optimal coagulation-flocculation, in which nearly all the aluminum (~98%) was removed from solution, caught on the membrane surface as an aluminum hydroxide mesh. At 0.06A the coagulation mechanisms are in transition due to the formation of a variety of aluminum hydrolysis species. The final pH was 5.5 (fig. 3.4.1-1) and the residual aluminum measured was 0.5 mg/l (fig. 3.4.2-1), which indicates that a large fraction (~21%) of the aluminum was not precipitated as aluminum hydroxide, but was present as soluble species (Al^{+3} and $Al(OH)^{+2}$). Moreover the positive ζ potential of the suspension indicates a transition through charge neutralization for all the currents, so we can assume the major factor causing the differences between the lower current and higher currents is a balance between the quantity of aluminum

hydroxide present, the presence of colloidal aluminum hydroxide which has not sufficiently flocculated and could cause a degree of pore blocking, and the structural stability of the flocs.

3.4.2.2 pH 6.5

At initial pH 6.5 filtration of kaolin causes significant flux decline, and by the end of the run it has reached 40% of the initial flux (fig. 3.4.2.2-1). Pre-EF of the suspension improves the flux, and for applied currents of 0.12A, 0.16A and 0.2A identical flux behavior is observed, by which the permeate flux reaches critical flux at above 60% of the initial flux. For an applied current of 0.06A there is a 5% drop in the flux compared to the other currents, and the permeate flux reaches critical flux at 55% of the initial flux. At pH 6.5 the dominant coagulation mechanism is sweep floc, due to increased formation of amorphous aluminum hydroxide, although at the higher currents the pH increases significantly (fig. 3.4.1-1) and speciation shifts towards $Al(OH)_4^-$ which decreases coagulation efficiency - indicated by the less positive ζ potential. This does not seem to affect the membrane behavior within the dosages used at this pH, because a wide range of currents produced the same results. Therefore, the improved membrane behavior observed here was due to the formation of aluminum hydroxide flocs in solution, which catch smaller particles and form a more permeable cake on the membrane surface. Moreover, aluminum hydroxide flocs are large enough to be sheared from the membrane surface and therefore the cake thickness is stable, resulting in a stable flux. Particle size counts performed between 5μm-20μm indicate that at 0.06A sizes obtained are on average smaller than those formed at other currents, therefore the cake is less porous and a minor difference in membrane behavior is observed. Particle size distribution measurements show that for 0.12A, 0.16A, and 0.2A the counts between 5μm-20μm are nearly identical, which can explain the similar flux obtained at these currents. Moreover, floc structure analysis at higher currents at pH 6.5 has shown that more porous flocs are obtained than at lower currents, which would result in a more porous cake and lower fouling degree.

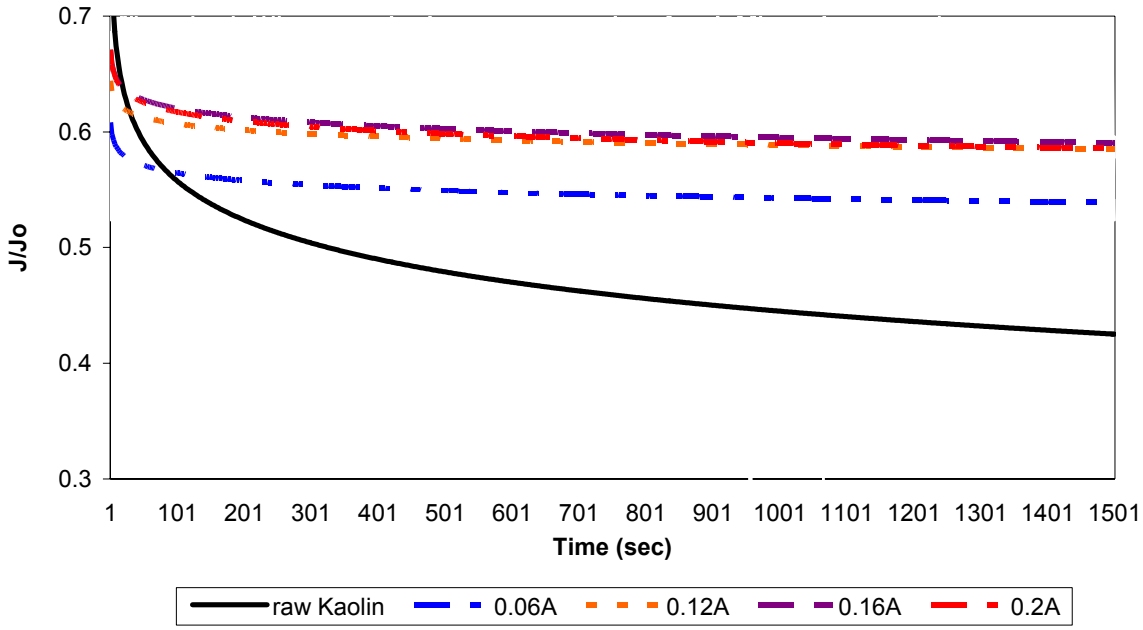

Figure 3.4.2.2-1 Permeate flux (J) as a fraction of initial flux (Jo) over the course of ultrafiltration of an electroflocculated kaolin suspension, C_{kaolin}=15mg/l, initial pH 6.5, at various applied currents.

3.4.2.3 pH 8

At initial pH 8 filtration of kaolin causes significant flux decline, and by the end of the run it has reached 50% of the initial flux (fig. 3.4.2.3-1).

Pre-EF does not improve the flux significantly, and for all currents similar flux behavior is observed, by which the permeate flux reaches steady state at 55% of the initial flux (only a 5% improvement relative to the flux obtained when filtering the raw kaolin). At pH 8 the ζ potential of kaolin is more negative, compared to that at pH 5 and 6.5, therefore the particles are more readily rejected from the membrane (which is hydrophilic and charged negatively), which can explain a slight increase in the initial flux relative to the flux at pH 5 and 6.5. At pH 8 the dominant species is $Al(OH)_4^-$, and therefore no real improvement is observed because coagulation conditions are not optimal. Some aluminum hydroxide precipitates, which is visible, and forms a cake on the membrane surface, but still primary kaolin particles

are present in large quantities in solution, because no efficient coagulation occurs. Colloidal aluminum hydroxide could also be present as flocculation conditions are not sufficient. These particles can enter the cake pores and thus reduce the flux, by pore blocking mechanism. The minor improvement in membrane behavior observed here was due to some formation of

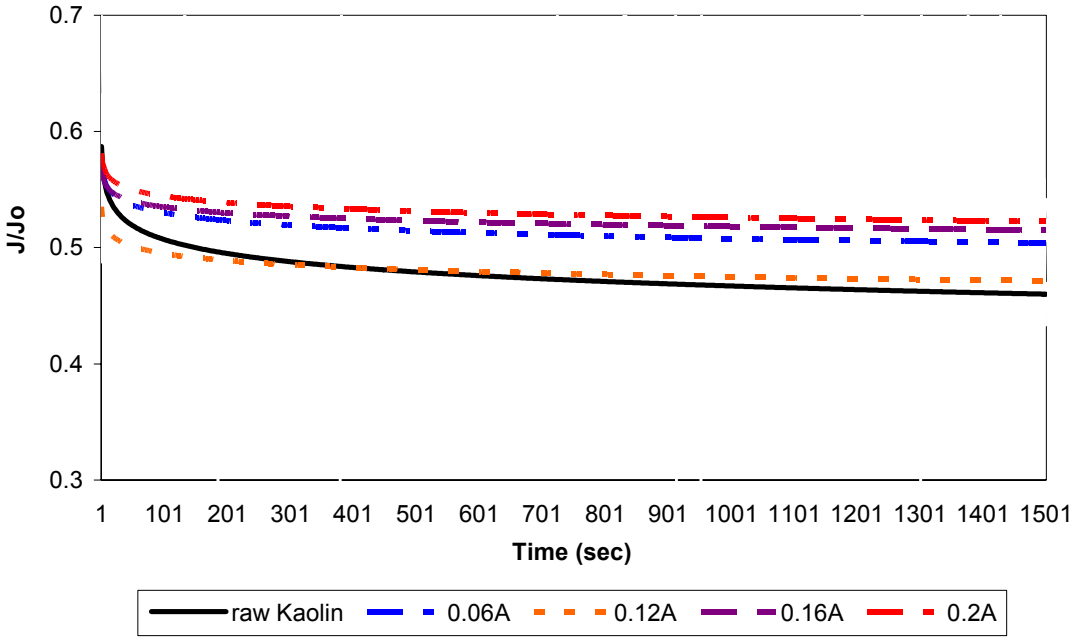

Figure 3.4.2.3-1 Permeate flux (J) as a fraction of initial flux (Jo) over the course of ultrafiltration of an electroflocculated kaolin suspension, C_{kaolin}=15mg/l, initial pH 8, at various applied currents.

aluminum hydroxide flocs in solution, which catch a fraction of the smaller particles. The permeate aluminum measurements indicate a large quantity of soluble aluminum which increases with applied current (0.68 mg/l (~28%) and 1.76 mg/l (~22%) for 0.06A and 0.2A respectively), thus corroborating the shift in speciation towards soluble aluminum mononuclear species $(Al(OH)_4^-$ at pH 8).

Particle size distribution measurements show nearly identical counts for all currents, between 5μm-20μm, which can explain the similar flux obtained at these currents. However, particle distribution measurements show much lower counts than those at pH 5 and 6.5, which indicates that less colloidal particles are present. At pH 5 and 6.5 more aluminum hydroxide

precipitates as colloidal matter, contributing to the particle counts. At pH 8 the aluminum solubility equilibrium has shifted towards the negative soluble species ($Al(OH)_4^-$), less aluminum hydroxide precipitates resulting in lower particle counts.

3.4.2.4 Cake characteristics

Figure 3.4.2.4-1 shows the visible differences in cakes formed on the membrane surface from filtration of a kaolin suspension and a pre-electroflocculated kaolin suspension.

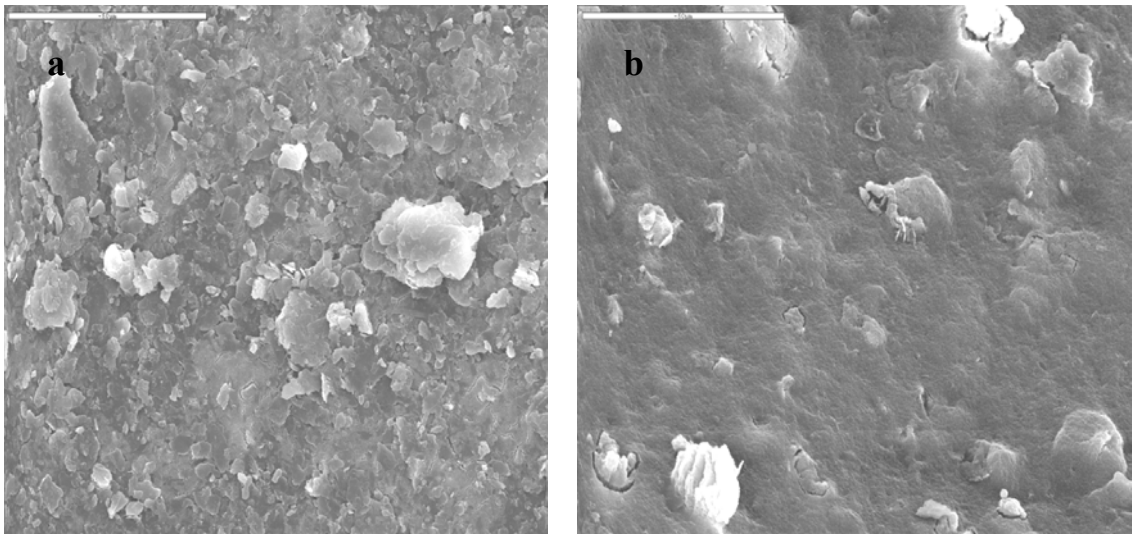

Figure 3.4.2.4-1 Cake on membrane after filtration **a.** after raw kaolin suspension **b.** after pre-electroflocculated kaolin suspension.

Filtration of the raw kaolin suspension produced a cake which exhibits a dense and compact form with the kaolin plates tightly packed together. The cake image obtained after filtration of a pretreated kaolin suspension shows a "loose" type of cake, lightly rested on the membrane surface.

Chapter 4 - General Discussion

This study has identified key mechanisms dictating the coagulation/flocculation behavior in EF, and related these to operational parameters such as applied current and reaction time. These parameters dictate first and foremost the amount of coagulant generated within the system, in this case the aluminum ion Al^{+3}. However, the applied current has an additional effect as it also causes the pH to rise, due to hydroxyl ion at the cathode, a product of the hydrolysis which occurs simultaneously. As such, unlike conventional coagulation, the final pH will always be higher than the initial pH. The continuous rise in pH, as more hydroxyl is produced, results in the shifting of coagulation mechanisms throughout the process, until the current is stopped, allowing the pH to stabilize and the species to reach equilibrium. This is evident by the changes in ζ potential as a function of current, which is directly linked to the surface charge of the particles and is indicative of the coagulant species in solution. The degree of pH change, however, can be controlled by adequate mixing conditions. Hence, the application of velocity gradient in EF is not only important to ensure aluminum hydroxide precipitation and floc formation, but also to control the pH increase which, without application of a sufficient mixing regime, can rise to values, depending on type of water being treated, which are detrimental to the process. Velocity gradients used in lab and full scale flocculation systems (10-30sec^{-1}) were found to be sufficient to stabilize the pH.

An additional mixing mechanism has been identified, which is induced by the passage of current through the system. When lowering the diffusion barrier between primary particles, without applying mixing conditions, aggregation of primary particle was observed when currents were applied. The extent of aggregation in these conditions is indicative of another transport mechanism other than Brownian diffusion. This transport could be induced by the electrical field formed by application of a current, and/or by bubble formation within the system.

When considering EF as an alternative to CF, the differences between the processes should be understood. These differences, small as they may be, are manifested in the chemical and physical characteristics of the treated suspension and resulting aggregates or flocs. Moreover, the kinetics of floc growth and the floc formation range are of utmost importance, as particle removal in water treatment relies primarily on precipitation of metal hydroxide and formation of a stable sweep floc regime. In EF the sweep floc regime is wider than in CF, due to the hydroxyl formation which pushes the equilibrium, according to Le Chatelier's principle, towards enhanced aluminum hydroxide precipitation. Based on the results, figures 4-1 and 4-2 demonstrate the differences of the sweep floc ranges in CF and EF, respectively.

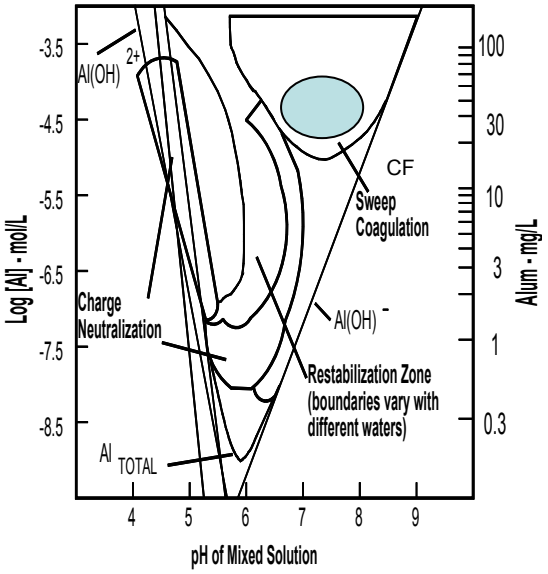

Figure 4-1 Sweep floc zone in CF

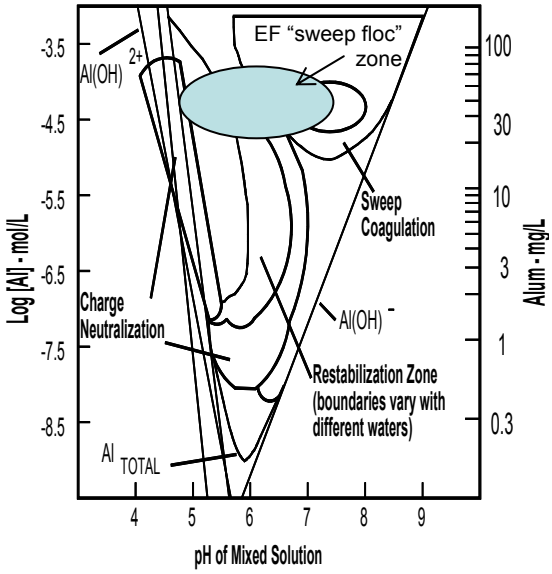

Figure 4-2 Sweep floc zone in EF

EF can be considered advantageous over CF as it is able to produce flocs over a wider range of doses and pH values. Thus overdosing effects in EF are less pronounced than in CF. This versatility produces a range of floc "types", depending on conditions of operation and has clear implications to many processes of importance in water and wastewater treatment as flocs can be "tailored" for specific processes, depending on requirements. The structural properties of these flocs and growth rates are dependent on specific operating parameters, primarily the initial pH and current applied.

Growth patterns of flocs formed in EF exhibited for *all* currents applied, for initial pH values of 5 and 6.5, sigmoidal growth behavior, including three typical stages: induction, exponential growth and fragmentation, as found in CF only within optimal dose limits. For adequate precipitation conditions, EF forms generally larger floc sizes than CF, for equivalent doses of aluminum. This, however, would depend on operating conditions, as low alum dosing in these conditions was found to produce equivalent floc size, although at a decreased growth rate. Floc growth in EF has been found to be quicker than in CF and shows a dependency of growth rate on current (dose), with higher growth rates obtained at higher currents. This dependency depends on the initial pH, and a higher dependency exists for enhanced precipitation zones (pH 6.5). This is derived from the stronger linkage between particles within this zone, coupled with increased mass and microbubble generation for higher currents – resulting in larger collision frequencies and collision efficiencies which in turn result in an enhanced growth rate.

Differences in structural evolution patterns between the two processes have also been identified – for adequate flocculation conditions (i.e sufficient growth) in CF, flocs evolve from a more compact structure into a more porous one. In EF, however, the evolution is generally from a less compact structure into a more compact one, although fluctuations have also been observed. EF produces more fragile flocs, which are more susceptible to shear forces, and undergo compaction and in some cases structural fluctuations. It seems that the flocculation mechanism in EF is of a diffusion limited type, with flocs forming at higher growth rates, compared to CF, exhibiting a higher collision frequency and collision efficiency. This behavior is especially evident at pH 6.5, where electrostatic repulsive forces are weaker. CF, on the other hand, exhibits a flocculation mechanism of a reaction limited nature, resulting in flocs which are more compact in the early stages of growth but are able to develop into more porous structures because they are less affected by shear forces.

EF produces flocs which *initially* are more porous than those formed in CF. By comparing the fractal dimension of resulting flocs, over a limited mixing period, to reported values in the literature regarding flocs formed in CF using alum, we find that flocs formed in EF generally

fall within the low range of values, indicating a more porous structure. *Without* taking into account restructuring effects, which occur at fragmentation stages when floc size is large enough to be affected by shear forces, a correlation was found between fractal dimension and aggregate size – lower fractal dimensions were obtained for larger aggregate sizes. This is consistent with flocculation models which have been developed based on conventional coagulation (Diffusion Limited Model and its variants). However, in real water systems, primary particles are not necessarily solid exhibiting fractal dimensions of Euclidean values (i.e.D_2=2) and in orthokinetic flocculation shear forces must be acknowledged, as these can cause fragmentation and restructuring. Thus, the final structures will depend on the shear forces within the system, and on the fragility of the flocs.

Although in EF current density can affect the aluminum dissolution rate, in this study floc growth was found to be independent of current density, and dependent on absolute current intensity.

Current application time was found to affect growth, and for longer dosing periods, larger flocs were obtained. As coagulant efficiency is dependent on the time of reaction in solution, this can be explained by conventional coagulation theory.

With regard to EF as a potential pretreatment to ultrafiltration – this study has proven the efficiency of the process on a practical level. EF can serve as an efficient pretreatment, with enhanced flux observed at pH 6.5 for higher currents, where sweep floc dominates and more porous floc structures are obtained. Although the major fouling factor is cake formation, the flux curves show indication of a degree of pore blocking for all pH values. This can be due to aluminum hydroxide colloidal particles which have not efficiently undergone flocculation, and/or kaolin primary particles still "free" in solution. The differences in critical flux can be attributed to cake properties, such as thickness and porosity, which are a function of the quantity of precipitate in solution and floc structure, respectively. At pH 5 and 8, the flux obtained from pre-electroflocculated suspensions was lower than that obtained at pH 6.5. At pH 5 and 8, less aluminum hydroxide precipitates and more primary kaolin particles are still present in suspension (not captured in the flocs forming), but also colloidal aluminum

hydroxide which has not sufficiently flocculated. These can enter the cake pores and cause "self contamination", resulting in increased flux decline. Moreover, for pH 6.5, particle counts indicate that larger flocs are present which can be readily sheared from the membrane surface resulting in a "thinner" cake, which can also explain flux enhancement, compared to other pH values.

These results demonstrate the potential of EF in general as an alternative to conventional flocculation and more specifically as a pretreatment to membrane ultrafiltration. This thesis provides the conceptual development and experimental justification which shed light on the mechanisms of the process. Thus, EF is a reliable and versatile technology that has considerable potential for water treatment and reuse.

4.1 Conclusions

EF, although an acknowledged technology, has never been researched at a level aimed at unraveling its underlying mechanisms. Research has focused on efficiency and performance, rather than on the fundamental basics which is the core of understanding the mechanisms and ultimately will lead to better system design and process control. This thesis has begun the process of elucidating the mechanisms of EF and evolving the technology from an empirical one to a firmly rooted scientific one, which has a promising future in water and wastewater treatment. The major conclusions of this research are summarized below:

- EF cannot be considered an "equivalent" process to CF. The hydrolysis which occurs simultaneously in EF has a major impact on the coagulation mechanisms which are in continuous transition while a current is applied and on resulting flocculation mechanisms as these are a function of aluminum hydroxide precipitation and surface repulsion forces.

- The final pH in EF will always be higher than the initial pH, thus differing from CF in which a decrease in pH occurs. The magnitude of pH rise can be controlled with sufficient mixing conditions.
- The applied current in EF affects particle transport, by the electrical field induced and/or by bubble formation within the system.
- EF is a versatile process exhibiting a wider sweep floc regime than CF, and is able to produce a wider range of floc "types" depending on conditions of operation.
- The flocculation rate in EF is generally higher than in CF. Growth rate is dependent on absolute current rather than current density, with higher growth rates obtained for higher currents. This dependency is increased in optimal aluminum hydroxide precipitation conditions.
- The floc structures formed in EF are initially more porous and fragile than those formed in CF. They are more susceptible to shear stress, and therefore more prone to compaction and restructuring.
- For optimal sweep floc conditions, the flocculation mechanism in EF is of a diffusion limited type while in CF it is more of a reaction limited nature.
- EF can serve as en efficient pretreatment to membrane ultrafiltration of colloidal particles. Differences in critical flux can be attributed to cake properties, such as thickness and porosity, but also to amount of colloidal aluminum hydroxide present that can cause a degree of pore blocking. Aluminum hydroxide precipitation conditions and surface charge of the evolving flocs dictate floc growth and structure – which vary according to initial pH and current applied. Best performance was observed for pH 6.5 for higher currents, where the balance between aluminum hydroxide precipitation and particle surface charge is optimal. These enable a diffusion limited type of reaction and growth into more porous structure (lower SE) resulting in a less compact cake.

4.2 Recommendations for further research

To improve the understanding of EF further refinement and development is required. This should be aimed primarily at a theoretical level, although practical implications should not be overlooked.

Parameters should be examined using a more advanced cell configuration. To develop more sophisticated reactor designs a greater understanding of the contact patterns is required.

Contaminant removal mechanisms should be examined. The chemistry behind removal of various contaminants should be explored using advanced chemical analysis such as XRD and SEM-EDAX. The flocs forming in EF could possess characteristics which differ from those formed in CF, such as chemistry (formation of AlO(OH)), which would affect the interaction with contaminants. In addition floc porosity could affect adsorption behavior.

Modeling of the process incorporating chemical and physical parameters will enable quantification and optimal operating conditions can be established.

The disinfection abilities of EF should be examined. Electrodes which are able produce disinfectant species such as free radicals can be incorporated into the reactor design, and current utilized for additional disinfection purposes.

To really advance EF on a practical level, a scale-up of bench-scale apparatus should be performed, and the practical (contaminant removal) and economic benefits (power consumption versus efficiency) of the process examined.

References

1. Abdessemed, D., Adin, A., Ben-Aim, R. (1998) Coupling flocculation with micro-ultrafiltration for wastewater treatment and reuse. Desalination **118**, 323.

2. Abuzaid, N.S., Bukhari, A.A., Al-Hamouz, Z.M. (1998) Removal of bentonite causing turbidity by electrocoagulation. Journal of Environmental Science and Health A **33** (7), 1341-1358.

3. Adin, A. and Vescan, N. (2002) Electroflocculation for particle destabilization and aggregation for municipal water and wastewater treatment. Proceedings of the American Chemistry Society **42** (2), 537-541.

4. Adler, P.M. (1981) Heterocoagulation in shear flow. Journal of Colloid Interface Science **83**, 106-115.

5. Alexandrova, L., Nedialkova, T., Nishkov, I. (1994) Electroflotation of metal ions in waste water. International Journal of Mineral Processing **41**, 285-294.

6. Altman, J. and Ripperberger, S. (1997) Particle deposition and layer formation at the crossflow microfiltration. Journal of Membrane Science **124** (1), 119-128.

7. Amirtharajah, A. and O'Melia, C.R. (1990) Coagulation Processes: destabilization, mixing and flocculation. Water Quality and Treatment, New-York, McGraw-Hill.

8. Argaman, Y. and Kaufman, W.J. (1970) Turbulence and flocculation. Journal of Sanitary Engineers Division Proceedings, American Society of Civil Engineers **96**, 223.

9. Balmer, L.M. and Foulds, A.W. (1986) Separating oil from oil-in-water emulsions by electroflocculation/electroflotation. Filtration and Separation **23** (11-12), 366-370.

10. Bard, A.J. and Faulkner, L.R. (2001) Electrochemical methods – fundamentals and applications. John Wiley and Sons, New-York.

11. Barkley, N.P., Farrel, C.W., Gardner-Clayson, T.W. (1993) Alternating current electrocoagulation for superfund site remediation. Air and Waste **43**, 784-789.

12. Belongia, B.M., Haworth, P.D., Baygents, J.C., Raghavan, S. (1999) Treatment of alumina and silica chemical mechanical polishing waste by electrodecantation and electrocoagulation. Journal of the Electrochemical Society **146** (11), 4124-4130.

13. Bottero, J.Y., Axelos, M., Tchoubar, D., Cases, J.M., Fripiat, J.J., Fiessinge, F. (1987) Mechanism of formation of aluminum trihydroxide from keggin Al13 polymers. Journal of Colloid and Interface Science **117** (1), 47-57.

14. Bourgeous, K.N., Darby, J.L., Tchobanoglous, G. (2001) Ultrafiltration of wastewater: effects of particles, mode of operation, and backwash effectiveness, Water Research **35** (1), 77-90.

15. Bowen, W.R., Doneva, T.A. (2000) Atomic force microscopy studies of membranes: effect of surface roughness on double-layer interactions and particle adhesion. Journal of Colloid and Interface Science **229**, 544-549.

16. Bowen, W.R., Jenner, F. (1995) Theoretical descriptions of membrane filtration of colloids and fine particles: An assessment and review. Advances in Colloid and Interface Science **56**, 141-200.

17. Bradley, S.M., Kydd, R.A., Howe, R.F. (1993) The structure of Al gels formed through base hydrolysis of Al^{+3} aqueous solutions. Journal of Colloid and Interface Science **159** (2), 405-412.

18. Brinkman, H.C. (1947) A calculation of the viscous forces extended by a flowing fluid on a dense swarm of particles. Applied Science Research A **1**, 27-34.

19. Bushell, G.C. and Amal, R. (1998) Fractal aggregates of polydisperse particles. Journal of Colloid and Interface Science **205**, 459-469.

20. Bushell, G.C., Yan, Y.D., Woodfield, D., Raper, J., Amal, R., (2002) On techniques for the measurement of the mass fractal dimension of aggregates. Advances in Colloid and Interface Science **95**, 1-50.

21. Camp, T.R., Stein, P.C. (1943) Velocity gradients and internal work in fluid motion. Journal of Boston Society of Civil Engineers **30**, 219-237.

22. Carmona, M., Khemis, M., Leclerc, J.-P., Lapicque, F. (2006) A simple model to predict the removal of oil suspensions from water using the electrocoagulation technique. Chemical Engineering Science **61**, 1237-1246.

23. Carroll, T., Gray, S.R., Bolto B.A., Booker N.A. (2000) The fouling of microfiltration membranes by NOM after coagulation treatment. Water Research **34** (11), 2861-2868.

24. Chakraborti, R.K., Gardner, K.H., Atkinson, J.F., Van Benschoten J.E (2003) Changes in fractal dimension during aggregation. Water Research **37**, 873-883.

25. Chen, G., Chen, X., Yue, P.L. (2000) Electrocoagulation and electroflotation of restaurant wastewater. Journal of Environmental Engineering **126** (9), 858-863.

26. Cheryan, M. (1998) Ultrafiltration and Microfiltration Handbook, Technomic Publishing, chapters 1-6.

27. Cho, J., Amy ,G., Pellegrino, J. (2000) Membrane filtration of natural organic matter: factors and mechanisms affecting rejection and flux decline with charged ultrafiltration (UF) membrane, Journal of Membrane Science **164**, 89-110.

28. Chowdhury, Z.K., Amy, G.L., Bales R.C. (1991) Coagulation of submicron colloids in water treatment by incorporation into aluminum hydroxide floc. Journal of Environmental Science and Technology **25**, 1766-1773.

29. Ciardelli, G. and Ranieri, N. (2001) The treatment and reuse of wastewater in the textile industry by means of ozonation and electroflocculation. Water Research **35** (2), 567-572.

30. Clark, M.M, Srivastava, R.M., David, R. (1993) Mixing and aluminum precipitation. Environmental Science and Technology **27** (10), 2181-2189.

31. Clark, M.M. and Flora, J.R.V. (1991) Floc restructuring in varied turbulent mixing. Journal of Colloid and Interface Science **147**, 407-421.

32. Clayfield, E.J. (1995) Electrocoagulation and separation of aqueous suspensions of ultrafine particles. Colloids and Surfaces A **104**, 101-109.

33. Clemens, O.A. (1981) Purifying oily wastewater by electrocoagulation. Plant Engineering (September) **17**, 124-125.

34. Cohen, R.D. and Probstein, R.F. (1986) Colloidal fouling of reverse osmosis membranes. Journal of Colloid and Interface Science **114** (1), 194-207.

35. Derjaguin, B.V. and Landau, L. (1941) Theory of the stability of strongly charged lyophobic sols and of the adhesion of strongly charged particles in solutions of electrolytes. Acta Physicochim. URSS **14**, 633-662.

36. Do, J.S. and Chen, M.L. (1994) Decolorization of dye-containing solutions by electrocoagulation. Journal of Applied Electrochemistry **24**, 785-790.

37. Dobolyi, E. (1978) Experiments aimed at the removal of phosphate by electrochemical methods. Water Research **12** (12), 1113-1116.

38. Drogui, P., Elmaleh, S., Rumean, M., Bernard, C., Rambaud, A. (2001) Hybrid process, microfiltration-electroperoxidation, for water treatment, Journal of Membrane Science **186**, 123-132.

39. Duan, J. and Gregory, J. (2003) Coagulation by hydrolyzing salts. Advances in Colloid and Interface Science **100-102**, 475-502.

40. Fair, G. M. and Gemmell, R. S. (1964) A mathematical model of coagulation, Journal of Colloid Science **19**, 360-372.

41. Flesch, J.C., Spicer, P.T., Pratsinis, S.E. (1999) Laminar and turbulent shear-induced flocculation of fractal aggregates. AIChE Journal **45** (5), 1114-1124.

42. Forrest, S.R. and Witten, T.A. (1979) Long-range correlations in smoke-particle aggregates. Journal of Physics A **12** (5), 109-117.

43. Foyn, E. (1963) Electrolytisk kloakkrensing i teknisk malestokk, Forsoksdriften pa Huk, Teknisk Ukeblad, 19.

44. Francois, R.J. (1988) Growth kinetics of hydroxide flocs. American Water Works Association **80**, 92-96.

45. Fu, L.F. and Dempsey, B.A. (1998) Modeling the effect of particle size and charge on the structure of the filter cake in ultrafiltration. Journal of Membrane Science **149**, 221-240.

46. Gorczyca, B. and Ganczarczyk, J.J. (1996) Image analysis of alum coagulated mineral suspensions. Environmental Technology **17**, 1361-1369.

47. Guan, J., Waite, T.D., Amal, R. (1998) Rapid structure characterization of bacterial aggregates. Environmental Science and Technology **32**, 3735-3742.

48. Han, M.Y., Lawler, D.F. (1991) Interactions of two settling spheres: settling rates and collision efficiencies. Journal of Hydraulic Engineers, American Society of Civil Engineers **117**, 1269-1289.

49. Han, M.Y. (1989) Mathematical modeling of heterogenous flocculant sedimentation. Ph.D Thesis, University of Texas, Austin.

50. Han, M.Y, and Lawler, D.F. (1992) The (relative) insignificance of G in flocculation. Journal of American Water Works Association **84**, 79-91.

51. Harris, H.S., Kaufman, W.J., Krone, R.B. (1996) Orthokinetic flocculation in water treatment, Journal of Sanitary Engineers Division Proceedings, American Society of Civil Engineers **92** (SA6), 95-111.

52. Holt, P.K., Barton, G.W., Wark, M., Mitchell,C.A. (2002) A quantitative comparison between chemical dosing and electrocoagulation. Colloids and Surfaces A: Physicochemical Engineering Aspects **211**, 233-248.

53. Hong, S., Faibish, R. S., Elimelech, M. (1997) Kinetics of permeate flux decline in crossflow membrane filtration of colloidal suspensions. Journal of Colloid and Interface Science **196**, 267-277.

54. Hoogland, M.R., Fane, A.G., Fell, C.J.D. (1990) The effect of pH on the crossflow filtration of mineral slurries using ceramic membranes, 1st International Conference on Ceramic Membranes, Montpellier, Trans Tech Publications, Montpellier, 153-162.

55. Huang, C.J. and Liu, J.C. (1999) Precipitate flotation of fluoride-containing wastewater from a semiconductor manufacturer. Water Research **33** (16), 3403-3412.

56. Ivanshvili, A.I., Przhegorlinskii, V.I. , Kalichenko, T.D. (1987) Comparative evaluation of the efficiency of electrocoagulation and reagent methods of clarifying wastewater. Soviet Journal of Water Chemistry and Technology **9** (5), 118-119.

57. Jiang, J.-Q., Graham, N., Andre, C., Kelsall, G.H., Brandon, N. (2002) Laboratory study of electro-coagulation-flotation for water treatment. Water Research **36** (16), 4064-4078.

58. Jiang, Q. and Logan, B.E. (1991) Fractal dimensions of aggregates determined from steady state size distributions. Environmental Science and Technology **25**, 2031-2038.

59. Johnson, S.B., Franks, G.V., Scales, P.J., Boger, D.V., Healy, T. H. (2000) Surface chemistry – rheology relationships in concentrated mineral suspensions. International Journal of Mineral Processing **58**, 267-304.

60. Jones, K.L. and O'Melia, C.R. (2001) Ultrafiltration of protein and humic substances: effect of solution chemistry on fouling and flux decline. Journal of Membrane Science 193, 163-173.

61. Judd, S.J. and Hillis, P. (2001) Optimization of combined coagulation and microfiltration for water treatment. Water Research **35** (12), 2895-2904.

62. Jullien, R. and Botet, R. (1987) Aggregation and Fractal Aggregates, Singapore: World Science.

63. Kim, J.-S., Akeprathumcha,i S., Wickramasinghe, S. R. (2001) Flocculation to enhance microfiltration. Journal of Membrane Science **182**, 162-172.

64. Klimpel, R.C. and Hogg, R. (1986) Effects of flocculation conditions on agglomerate structure. Journal of Colloid and Interface Science **113**, 121-131.

65. Kruyt, H.R. (1952) Colloid Science. Volume 1, Irreversible Systems: v-vi, Elsevier, Amsterdam.

66. Kumar, P.R., Chaudhari, S., Khilar, K., Mahajan, S.P. (2004) Removal of arsenic from water by electrocoagulation. Chemosphere **55** (9), 1245-1252.

67. Kusters, K.A., Wijers, J.G., Thoenes, D. (1997) Aggregation kinetics of small particles in agitated vessels. Chemical Engineering Science **52** (1), 107-121.

68. Laher, V.K. and Healy, T.W. (1963) Adsorption-flocculation reactions of macromolecules at the solid-liquid interface. Review, Pure Applied Chemistry **13**, 112-132, 1963.

69. Lahousine-Turcard, V., Weisner, M.R., Bottero J.Y. (1990) Fouling in tangential-flow ultrafiltration: the effect of colloid size and coagulation pretreatment. Journal of Membrane Science **52**, 173-190.

70. Larue, O., Vorobiev, E., Vu, C., Durand, B. (2003) Electrocoagulation and coagulation by iron of latex particles in aqueous suspensions. Separation and Purification Technology **31**, 177-192.

71. Lawler, D.F. (1993) Physical aspects of flocculation: from microscale to macroscale. Water Research **27**, 164-180.

72. Lawler, D.F. (1997) Particle size distributions in treatment processes: theory and practice. Journal of Water Science and Technology **36** (4), 15-23.

73. Lee, D.G., Bonner, J.S., Garton, L.S., Ernest, A.N.S., Autenrieth, R.L. (2000) Modeling coagulation kinetics incorporating fractal theories: a fractal rectilinear approach. Water Research **34** (7),1987-2000.

74. Lee, J.-D., Lee, S.-H., Jo, M.-H., Park, P.-K., Lee, C.-H., Kwak, J.-W. (2000) Effect of coagulation conditions on membrane filtration characteristics in coagulation-microfiltration process for water treatment. Environmental Science and Technology **34**, 3780-3788.

75. Letterman, R.D., Amirtharajah, A., O'Melia, C.R. (1999) Coagulation and Flocculation. In AWWA "Water Quality and Treatment", Letterman, R.D. (ed.)

76. Li, X. and Logan, B.E. (1997) Collision frequencies between fractal aggregates and small particles in a turbulently sheared fluid. Environmental Science and Technology **31**, 1237-1242.

77. Li, D., Ganczarczyk, J.J. (1989) Fractal geometry of particle aggregates generated in water and wastewater treatment processes. Environmental Science and Technology **23** (11), 1385-9.

78. Li, H., Addai-Mensah, J., Thomas, J.C., Gerson, A.R. (2005) The influence of Al(III) supersaturation and NaOH concentration on the rate of crystallization of $Al(OH)_3$ precursor particles from sodium aluminate solutions. Journal of Colloid and Interface Science **286**, 511-519.

79. Lin, C.-F., Lin, T.-Y., Hao, O. J. (2000) Effects of humic substance charateristics on UF performance. Water Research **34** (4), 1097-1106.

80. Lin, S.H. and Lin, C.S. (1998) Reclamation of wastewater effluent from a chemical fiber plant. Desalination **120**, 185-195.

81. Lin, S.H. and Peng, C.F. (1994) Treatment of textile waste-water by electrochemical method. Water Research **28** (2), 277-282.

82. Lin, M.Y., Lindsay, H.M., Weitz, D.A., Ball, R.C., Klein, R., Meakin, P. (1989) Universality in colloid aggregation. Nature **339**, 360-362.

83. Lyklema, J. (1978) Surface chemistry of colloids in connection with stability, Ives K.J. (Ed.). The Scientific Basis of Flocculation, Sijthoff and Noordhoff, The Netherlands.

84. MacDonough, R.M., Fane, A.G., Fell, C.J.D. (1989) Charge effects in the cross-flow filtration of colloids and particulates. Journal of Membrane Science **43**, 69-85.

85. Mallikarjuan, R. and Venkatachalam, S. (1984) Electroflotation: A Review. International Symposium on Electrochemistry in Mineral and Metal Processing (165th meeting of the Electrochemical Society), Cincinnati, Ohio, USA, 233-256.

86. Mameri, N., Lounici, H., Belhocine, D., Grib, H., Piron, D.L., Yahiat Y. (2000) Deflouridation of Sahara water by small plant electrocoagulation using bipolar aluminium electrodes. Separation Purification Technology **24**, 113-119.

87. Mameri, N., Yeddou, A.R., Louncin,i H., Belhocine ,D., Grib ,H., Bariou, B (1998) Defluoridation of Septentrional Sahara water of North Africa by electrocoagulation process using bipolar aluminum electrodes. Water Research **32** (5), 1604-1612.

88. Mandelbrot, B.B.(1987) The fractal geometry of nature. Freeman, New-York.

89. Matijevic, E., Abramson, M.B., Ottewill, R.H., Shulz K.F., Keiker M. (1961) Adsorption of thorium ions on silver iodide sols. Journal of Physical Chemistry **65**, 1724-1729.

90. Matijevic, E., Janaues, G.E., Kerker, M. (1964) Reversal charge of lyphobic colloids by hydrolyzed metal ions. I. Aluminium nitrate, Journal of Colloid Science **19**, 333-346.

91. Matteson, M.J., Dobson, R.L., Glenn, R.W., Jr., Kukunoor, N.S., Waits, W.H. III., Clayfield, E.J. (1995) Electrocoagulation and separation of aqueous suspensions of ultrafine particles. Colloids and Surfaces A **104**, 101-109.

92. Meakin, P. (1998) Fractal aggregates. Advances in Colloid and Interface Science. **28**, 249-331.

93. Michaels, A.S., Aggregation of suspensions by polyelectrolytes (1954) Ind. Eng. Chem. **46**, 1485-1490.

94. Mills, D. (2000) A new process for electrocoagulation. Journal of American Water Works Association **92** (6): 34-43.

95. Mollah, A.Y.A., Schennech, R., Parga, J.R. and Cocke, D.L. (2001) Electrocoagulation (EC) – Science and applications. Journal of Hazardous materials B **84**, 29-41.

96. Murugananthan, M., Raju, G.B., Prabhakar, S. (2004) Removal of sulfide, sulfate and sulfite ions by electrocoagulation. Journal of Hazardous Materials B **109**, 37-44.

97. Nowostawska, U., Sander, S.G., McGrath, K.M., Hunter K.A. (2005) Effects of coagulants on the surface forces of colloidal alumina under water treatment conditions. Colloids and Surfaces A **266**, 214-222.

98. Ogutveren, U.B. and Koparal, S. (1992) Electrochemical treatment of water containing dye-stuffs: anodic oxidation of congo red and xiron blau 2RHD. International Journal of Environmental Studies 42, 41-52.

99. Ogutveren, U.B. and Koparal, S. (1997) lectrocoagulation for oil-water emulsion treatment. Journal of Environmental Science and Health A 32 (9-10), 2507-2520.

100. Oles, V. (1992) Shear-induced aggregation and breakup of polystyrene latex particles. Journal of Colloid and Interface Science **154**, 351-358.

101. O'Melia, C.R. (1972) Coagulation and flocculation. In Physicochemical Processes for Water Quality Control W.J., Weber Jr. (ed.), Wiley Interscience, New York.

102. Packham R. F. (1965) Some studies of the coagulation of dispersed clays with hydrolyzing salts. Journal of Colloid Science **20**, 81-92, 1965.

103. Parker D.S., Kaufman W.J., Jenkins D. (1972) Floc break-up in turbulent flocculation processes. Journal of Sanitary Engineers Division Proceedings, American Society of Civil Engineers **98** (SA1), 79-99.

104. Peuchot, M. and Ben-Aim, R. (1992) Improvement of cross-flow microfiltration performances with flocculation. Journal of Membrane Science **68**, 241-248.

105. Picard, T., Cathalifaud-Feuillade, G., Mazet, M., Vandensteendam ,C. (2000) Cathodic dissolution in the electrocoagulation process using aluminum electrodes. Journal of Environmental Monitoring **2**, 77-80.

106. Posselt, H.S., Anderson, F.J., Weber, W.J. Jr. (1968) Cation sorption on colloidal hydrous manganese dioxide. Environmental Science and Technology **2** (12), 1087-1093.

107. Potanin, A.A. (1991) On the mechanism of aggregation and breakup of polystyrene. Journal of Colloid and Interface Science **145**, 140-157.

108. Pouet, M. F. and Grasmick, A. (1995) Urban wastewater treatment by electrocoagulation and flotation. Water Science and Technology **31** (3-4), 275-283.

109. Richens, D.T (1997) The Chemistry of Aqua Ions, Wiley, Chichester.

110. Ruehrwein, R.A. and Ward, D.W. (1952) Mechanism of clay aggregation by polyelectrolytes. Soil Science **73**, 485-492.

111. Sato, D., Kobayashi, M., Adachi, Y. (2004) Effect of floc structure on the rate of shear coagulation (2004) Journal of Colloid and Interface Science **272**, 345-351.

112. Schafer, A.I., Schicker, U., Fischer, M.M., Fane, A.G., Waite, T.D. (2000) Microfiltration of colloids and natural organic matter. Journal of Membrane Science 171, 151-172.

113. Schmidt-Ott, A., Baltensperger, U., Gaggeler, H.W., Jost, D.T. (1990) Scaling behaviour of physical parameters describing agglomerates. Journal of Aerosol Science **21** (71), 1-717.

114. Selomulya, C., Bushell, G., Amal, R., Waite, T.D. (2003) Understanding the role of restructuring in flocculation: The application of a population balance model. Chemical Engineering Science **58**, 327-338.

115. Shen, F., Gao, P., Chen, X., Chen, G. (2003) Electrochemical removal of fluoride ions from industrial wastewater. Chemical Engineering Science **58**, 987-993.

116. Smoluchowski, M. (1917) Versuch einer mathematischen theorie der koagulations – kinetik kolloides losungen, Z. Physic. Chem. **92**, 129-168.

117. Soffer, Y., Ben-Aim R., Adin A. (2000) Membrane for water reuse: effect of pre-coagulation on fouling and selectivity. Water Science and Technology **42** (1-2), 367-372.

118. Song, L. (1998) Flux decline in crossflow microfiltration and ultrafiltration: mechanisms and modeling of membrane fouling. Journal of Membrane Science **139**, 183-200.

119. Sorensen, C.M. (1997) Surface and colloid chemistry: Birdi, K.S., Ed., CRC Press: Boca Raton, FL, Chapter 13, 533-558.

120. Spicer, P.T. and Pratsinis, S.E. (1996) Shear-induced flocculation: The evolution of floc structure and the shape of the size distribution at steady-state. Water Research **30** (5), 1049-1056.

121. Sposito, G. (1996) The environmental chemistry of aluminum. Second, CRC Press Ltd., Florida.

122. Stuart, F.E. (1946) Electronik principle of water purification. Journal of New England Water Works Association **60**, 236.

123. Stumm, W. and Morgan, J.J. (1962) Chemical aspects of coagulation. Journal of American Water Works Association **54**, 971-994.

124. Stumm, W. and O'Melia, C.R. (1968) Stochiometry of coagulation. Journal of American Water Works Association **60**, 514-539.

125. Tamamushi, B. and Tamaki, K. (1959) The action of long-chain cations on negative silver iodide sol. Koll.-Z **163**, 122-126.

126. Tambo, N. (1991) Basic concepts and innovative turn of coagulation/flocculation. Water Supply **9**, 1-10.

127. Tambo, N. and Watanabe, Y. (1979) Physical characteristics of flocs I: the floc density and aluminum floc. Water Research **13**, 409-419.

Abstract

Electroflocculation (EF) is gaining popularity and becoming recognized an alternative process to conventional coagulation/flocculation (CF), although both are somewhat different. Research into this alternative technology has focused on efficiency and performance rather than on the fundamental basics which is the core of understanding the mechanisms of EF and ultimately will lead to better system design and process control.

In EF the active coagulant species are generated in situ by electrolytic oxidation of an appropriate anode material, thus differing from CF in which chemical coagulants such as metal salts or polymers and polyelectrolytes are used. The electrical current applied in EF creates a unique chemical/physical environment which affects coagulation mechanisms and subsequent aggregate/floc formation. This is due to competing redox reactions within the system, the first and foremost being hydrolysis. Coagulation mechanisms depend primarily on factors such as pH and coagulant dosage, which govern speciation of the active mononuclear species, hence the current has an additional affect as it both governs the dissolution of the metal coagulant into the system and also causes the pH to rise, as hydroxyl is simultaneously formed at the cathode. In addition, the dosing regime is an additive process over time in which negative counter ions are not introduced, and microbubbles are formed as hydrogen and oxygen are also products of the hydrolysis. It is also possible that the electrical field imposed could affect ion and particle transport.

The aim of this research is to gain a better understanding of the EF process, primarily on a theoretical level, but also to evaluate the applicability of the process as a viable alternative to conventional coagulation. The mechanisms of coagulation and flocculation in EF are elucidated, while connecting changes in suspension characteristics, floc growth patterns, structural evolution and floc morphology to operational parameters. A comparison with CF was performed, with regard to destabilization mechanisms and floc structural evolution. Finally, the applicability of the process was examined, as a viable alternative pretreatment process in membrane ultrafiltration.

128. Tence, M., Chevalier J.P., Jullien R. (1986) On the measurement of the fractal dimension of aggregated particles by electron-microscopy experimental method, corrections and comparison with numerical models. Journal De Physique **47** (11), 1989-1998.

129. Thill, A., Lambert, S., Moustier, S., Ginestet, P., Audic, J.M., Bottero, J.Y. (2000) Structural interpretations of static light scattering patterns of aggregates II. Experimental study. Journal of Colloid and Interface Science **228**, 386-392.

130. Thomas, D.N., Judd, S.J., Fawcett, N. (1999) Flocculation modeling: a review. Water Research **33** (7), 1579-1592.

131. Veerapaneni, S. and Wiesner, M.R. (1996) Hydrodynamics of fractal aggregates with radially varying permeability. Journal of Colloid and Interface Science **177**, 45-57.

132. Verwey, E.J.W. and Overbeek, J. Th. G. (1948) Theory of stability of lyphobic colloids, Elsevier, Amsterdam.

133. Vik, E.A., Carlson, D.A., Eikum, A.S., Gjessing, E.T. (1984) Electrocoagulation of potable water. Water Research **18** (11), 1355-1360.

134. Waite, T.D. (1999) Measurement and implications of floc structure in water and wastewater treatment. Colloids and Surfaces A **151**, 27-41.

135. Weisner, M.R., Clark, M.M. and Mallevialle, J. (1989) Membrane filtration of coagulated suspensions. Journal of Environmental Engineering **115** (1), 20-40.

136. Zhang, J. and Buffle, J. (1996) Multi-method determination of the fractal dimension of hematite aggregates. Colloids and Surfaces A **107**,175-187.

137. Zhu, B., Clifford, D.A., Shankararaman, C. (2005) Comparison of electrocoagulation and chemical coagulation pretreatment for enhanced virus removal using microfiltration membranes. Water Research **39** (13), 3098-3108.

Appendix

Published papers

Electroflocculation as potential pretreatment in colloid ultrafiltration

T. Harif, M. Hai and A. Adin

Soil&Water Sciences Department, Faculty of Agricultural, Food and Environmental Quality Sciences, The Hebrew University of Jerusalem, POB 12, Rehovot 71612, Israel. E-mail: tharif@vms.huji.ac.il; dariels@pob.huji.ac.il; adin@vms.huji.ac.il

Abstract Electroflocculation (EF) is a coagulation/flocculation process in which active coagulant species are generated in situ by electrolytic oxidation of an appropriate anode material. The effect of colloidal suspension pretreatment by EF on membrane fouling was measured by flux decline at constant pressure. An EF cell was operated in batch mode and comprised of two flat sheet electrodes - an aluminum anode and stainless steel cathode - which were immersed in the treated suspension, and connected to an external DC power supply. The cell was run at constant current between 0.06A-0.2A. The results show that pre-EF enhances the permeate flux at pH 5 and 6.5, but only marginal improvement is observed at pH 8. At all pH values cake formation on the membrane surface was observed. The differences in membrane behavior can be explained by conventional coagulation theory and transitions between aluminum mononuclear species which affect particle characteristics and consequently cake properties. At pH 6.5, where sweep floc mechanism dominates due to increased precipitation of aluminum hydroxide, increased flux rates were observed. It is evident that EF can serve as an efficient pretreatment to ultrafiltration of colloid particles.
Keywords Electroflocculation; ultrafiltration; coagulation; filtration; fouling; colloid; aluminum

Introduction

Electroflocculation (EF) is a coagulation/flocculation process in which active coagulant species are generated in situ by electrolytic oxidation of an appropriate anode material. The EF process can substitute for chemical coagulation aimed at destabilizing emulsions and colloidal suspensions. In its simplest form, an EF reactor may be made up of an electrolytic cell containing one anode and one cathode. When connected to an external power source, an oxidation reaction occurs at the anode and a reduction reaction at the cathode. The specific chemical and electrochemical reactions occurring within the EF cell depend upon the type of metal used as the anode. The anode material most commonly used is aluminum or iron because when electrochemically oxidized they produce the most commonly used ionic coagulants, Al^{+3} and Fe^{+3} (or Fe^{+2}) respectively .The basic reactions that occur with aluminum anodes are described in Eqs. (1)-(3):

(-) Cathode: $2H_2O + 2e^- \rightarrow H_{2\,(g)} + 2OH^-_{(aq)}$ (1)

(+) Anode: $2H_2O \rightarrow O_{2\,(g)} + 4H^+_{(aq)} + 4e^-$ (2)

(+) Anode: $Al_{(s)} \rightarrow Al^{3+}_{(aq)} + 3e^-$ (3)

The aluminum cation hydrolyses upon addition to solution. Mononuclear complexes are initially formed as described by Eqs. (4)-(7).

$Al^{+3}_{(aq)} + H_2O \rightarrow AlOH^{+2}_{(aq)} + H^+_{(aq)}$ (4)

$AlOH^{+2}_{(aq)} + H_2O \rightarrow Al(OH)_2^+{}_{(aq)} + H^+_{(aq)}$ (5)

$Al(OH)_2^+{}_{(aq)} + H_2O \rightarrow Al(OH)_{3(s)} + H^+_{(aq)}$ (6)

$Al(OH)_{3(s)} + H_2O \rightarrow Al(OH)_4^-{}_{(aq)} + H^+_{(aq)}$ (7)

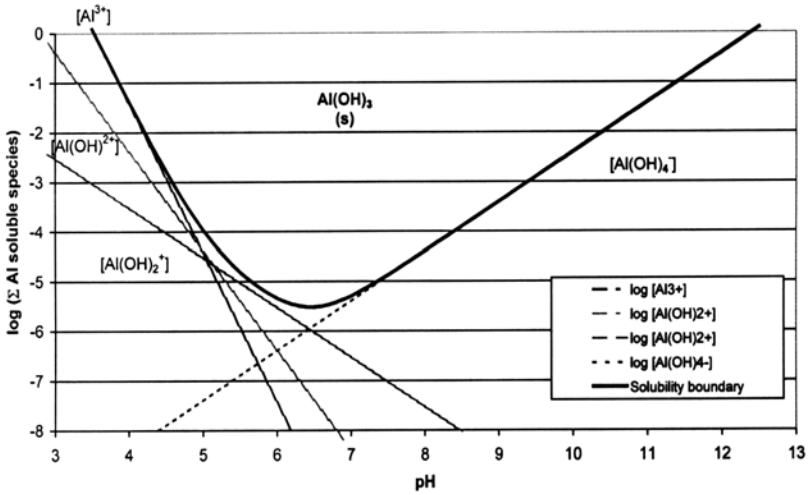

Fig.1. Solubility diagram of aluminum hydroxide $Al(OH)_{3(s)}$ with mononuclear species.

The speciation of aluminum systems has been well documented in the literature (Sposito, 1996; Duan and Gregory, 2003, Letterman et al, 1999). This paper will assume that mononuclear hydrolyzed species adequately predict aluminum hydroxide precipitation.

The type of coagulant required in the system dictates the choice of the anode material in an EF reactor. The theoretical dosage can be calculated using Faraday's law, which describes a linear relationship between current intensity and the amount of metal dissolved. In order to achieve the desired current, and overcome the IR drop (caused by the cell itself and polarization factors), steps can be taken to lower the system resistance (e.g. minimize distance between electrodes, increase conductivity) or a potential greater than the theoretical potential must be applied to the cell. The cathode material is of less importance, although, due to oxygen gas formation at the anode, and hydroxide ion formation at the cathode, the surface of the cathode can become chemically oxidized, producing aluminum oxide, which forms a passivation layer, and also can undergo pitting due to a highly basic local environment. This increases the resistance within the cell, causing a drop in voltage across the cell, which, in turn, decreases the metal dissolution at the anode. Using cathodes made from inert metals, or metals that oxidize slowly, or using an ac generator, can overcome this problem (Ivanishvili et al., 1987).

Only in the past decade has awareness grown as to the advantages of using the technology for electrochemical treatment of water and wastewater. Today, electrochemical processes are being used in a wide range of applications (Mollah et al., 2000, Adin and Vescan, 2002). Treatment of wastewater by EF has been practiced for most of the 20th century, yet limited scientific research has explored the efficiency of the technology as an alternative process for water treatment. Preliminary work has been done on colloid and organic matter removal (Vik et al., 1984, Matteson et al., 1995), although in general, technological developments have focused on commercialization of the process by minimizing electrical power consumption and maximizing effluent throughput rates (Mills et al., 2000).

Membrane filtration is a widely applied technology in water and wastewater treatment (Bourgeous et al., 2001), although membranes are highly susceptible to fouling. Fouling is caused by a combination of factors: 1. accumulation of materials on the membrane surface which precipitate or form a layer that resists the flow of permeate (cake formation) 2. internal blocking by materials entering the membrane pores 3. pore blocking 4. accumulation of materials near the membrane surface, in the concentration boundary (referred to as the concentration polarization layer) 5. changes in the membrane structure (Carroll et al., 2000). In most cases, when treating water, the concentration polarization layer, if formed, contributes negligible resistance compared to the actual cake resistance (Waite et al., 1999). The connection between aggregation conditions, either in suspension, or at the membrane surface to cake properties has been acknowledged (Fu and Dempsey, 1998). The porosity of the cake has a major impact on its resistance, and increased

porosity results in improved permeate flux. When the pressure across the membrane's surface (trans-membrane pressure-TMP) is constant, the fouling rate can be expressed as J/Jo (permeate flux/initial flux), which typically exponentially declines. Pre-treatment of the feed, using conventional coagulation/flocculation methods, has proven effective in reducing the fouling behavior of membranes (Lahoussine-Turcaud et al., 1990; Soffer et al., 2000; Judd and Hillis, 2001; Kim et al., 2001).

The introduction of the active coagulant species (metal ions) is an additive process over time, negative counter-ions are not introduced, an electrical field exists which could affect particle transport, the pH rises due to hydroxide formation at the cathode, bubbles are present due to the hydrolysis which occurs and can be a negative steric factor affecting aggregate growth. Moreover, the process forms a dynamic electrochemical environment where many other electrochemical reactions occur, depending on the chemistry of the treated suspension.

This research examines the fouling behavior of a UF membrane in a coupled EF-UF process by measuring flux decline at constant pressure. Cake formation on the membrane surface is examined using electronic microscopy techniques, and correlations between characteristics of an electroflocculated kaolin suspension fed into the system (particle size distribution, ζ potential, pH), cake structure, and membrane performance are investigated.

Materials and Methods

Colloidal suspensions 0.3gr of kaolin was suspended in 20 liters of distilled water (15mg/l final concentration) and homogenized using an Ultraturax 2000. 1.66gr of $NaHCO_3$ was added (final concentration 83mg/l), the pH was corrected to 5, 6.5 and 8, with NaOH or H_2SO_4, and conductivity was increased to 1mS/cm with $NaNO_3$.

Electroflocculation The electroflocculation unit was a batch cell comprised of two flat sheet electrodes (an aluminum anode and stainless steel cathode), with an active area of $9cm^2$, which were immersed in the treated suspension, and connected to an external DC power supply. The cell was run at constant current (range used was 0.06A-0.2A), for a fixed 7 minutes dosing period, and the doses were equivalent to aluminum content in 30, 60, 80 and 100 mg/l commercial alum ($Al_2(SO_{4)3}18H_2O$).

Membranes The ultrafiltration membranes used in this study were hydrophilic polyethersulfone flat sheet membranes manufactured by Microdyn-Nadir (Germany), with a nominal molecular weight cut-off of 50kDa, and pure water flux > $250l/m^2h$. Prior to use the membranes were soaked for 12 hours in distilled water.

Ultrafiltration Unit The membrane filtration unit was comprised of a nitrogen gas cylinder, which maintained a constant pressure of 3 bars throughout the unit. A polypropylene feed reservoir, with a volume of 1250ml, held the colloidal suspension prior to the membrane module. The membrane module, made from polypropylene, was operated as a stirred cell. It contained an internal magnetic stirrer bar suspended close to the upper surface of the membrane with motion induced by a magnetic stirrer table placed beneath it. A flat disc membrane with an area of $11.3cm^2$ was held in place with an O-ring. The permeate was collected in a chemical glass mounted onto an electronic balance, which was connected to a computer containing software that calculated the permeate flux from permeate weight accumulation.

Particle Size Analysis Particle size distribution measurements were performed over a range of 2μm-300μm, using a HIAC Royco Liquid Particle Counting System.

ζ potential The ζ potential of the post electroflocculated suspension was measured using a Malvern Zetamaster S.

Cake characterization Membranes exhibiting cake formation were dried (at room temperature) and photographed using scanning electronic microscopy (SEM)**.**

Aluminum measurements Residual aluminum in the permeate was measured using ICP (Cole-Parmer).

Experimental Procedure. One liter of the kaolin suspension underwent EF for 7 minutes, in a rapid mix regime (using magnetic stirrer at 120 rpm), and then was transferred to a jar test apparatus (Phipps and Bird, USA) for an additional 20 minutes slow mixing (30 rpm). Samples were taken from the flocculated suspension for particle characterization (particle size distribution and ζ potential), before filtering through the membrane unit. The flux was measured through the membrane, at room temperature (~20^{o}C) at constant pressure (3 bars) over a 25 minute time span.

Results and Discussion

Characteristics of an electroflocculated kaolin suspension. The current applied in the EF process has a double effect, by both generating the coagulant species and by causing hydrolysis in which excess hydroxyl ions are formed at the cathode, resulting in an increase in pH (eq. 1.). In these dynamic conditions, coagulation mechanisms shift, depending on the current applied. The shift in pH and consequent shifting speciation of aluminum mononuclear complexes, causes the ζ potential of the electroflocculated suspensions to change, which serves as an indicator for coagulation efficiency. Fig.2. shows the change in pH and ζ potential as a function of applied current for a 15mg/l kaolin suspension at different initial pH values. The ζ potential of the kaolin suspensions, without applying any current, were: -17.9mV, -21.7mV and -23.7mV for pH 5, 6.5 and 8 respectively.

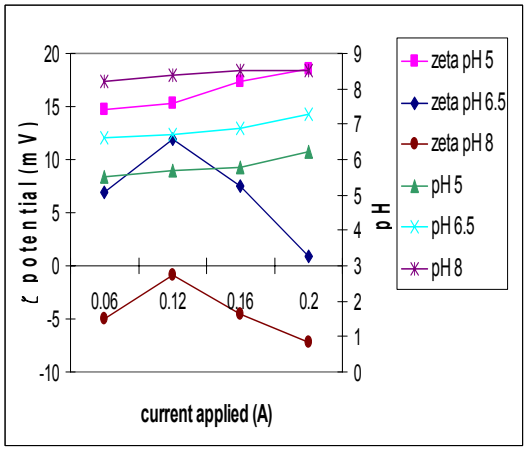

Fig. 2. Change in pH and z potential vs. applied current for different initial pH values. C_0=15mg/l, t=7min.

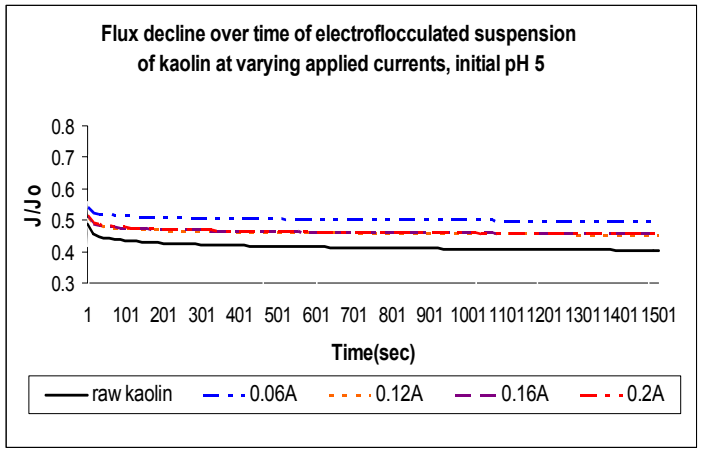

Fig. 3. Permeate flux (J) as a fraction of initial flux (J_0) over the course of ultrafiltration of an electroflocculated kaolin suspension, initial pH 5, at various applied currents.

Membrane Filtration. The permeate flux was measured for suspensions, that had undergone electroflocculation using aluminum as the anode material. The aluminum doses were controlled by the applied current, which was kept constant during each run. The results show that pre-EF enhances the permeate flux, at all initial pH ranges, 5, 6.5 and 8.

pH 5 (initial) At initial pH 5 filtration of kaolin causes significant flux decline, and by the end of the run it has reached 40% of the initial flux (Fig. 3.) Pre-EF of the suspension improves the filtration, and at all currents we observe flux enhancement. At 0.06A the maximum flux enhancement occurs, by which the flux has improved by 15%, reaching steady state at 55% of the initial flux. At 0.12A, 0.16A and 0.2A similar behavior is observed, by which the permeate flux reaches steady state at 60% of the initial flux. The difference in membrane behavior obtained after EF at 0.06A relatively to the other applied currents can be explained by the transition to a different coagulation mechanism, which occurs at higher doses of aluminum. At pH 5 the governing aluminum species in solution are Al^{+3} and $Al(OH)^{2+}$, and therefore we assume that at this initial pH the dominant coagulation mechanism is adsorption and charge neutralization,

although some aluminum hydroxide does precipitate in these conditions. In this case it appears that at the minimum applied current, 0.06A, adsorption and charge neutralization is the dominant coagulation mechanism, thus producing aggregates that form a stable cake on the membrane surface, which has a higher porosity than the dense, compact cake formed by filtration of kaolin (Fig. 6.). At the higher currents, 0.12A, 0.16A and 0.2A we observe improved membrane behavior due to increased formation of aluminum hydroxide in solution, which catches the smaller particles (by "sweep floc" mechanism) thereby enhancing the permeate flux. The decline in flux relative to the flux obtained at 0.06A, is due to increased cake formation of gelatinous aluminum hydroxide on the membrane surface. From SEM analysis, aluminum hydroxide seems to form a "blanket" on the membrane surface, and exhibits different characteristics than the cake formed from filtration of raw kaolin, which appears to be very dense and tightly packed (Figs. 6. and 7.). In addition, aluminum hydroxide flocs, unlike kaolin particles (which have an average size of 1μm), are large enough to be sheared from the membrane surface (Weisner et al., 1989). This, however, may not be the sole factor that causes this difference between the two types of suspensions – density and morphology may also play an important role here, which is still a matter of conjecture. Particle size distribution measurements of the electroflocculated suspension show an increase in particle counts for particles between 5μm-10μm for the higher applied currents. Since permeability of the filter cake and back transport by hydrodynamic forces both increases with increasing particle size (Fu and Dempsey, 1998), this can also explain the flux enhancement. The residual aluminum measured in the permeate at the higher currents was 0.030mg/l and 0.039mg/l (for 0.16A and 0.2A respectively), indicating optimal coagulation-flocculation, in which nearly all the aluminum (~98%) was removed from solution, caught on the membrane surface as an aluminum hydroxide mesh. At 0.06A the coagulation mechanisms are in transition due to the formation of a variety of aluminum hydrolysis species. The final pH was 5.5 (Fig. 2.) and the residual aluminum measured was 0.5 mg/l, which indicates that a large fraction (~21%) of the aluminum was not precipitated as aluminum hydroxide, but was present as soluble species (Al^{+3} and $Al(OH)^{+2}$). Moreover the positive ζ potential of the suspension indicates a transition through charge neutralization for all the currents, so we can assume the major factor causing the differences between the lower current and higher currents is the quantity of aluminum hydroxide present.

pH 6.5 (initial) At initial pH 6.5 filtration of kaolin causes significant flux decline, and by the end of the run it has reached 40% of the initial flux (Fig.4.). Pre-EF of the suspension improves the flux,and for applied currents of 0.12A, 0.16A and 0.2A identical flux behavior is observed, by which the permeate flux reaches steady state at above 60% of the initial flux. For an applied current of 0.06A there is a 5% drop in the flux compared to the other currents, and the permeate flux reaches steady state at 55% of the initial flux. At pH 6.5 the dominant coagulation mechanism is sweep floc, due to increased formation of amorphous aluminum hydroxide, although at the higher currents the pH increases significantly (Fig. 2.) and speciation shifts towards $Al(OH)_4^-$ which decreases coagulation efficiency - indicated by the less positive ζ potential. This does not seem to affect the membrane behavior within the dosages used at this pH, because a wide range of currents produced the same results. Therefore, the improved membrane behavior observed here was due to the formation of aluminum hydroxide flocs in solution, which catch smaller particles and form a more permeable cake on the membrane surface. Moreover, aluminum hydroxide flocs are large enough to be sheared from the membrane surface and therefore the cake thickness is stable, resulting in a stable flux. Particle size counts performed between 5μm-20μm indicate that at 0.06A sizes obtained are on average smaller than those formed at other currents, therefore the cake is less porous and a minor difference in membrane behavior is observed. In addition, particle size distribution measurements show that for 0.12A, 0.16A, and 0.2A the counts between 5μm-20μm are nearly identical, which can explain the similar flux obtained at these currents.

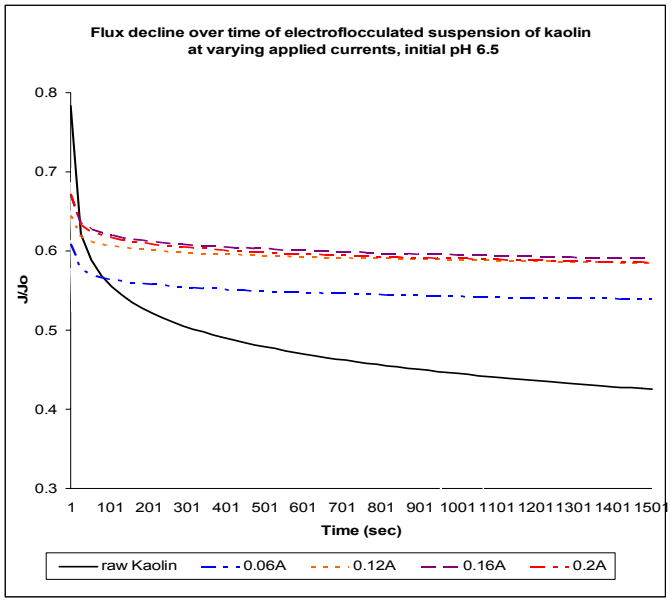

Fig.4. Permeate flux (J) as a fraction of initial flux (Jo) over the course of ultrafiltration of kaolin suspension, initial pH 6.5, at various applied currents.

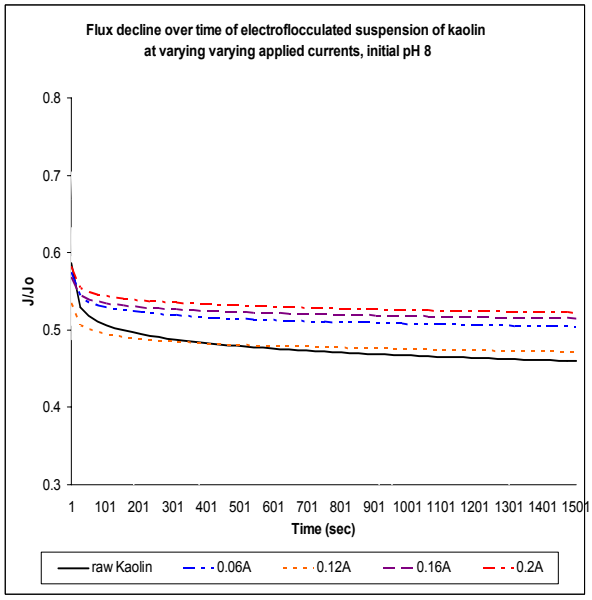

Fig.5. Permeate flux (J) as a fraction of initial flux (Jo) over the course of ultrafiltration of kaolin suspension, initial pH 8, at various applied currents.

pH 8 (initial) At initial pH 8 filtration of kaolin causes significant flux decline, and by the end of the run it has reached 50% of the initial flux (Fig. 5). Pre-EF does not improve the flux significantly, and for all currents similar flux behavior is observed, by which the permeate flux reaches steady state at 55% of the initial flux(only a 5% improvement relative to the flux obtained when filtering the raw kaolin). At pH 8 the ζ potential of kaolin is more negative, compared to that at pH 5 and 6.5, therefore the particles are more readily rejected from the membrane (which is hydrophilic and charged negatively), which can explain a slight increase in the flux relative to the flux at pH 5 and 6.5. At pH 8 the dominant species is $Al(OH)_4^-$, and therefore no real improvement is observed because coagulation conditions are not optimal. Some aluminum hydroxide precipitates, which is visible, and forms a cake on the membrane surface, but still small particles are present in large quantities in solution, because no efficient coagulation occurs. These particles can enter the cake pores and thus reduce the flux. The minor improvement in membrane behavior observed here was due to some formation of aluminum hydroxide flocs in solution, which catch a fraction of the smaller particles. The permeate aluminum measurements indicate a large quantity of soluble aluminum which increases with applied current (0.68 mg/l (~28%) and 1.76 mg/l (~22%) for 0.06A and 0.2A respectively), thus corroborating the shift in speciation towards soluble aluminum mononuclear species ($Al(OH)_4^-$ at pH 8).
Particle size distribution measurements show nearly identical counts for all currents, between 5μm-20μm, which can explain the similar flux obtained at these currents. However, particle distribution measurements show much lower counts than those at pH 5 and 6.5, which indicates that less colloidal particles are present. At pH 5 and 6.5 aluminum hydroxide precipitates as colloidal matter, contributing to the particle counts. At pH 8 the aluminum solubility equilibrium has shifted towards the negative soluble species ($Al(OH)_4^-$), less aluminum hydroxide precipitates resulting in lower particle counts.

Figs.6. and 7. show the visible differences in cakes formed on the membrane surface from filtration of a kaolin suspension and a pre-electroflocculated kaolin suspension.

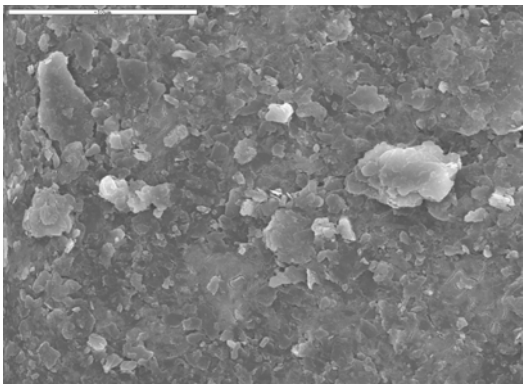

Fig.6. Cake after filtration of raw kaolin.

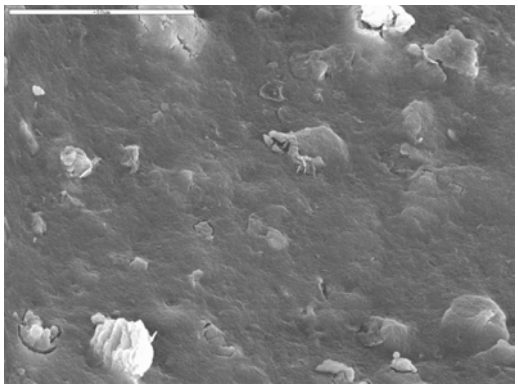

Fig.7. Cake after filtration of pre-electroflocculated kaolin.

Conclusions

Electroflocculation can serve as an efficient pretreatment to ultrafiltration of colloid particles. The fouling behavior of the membrane could be explained by applying conventional coagulation theory. Increased flux rates were observed at pH 6.5, and currents of 0.12A-0.2A, where sweep floc mechanism dominates due to increased precipitation of $Al(OH)_{3(s)}$. At all pH values cake formation on the membrane surface was observed indicating that cake resistance is a primary fouling factor. The differences in flux can be attributed to cake properties (i.e., thickness, porosity) which are determined by particle characteristics. At pH 5 and 8, the flux obtained from pre-electroflocculated suspensions was less than that obtained at pH 6.5. At pH 5 and 8, the solubility equilibrium is in transition and less aluminum hydroxide precipitates, therefore smaller particles are still present in suspension (not removed by sweep floc mechanism). These can enter the cake pores and cause "self contamination", resulting in increased flux decline. Moreover, particle counts indicate that at pH 6.5 larger flocs are present which can be readily sheared from the membrane surface resulting in a "thinner" cake, which can also explain flux enhancement. These results demonstrate the potential of electroflocculation as pretreatment to ultrafiltration, and stress the importance of research with different types of contaminants.

Acknowledgements

The work was partially supported by BMBF Germany and Israeli ministry of Science. The samples of membranes were kindly provided by MICRODYN-NADIR.

References

Adin, A. and Vescan, N. (2002). Electroflocculation for particle destabilization and aggregation for municipal water and wastewater treatment. *Proc. Amer. Chem. Soc.*, **42**(2), 537-541.

Bourgeous K. N., Darby J. L. and Tchobanoglous G.(2001). Ultrafiltration of wastewater: effects of particles, mode of operation, and backwash effectiveness. *Wat. Res.*, **35**(1), 77-90.

Carroll T., Gray S. R., Bolto B. A. and Booker N. A. (2000). The fouling of microfiltration membranes by NOM after coagulation treatment. *Wat. Res.*, **34**(11), 2861-2868.

Duan J. and Gregory J. (2003). Coagulation by hydrolyzing salts. *Adv. Colloid Interface. Sci.*, **100-102**, 475-502.

Fu L. F. and Dempsey B. A. (1998). Modeling the effect of particle size and charge on the structure of the filter cake in ultrafiltration. *J. Membrane Sci.*, **149**, 221-240.

Holt P. K., Barton G. W., Wark M. and Mitchell C.A. (2002). A quantitative comparison between chemical dosing and electrocoagulation. *Colloids and Surfaces A: Physicochem. Eng. Aspects*, **211**, 233-248.

Ivanshvili A. I., Przhegorlinskii V. I. and Kalichenko T. D. (1987). Comparative evaluation of the efficiency of electrocoagulation and reagent methods of clarifying wastewater. *Soviet J. Wat. Chem. and Tech*., **9** (5): 118-119.

Judd S. J. and Hillis P. (2001). Optimization of combined coagulation and microfiltration for water treatment. *Wat. Res.*, **35** (12): 2895-2904.

Kim J.-S., Akeprathumchai S. and Wickramasinghe S. R. (2001). Flocculation to enhance microfiltration. *J. Membrane Sci.*, **182**, 162-172.

Lahousine-Turcard V., Weisner M. R. and Bottero J. Y (1990b). Fouling in tangential-flow ultrafiltration: the effect of colloid size and coagulation pretreatment. *J. Membrane Sci*, **52**, 173-190.

Letterman R.D., Amirtharajah A. and O'Melia C. R. (1999). Coagulation and flocculation in water quality and treatment, in: Letterman R. D. (Ed.), A Handbook of Community Water Supplies, Fifth, *AWWA, McGraw-Hill, New York.*

Matteson M. J., Dobson R. L., Glenn R. W., Jr., Kukunoor N. S., Waits W. H. III. and Clayfield E. J. (1995). Electrocoagulation and separation of aqueous suspensions of ultrafine particles. *Colloids and Surfaces A: Physicochem. Eng. Aspects* **104**, 101-109.

Mills D. (2000). A new process for electrocoagulation. *AWWA*, **92** (6): 34-43.

Mollah A. Y. A., Schennech R., Parga J. R. and Cocke D. L. (2001). Electrocoagulation (EC) – Science and applications. *J. Haz. Mat.*, **B84**, 29-41.

Soffer Y., Ben Aim R. and Adin A. (2000). Membrane for water reuse: Effect of pre-coagulation on fouling and selection. *Wat. Sci. and Tech.*, **42**(1-2): 367-372.

Sposito G. (1996). The environmental chemistry of aluminum. Second, *CRC Press Ltd., Florida.*

Vik E. A., Carlson D. A., Eikum A. S. and Gjessing E. T. (1984). Electrocoagulation of potable water. *Wat. Res.*, **18** (11), 1355-1360.

Waite T. D. (1999). Measurement and implications of floc structure in water and wastewater treatment. *Colloids and Surfaces A: Physicochem. Eng. Aspects*, **151**, 27-41.

Weisner M. R., Clark M.M. and Mallevialle J. (1989). Membrane filtration of coagulated suspensions. *J. Envir. Eng.*, **115** (1), 20-40.

Characteristics of aggregates formed by electroflocculation of a colloidal suspension

T. Harif and A. Adin

Soil &Water Sciences Department, Faculty of Agricultural, Food and Environmental Quality Sciences, The Hebrew University of Jerusalem, POB 12, Rehovot 71612, Israel. E-mail: tharif@vms.huji.ac.il; adin@vms.huji.ac.il

Abstract Electroflocculation (EF) is becoming recognized as an alternative process to conventional coagulation/flocculation, although both are somewhat different. The electrical current applied in EF to generate the active coagulant species creates a unique chemical/physical environment which affects coagulation mechanisms and subsequent aggregate formation. The chemical and physical characteristics of an electroflocculated kaolin suspension and the morphology/fractal dimension of the resulting aggregates were examined. An EF cell was operated in batch mode and comprised of two concentric electrodes - a stainless steel cathode (outer electrode) and an aluminum anode (inner electrode).The cell was run at constant current between 0.05A-0.3A, velocity gradients were 0-30 sec^{-1}. The results show that the simultaneous hydrolysis occurring has a profound affect on the final pH and consequently on the coagulation mechanisms as indicated by differences in ζ potential measured. Moreover, the electrical field induced by passage of a current has an apparent effect on particle transport. A linear correlation between floc size and current was observed and lower fractal dimensions were obtained for larger floc sizes. The fractal dimensions of the flocs obtained in EF are on average lower than those reported for conventional coagulation.
Keywords Electroflocculation; coagulation; aluminum; species; aggregate; fractal dimension

1. Introduction

Electroflocculation (EF) is gaining popularity and is becoming recognized as an alternative to conventional coagulation/flocculation processes. EF generates active coagulant species in situ by electrolytic oxidation of an appropriate anode material, thus differing from the conventional process in which chemical coagulants such as metal salts or polymers and polyelectrolytes are used for destabilizing emulsions and colloidal suspensions. EF creates unique chemical and physical conditions because the electrical current has a secondary effect within the system, first and foremost due to the hydrolysis which occurs.

Preliminary work has been done on colloid and organic matter removal using EF (Vik et. al., 1984; Matteson et. al., 1995), and over the past decade increased research has explored EF in a wide range of applications (Pouet and Grasmick, 1995; Belongia et. al., 1999; Do and Chen, 1994; Mollah et. al., 2000; Adin and Vescan, 2002; Mills, 2000). Despite growing awareness of the process, no substantial research has been conducted on the mechanisms of coagulation and flocculation in EF, which are directly affected by the unique conditions the process creates. The morphology of resulting aggregates is directly connected to these mechanisms, and is primary factor in understanding them. This research explores the morphology of aggregates formed in the EF process, while using a two-dimensional fractal dimension to quantify their structure. This is the first time morphological characteristics of aggregates formed in EF have been reported.

Description of the technology:

In its simplest form, an EF reactor may be made up of an electrolytic cell containing one anode and one cathode. The anode metals most commonly used are aluminum or iron because when electrochemically oxidized they produce the most commonly used ionic coagulants, Al^{+3} and Fe^{+3} (or Fe^{+2}) respectively. The cathode material is of less importance, although, due to competing redox reactions, by-products are formed which can affect the cathode surface if highly reactive metals are

used. Cathodic dissolution can occur, due to a highly basic local environment caused by hydroxl ion formation at the cathode (Picard et al., 1999). Using cathodes made from inert metals, or metals that oxidize slowly, or using an ac generator, can overcome this problem (Ivanishvili et al., 1987).
The theoretical dosage of the active metal ions can be calculated using the second Faraday's law which describes a linear relationship between current intensity and the amount of metal dissolved:

$w = ItM/Fn\bar{e}$ (1)

w is the weight of the metal generated (gr), I the current intensity (A), t the time (sec), M the molecular weight of the metal (gr/mol), F Faraday's constant (96485 C/mol), $n\bar{e}$ the number of electrons involved in the reaction.

EF using aluminum as coagulant:

The redox reactions that occur with aluminum anodes are described in Eqs. (2)-(4):

(-) Cathode: $2H_2O + 2e^- \rightarrow H_{2\,(g)} + 2OH^-_{(aq)}$ (2)

(+) Anode: $2H_2O \rightarrow O_{2\,(g)} + 4H^+_{(aq)} + 4e^-$ (3)

(+) Anode: $Al_{(s)} \rightarrow Al^{3+}_{(aq)} + 3e^-$ (4)

In the case of Al^{+3}, the water molecules in the primary hydration shell are polarized because of the high charge on the metal ion, leading to their replacement by hydroxyl ions. This results in the formation of aluminum hydroxide mononuclear species, which have a lower positive charge as described by Eqs. (5)-(8).

$Al^{+3}_{(aq)} + H_2O \rightarrow AlOH^{+2}_{(aq)} + H^+_{(aq)}$ (5)

$AlOH^{+2}_{(aq)} + H_2O \rightarrow Al(OH)_2^+{}_{(aq)} + H^+_{(aq)}$ (6)

$Al(OH)_2^+{}_{(aq)} + H_2O \rightarrow Al(OH)_{3(s)} + H^+_{(aq)}$ (7)

$Al(OH)_{3(s)} + H_2O \rightarrow Al(OH)_4^-{}_{(aq)} + H^+_{(aq)}$ (8)

The hydrolysis proceeds as the pH is increased, giving first the doubly- and single-charged cationic species and then uncharged aluminum hydroxide, $Al(OH)_3$, which is of very low solubility and precipitates at intermediate pH values. With further increase in pH, the soluble anionic form $Al(OH)_4^-$ becomes dominant.

It is known that dimeric, trimeric and polynuclear hydrolysis products of Al^{+3} can form, although these can often be ignored, especially in dilute solutions, and may not affect the overall speciation. The complexity of the aqua-aluminum system is neither completely understood nor completely quantified (O'Melia, 1972; Sposito, 1996; Letterman et al, 1999; Duan and Gregory, 2003). This paper will assume that mononuclear hydrolyzed species adequately predict aluminum hydroxide precipitation.

EF and coagulation mechanisms

Coagulation mechanisms depend primarily on factors such as pH and coagulant dosage, which govern speciation of the active mononuclear species (Amirtharajah and O'Melia, 1990). In EF the current in fact has a "double" affect on the speciation and consequent coagulation mechanisms – it both governs the dissolution of aluminum into the system, and also causes the pH to rise. Unlike conventional coagulation, the speciation in this environment is in constant transition, until the current is stopped, enabling the pH to stabilize and the species to reach equilibrium. This causes the coagulation mechanisms to shift throughout the process, depending on the speciation at each given time. Moreover, in EF the dosing regime is an additive process over time in which negative counter-ions are not introduced. Negative counter-ions influence the metal hydrolyzed species, which are coordinated with hydroxyl ions, because they can replace the hydroxyl, thereby changing the charge of the active species (Duan and Gregory, 2003). The absence of these counter-ions can affect the coagulation mechanism which depends on the types of species present in solution. The hydrolysis, in addition to raising the pH, also produces hydrogen gas at the cathode and oxygen gas at the anode which form micro-bubbles and could be a steric factor affecting aggregate growth. It is also possible that the electrical field imposed could affect ion and particle transport.

ζ potential and coagulation

In the most basic case, the net inter-particle force between primary particles is governed by the sum of the attractive van der Waals and the repulsive electrical double layer forces, as defined by the DLVO theory (Derjaguin and Landau, 1941; Verwey and Overbeek, 1948). The ζ potential depends on the potential at the surface of the particle and the composition of the Stern layer (Lyklema et al., 1978).It is an indirect measurement of the charge on particles, and its value determines the extent of the electrostatic forces of repulsion between charged particles, which indicates the extent of stability of the suspension. These forces change with the addition of a coagulant, and the ζ potential serves as a destabilization indicator.

Aggregate characteristics and morphology

The characteristics of the aggregates formed in the process are a key factor in understanding the mechanisms of EF. Fractal mathematics enables the representation of the apparently wild, complex structures of aggregates by simple parameters known as fractal dimensions (Mandelbrot, 1975). The expression which describes the whole concept of fractal structure is:

$N_l \alpha l^{-D}$ (9)

N_l = number of particles

l = diameter of sphere

D = (number) fractal dimension

An object can be defined as fractal, with a fractal dimension, D, if N_l asymptotically grows as l^{-D} when $l \rightarrow 0$. For linear, planar and three dimensionally compact objects, the exponent D, will have maximum values of 1, 2, and 3 respectively, while for porous aggregates (colloidal assemblages), D may take a fractional value. Aggregates are not really fractal in the strict sense of the word, since their scaling is only observed over a finite range of length scales and the fractal dimension can only be properly defined when using an asymptotic limit to infinitely small lengths. Therefore, aggregates are not true fractals but can be referred to as natural fractals (Jullien and Botet, 1997). Much research has been conducted on the fractal dimension of aggregates in various systems (Forrest and Witten, 1979, Tambo and Watanabe, 1979; Klimpel and Hogg, 1986; Oles, 1992) and the effect of structure on growth (Kusters et al., 1997). Assumptions have been made that aggregation behavior is independent of the detailed chemical nature of the colloid system (Lin et al., 1989), although certain colloid systems have been found to deviate from this universality, depending on the way the aggregation was induced (Zhang and Buffle, 1996).

Fractal analysis is used in this research in conjunction with morphology analysis and particle size distribution to gain a comprehensive analysis of the aggregates formed in the EF process.

2. Materials and Methods

Colloidal suspension

0.3gr of kaolin ($AlSi_2O_5(OH)_4$) was suspended in 20 liters of distilled water (15mg/l final concentration) and homogenized using an Ultraturax 2000. 1.66gr of $NaHCO_3$ was added (final concentration 83mg/l), the pH was corrected to 5 and 6.5 with NaOH or H_2SO_4, and conductivity was increased with $NaNO_3$.

EF cell

An EF unit which can be operated as a batch or continuous unit was designed (fig 1.).It consisted of a cylindrical plexyglass shell, with a volume dimension of 77.64cm^3 (H=6.5cm, D=3.9cm) and two concentric electrodes, inserted one inside the other, creating a space into which water could flow to be treated. The outer electrode (H=6.5cm, D=3.8cm) was stainless steel and served as the cathode. The inner electrode was aluminum, which was the anode (H=6.5cm, D=1.8cm). The anode was perforated with 28 holes, each with a diameter of 0.5cm, leaving an effective anode area of 31.27cm^2. Through the anode a baffle was fitted, which was connected to a motor, powered by an external power source. Adequate mixing conditions were created within the cell due to the holes

perforated through the anode. The electrodes were connected to a DC external power source .The cell was used in all experiments as a batch cell.

Particle Size Analysis

Particle size distribution (PSD) measurements were performed over a range of 2μm-300μm, using a HIAC Royco Liquid Particle Counting System.

Aggregate morphology/fractal dimension

The aggregates resulting from the process were photographed using an Olympus DP70 digital camera which was mounted on a Reichart microscope. Morphological characterization of suspended aggregates is a microscopic technique which is complementary to macroscopic methods for characterizing flocculated suspensions. Image analysis was used to morphologically characterize the resulting aggregates (i.e primary kaolin particles vs. aluminum hydroxide floc) and for quantifying their structure using a two-dimensional fractal dimension (D_2). To calculate D_2, the images were processed using standard software (photoshop), and then were analyzed using NIH-Image software which uses the box counting method. The fractal dimension measured by this technique is:

$D = \lim_{L \to 0} - \log(N)/\log(L)$ (10)

N is the number of squares required to cover the object, and L is the resolution or size of the square. Plotting the number of squares against the resolution on a log-log plot returns the fractal dimension of the aggregate. One image (one aggregate) was used for each analysis, following application of thresholding. Several images were acquired for each measurement and the fractal dimensions obtained are based on an average of 7-8 aggregates.

ζ Potential

The ζ potential of the post electroflocculated suspension was measured using a Malvern Zetamaster S. Each result was an average of three readings.

Experimental Procedure

The cell was filled with the kaolin suspension, a velocity gradient (G) was set ($0sec^{-1}$, $10sec^{-1}$ or $30sec^{-1}$), and a current was applied for 1min. The G values were chosen according to typical values used for slow mixing in lab apparatus and larger scale systems. The suspension underwent an additional 5 min mixing, after which a sample of the effluent was taken for analysis. The cell was operated in galvanostatic mode: the current was set and the potential found its own value dependent on the system's overall resistance. This ensured coagulant production at a predetermined rate, defined by Faraday's law. The currents used for the experiments were 0.05A, 0.1A, 0.2A, 0.3A producing $1.6mA/cm^2$, $3.2mA/cm^2$, $6.4mA/cm^2$, $9.6mA/cm^2$ respectively. The current densities are in good accordance with figures reported in the literature (Holt et al, 2002; Mameri et al, 1998). The respective aluminum doses obtained were: 4mg/l, 8mg/l, 16mg/l, 24mg/l, for a dosing time of 1 min. Some experiments explored the effect of current density on the resulting aggregates, and these were carried out using 1/2 the current densities, and a dosing time of 2 min.

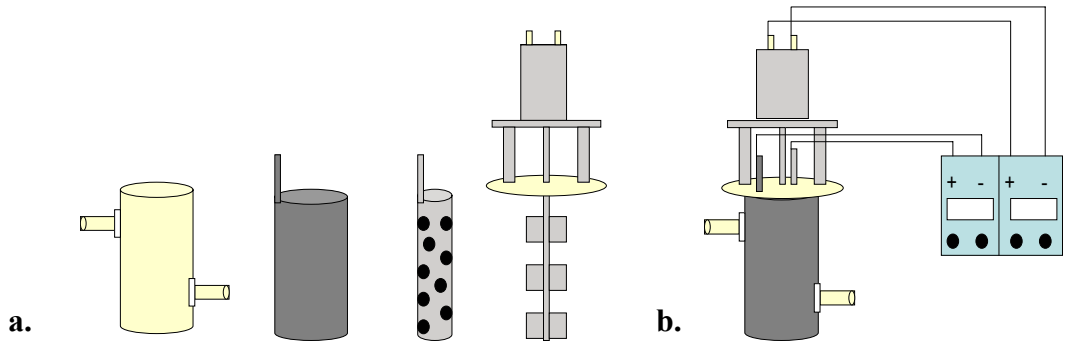

Fig.1: a. EF cell components: (from left to right) outer cell, outer electrode (stainless steel cathode), inner electrode (aluminum anode, perforated), mechanical baffle (with electrical motor). b. Components combined into EF cell and connected to DC power supply.

3. Results and Discussion

3.1 Characteristics of an electroflocculated kaolin suspension

Fig.2. shows the change in ζ potential and pH as a function of applied current for a 15mg/l kaolin suspension at two different initial pH values: 5 and 6.5. The ζ potentials of the kaolin suspensions, without applying any current, were: -17.9mV and -21.7mV for pH 5 and 6.5 respectively.

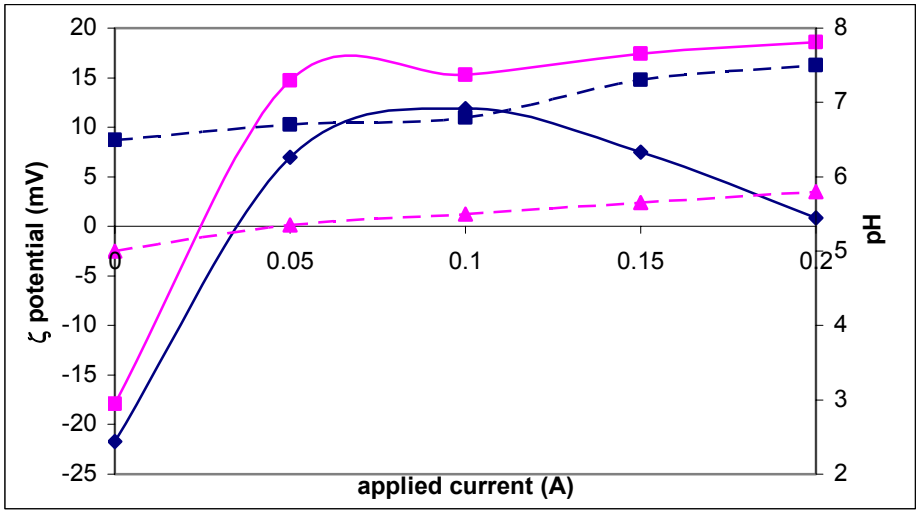

Fig.2. Change in ζ potential (solid line) and pH (dashed line) vs. applied current for initial pH 5 and 6.5. C_{kaolin}=15mg/l, conductivity=1mS/cm, $t_{dosing+mixing}$=6min, G=30sec^{-1}

The dynamic conditions EF creates cause coagulation mechanisms to shift, depending on the current applied. The rise in pH and consequent shifting speciation of aluminum mononuclear complexes, changes the ζ potential which serves as an indicator for coagulation efficiency.

At pH 5 the governing aluminum mononuclear species in solution are Al^{+3} and $Al(OH)^{2+}$ (Duan and Gregory, 2003), and it is assumed that dominant coagulation mechanism is adsorption and charge neutralization. Therefore, the ζ potential of the suspension under these conditions becomes more positive as a function if the applied current, until stabilizing at +17mV, for an applied current of 0.1A and above (within the measured range). At 0.1A, the pH rises to 5.7 and conditions become favorable for aluminum hydroxide ($Al(OH)_3$) precipitation (transition to "sweep-floc"). $Al(OH)_3$ is charged positively below its iso-electric point (i.e.p, between 8-9), and therefore in the precipitation zone the ζ potential stabilizes at a positive value. Increased $Al(OH)_3$ precipitation stabilizes the pH due to the removal of the excess hydroxyl ions from solution. This coagulation mechanism combines both destabilization and transport processes.

At pH 6.5 the governing coagulation mechanism is "sweep-floc", as at this pH formation of amorphous $Al(OH)_3$ is considered optimal. At this pH other positive mononuclear species, Al^{+3} and $Al(OH)^{2+}$, are also present, although in reduced amounts. These contribute to the charge neutralization and ultimately charge reversal, indicated by the change in ζ potential towards more positive values, reaching a maximum of +12mV, at 0.1A (fig. 2.). At currents higher than 0.1A, a drop in the ζ potential occurs, and its value becomes less positive. At 0.2A, at a final pH of 7.5, the ζ potential reaches an i.e.p, due to the presence of negative mononuclear species which counteract the effect of the positive species in solution. At 0.1A, the pH is 6.8. At currents above this the pH increases even more and speciation shifts towards $Al(OH)_4^-$ - indicated by the less positive ζ potential.

3.2 Effect of mixing conditions in EF process

Experiments were conducted at pH 5, without applying a G (G=0sec^{-1}) and these produced suspensions with a higher final pH, than those treated applying a G (fig. 3).

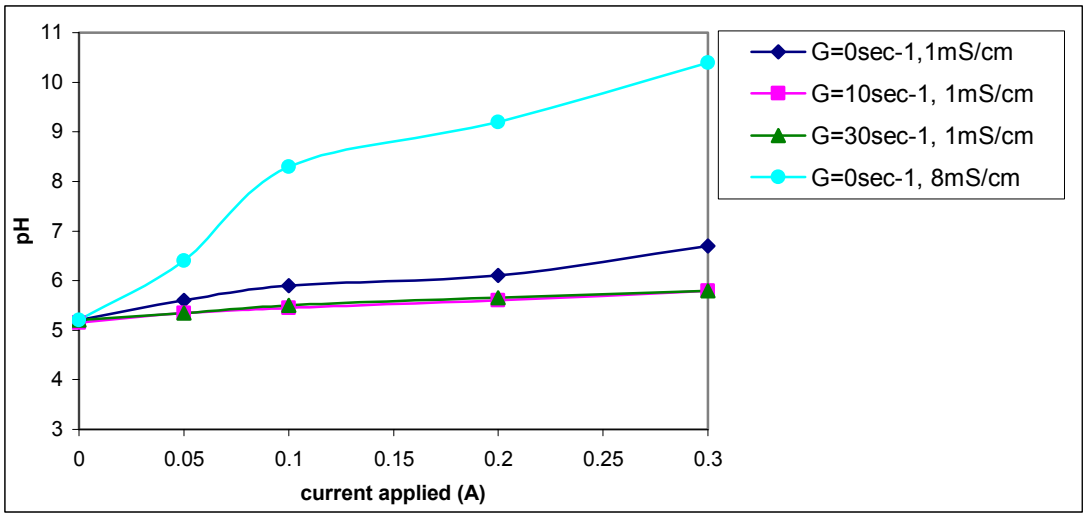

Fig.3. Change in pH vs. applied current, for varying velocity gradients.
C_{kaolin}=15mg/l, conductivity=1mS/cm, 8mS/cm, $t_{dosing+mixing}$=6min, initial pH 5.

For conductivity values of 1mS/cm, and G of both $10sec^{-1}$ and $30sec^{-1}$ a similar result is obtained, the final pH not exceeding 6, for the maximum current used, 0.3A. However, the pH rises to 6.6, when a G is not applied ($G=0sec^{-1}$). For high conductivity values (8mS/cm), the rise in pH was even more substantial for $G=0sec^{-1}$ (fig.3.), reaching 10.1 at 0.3A, for initial pH 5. Applying a G ($10sec^{-1}$ and $30sec^{-1}$) did lower the pH to similar values shown in fig.3 for 1mS/cm suspensions. The significant increase in pH at high conductivities, when mixing conditions aren't imposed, is most likely due to a screening effect other charged particles produce when in high concentration in solution. If other ions are present in large concentrations, the aluminum ions at the anode and the hydroxyl ions at the cathode won't be able to diffuse across the solution and come in contact efficiently, because a dense barrier of other ions exists between them. Mixing "breaks" this barrier and enables efficient contact, thus resulting in $Al(OH)_3$ precipitation and a lower final pH. The application of a G is a key factor in maintaining a relatively stable pH throughout the EF process. The effect of mixing conditions on $Al(OH)_3$ precipitation has been studied in some detail by Clark et al. (1993), who has indicated that with more intense mixing, precipitation would be favored.

3.3 Aggregates formed in EF

Fig.4. shows types of aggregates obtained after EF (magnification x10).

The visible data shows distinct differences between aggregates, both in morphology and in size, obtained under different EF conditions. In general, a difference is evident between kaolin aggregates and $Al(OH)_3$ flocs. The former has a dense, compact structure, and the latter a more open, loose structure. Under control conditions, without applying current or velocity gradient (a.), the primary kaolin particles appear dispersed. Some minor aggregation of primary kaolin particles has occurred (indicated by larger black clusters). This can probably be explained by a degree of Brownian diffusion occurring, coupled with double layer compression (Verwey and Overbeek, 1948) promoted by the addition of electrolyte ($NaNO_3$) to achieve adequate conductivity values (minimum 1mS/cm) for operation of the EF cell. Applying a current and G induces flocculation which results in precipitation of $Al(OH)_3$ and formation of flocs which enmesh the primary kaolin particles. These flocs increase in size as the current increases (b. and c.). At initial pH 5 (as shown in fig.4), raising the current shifts the coagulation mechanism from adsorption and charge neutralization more towards sweep-floc, because the pH shifts to values which favor $Al(OH)_3$ precipitation. Under these conditions, a higher current will increase precipitation of $Al(OH)_3$ and consequently larger flocs will form. For higher conductivity values (8mS/cm), significant kaolin aggregation occurs, and no precipitation is observed, when a current is applied alone (d.), without applying a G. The high level of electrolyte in solution, coupled with the aluminum dose has most likely lowered the repulsion

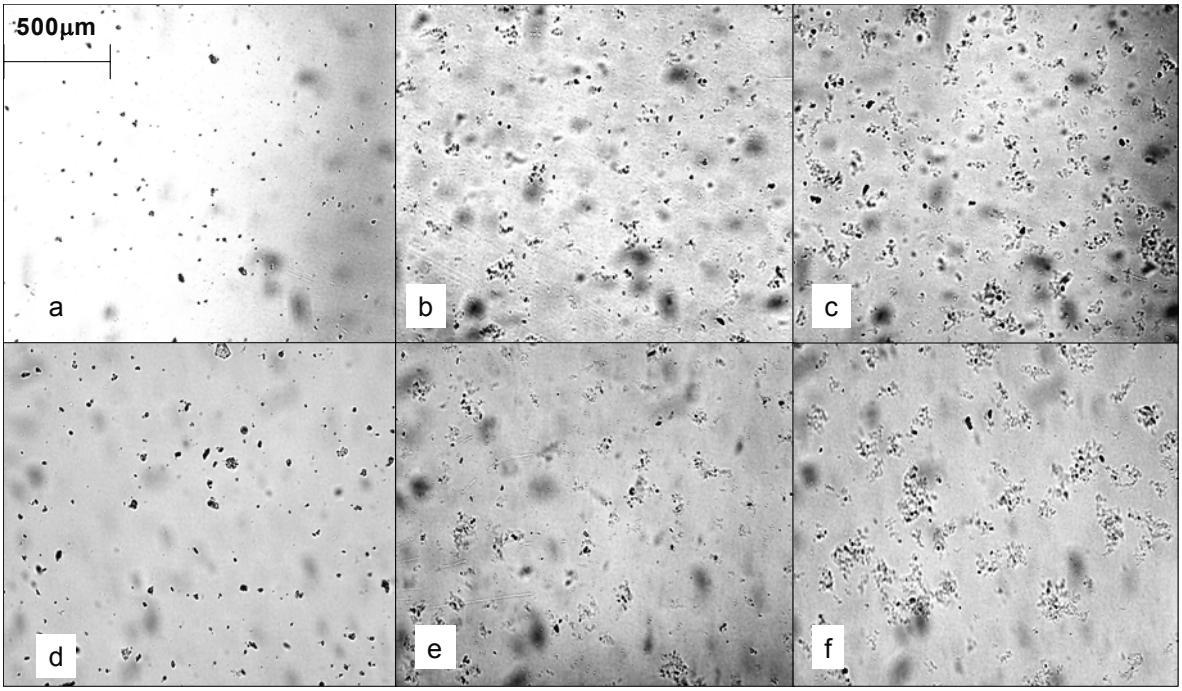

Fig.4: **a.** pH 5, 1mS/cm, 0A, G=0sec^{-1} **b.** pH 5, 1mS/cm, 0.05A, G=30sec^{-1} **c.** pH 5, 1mS/cm, 0.1A, G=30sec^{-1} **d.** pH 5, 8mS/cm, 0.1A, G=0sec^{-1} **e.** pH 5, 8mS/cm, 0.1A, G=10sec^{-1} **f.** pH 5, 8mS/cm, 0.3A, G=10sec^{-1}

barrier between primary particles, and enabled aggregation. Some aggregates observed are large in size (up to 50μm), and considering the time span of the experiments, it is unlikely Brownian diffusion is the primary transport mechanism. This raises questions regarding the effect of the electric field on particle transport in the EF process, which could explain the enhanced kaolin aggregation without applying a G. For high conductivity values, when both current and G are applied, similar results to those at lower conductivity values are obtained, and increased $Al(OH)_3$ precipitation is observed (e. and f.). At pH 6.5, for all currents, with application of a G, $Al(OH)_3$ precipitation was observed. Moreover, floc size increased with current increase. At pH 6.5, the dominant coagulation mechanism is sweep-floc, for all currents applied. Although speciation shifts towards negative mononuclear species at the higher currents (0.2A, 0.3A produce a final pH of 7.3 and 7.5 respectively), increased precipitation occurs at the beginning of the process, due to the large amount of Al^{+3} introduced into solution. Despite the existence of negative mononuclear species at the end of the process, their effect on coagulation is negligible, because $Al(OH)_3$ flocs have already formed extensively.

3.3.2 Fractal Dimension

The fractal dimension of aggregates/flocs in the experiments was based on imaging, and therefore is two-dimensional and is referred to as D_2. The fractal dimension was used to quantify aggregate/floc structure, and subsequently served as a mathematical parameter for tracking differences between aggregates formed in different experiments, resulting from varying operational parameters, such as applied current (Al^{+3} dose), current density, pH, conductivity and G. Table 1. summarizes the results.

Current (A)	Al^{+3} Dose (mg/l)	Current Density (mA/cm^2)	G (sec^{-1})	Conduct. (mS/cm)	T_{dose} (min)	pH	Ave. Fractal Dimension (D_2)	Standard Deviation
0	0	0	0	1	1	5	1.68	0.04
			10				1.70	0.07
			30				1.62	0.09
0.05	4	1.6	0	1	1	5	1.68	0.09

			10				1.46	0.05
			30				1.52	0.08
0.1	8	3.2	0	1	1	5	1.68	0.08
			10				1.51	0.06
			30				1.48	0.04
0.2	16	6.4	0	1	1	5	1.67	0.05
			10				1.48	0.07
			30				1.39	0.01
0.3	24	9.6	0	1	1	5	1.60	0.06
			10				1.52	0.07
			30				1.45	0.08
0	0	0	0	1	1	6.5	1.64	0.07
			10				1.64	0.05
			30				1.63	0.07
0.05	4	1.6	0	1	1	6.5	1.65	0.11
			10				1.57	0.09
			30				1.48	0.03
0.1	8	3.2	0	1	1	6.5	1.67	0.07
			10				1.49	0.04
			30				1.48	0.05
0.2	16	6.4	0	1	1	6.5	1.68	0.04
			10				1.51	0.05
			30				1.45	0.04
0.3	24	9.6	0	1	1	6.5	1.50	0.04
			10				1.48	0.06
			30				1.51	0.04
0.025	4	0.8	10	1	2	5	1.51	0.04
			30				1.50	0.06
0.05	8	1.6	10	1	2	5	1.48	0.07
			30				1.46	0.05
0.1	16	3.2	10	1	2	5	1.47	0.05
			30				1.44	0.04
0.15	24	4.8	10	1	2	5	1.43	0.06
			30				1.41	0.05
0	0	0	0	8	1	5	1.66	0.09
			10				1.59	0.07
			30				1.67	0.05
0.05	4	1.6	0	8	1	5	1.70	0.08
			10				1.50	0.06
			30				1.51	0.05
0.1	8	3.2	0	8	1	5	1.65	0.04
			10				1.47	0.07
			30				1.46	0.05
0.2	16	6.4	0	8	1	5	1.61	0.08
			10				1.46	0.04
			30				1.43	0.07
0.3	24	9.6	0	8	1	5	1.65	0.06
			10				1.48	0.03
			30				1.42	0.1

Table 1: Average two-dimensional (D_2) fractal dimensions obtained for different operational parameters.

The values obtained without applying a G are similar for most experiments, and are between 1.60$\pm$0.06 and 1.70$\pm$0.08. These are representative of kaolin aggregation in a dilute electrolyte, as in these conditions $Al(OH)_3$ precipitation is limited as no mixing is induced. However, at pH 6.5 and 0.3A, the D_2 calculated is low compared to these values – 1.50$\pm$0.04.This can be explained by the fact that the high Al^{+3} dosage and pH have created some degree of $Al(OH)_3$ precipitation, despite absent mixing conditions. This is probably via diffusion, as large amounts of Al^{+3} and OH^- ions are

created in these conditions. The more open and loose structure which characterize $Al(OH)_3$ flocs, as opposed to kaolin aggregates, is the reason for the lower average D_2. In general, a trend is observed in which D_2 decreases as the current increases, when a G is applied, although differences obtained from 0.05A and above are not significant. Moreover, t-tests comparing D_2 values obtained for different currents between sets (i.e. different currents at same G), both at pH 5 and 6.5, indicated that these differences are indeed not appreciable ($P>0.05$). Fig. 5 shows the differences in D_2 obtained at pH 5, as a function of applied current and G.

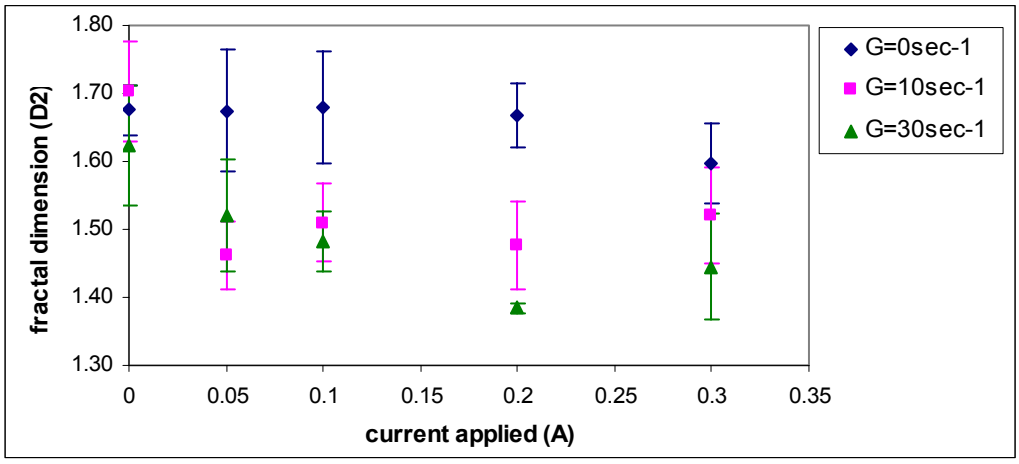

Fig.5. Fractal dimension, D_2, vs. current intensity, for different G values, pH 5, 1mS/cm. Error bars represent one standard deviation.

D_2 for all currents applied, in the absence of mixing conditions, does not significantly change, and is between 1.60 ± 0.06 and 1.68 ± 0.09. Application of a G does lower the resulting average D_2, because mixing induces precipitation and floc formation. There is not an appreciable difference (based on t-tests) between D_2 values, when applying a G, for all currents. Therefore, the resulting D_2 values for $G=10sec^{-1}$ or $G=30sec^{-1}$ are considered similar. For a doubled dosing period (2 min), there appears to be a more distinct difference between D_2 values obtained for different currents. For currents of 0.025A and 0.15A, and $G=10sec^{-1}$, the resulting D_2 values were 1.51 ± 0.04 and 1.43 ± 0.06, respectively. Therefore, for an increased dosing period (2 min), lower currents produced higher D_2 values, than for higher currents. When comparing current densities, for 1min and 2 min dosing, no significant differences are observed. For different current densities and identical doses, a trend is observed, at higher dosage levels: lower current densities produced lower D_2 values. To achieve equivalent doses using half current densities, a doubled dosing period was required. In these conditions, despite the lowered dissolution rate of Al^{+3} ions (mg/sec), the ions first dissolved have a longer effective time to react in solution. This could lead to better growth and consequently larger flocs exhibiting lower D_2 values.

When comparing D_2 values obtained from suspensions with different conductivities (1mS/cm vs. 8mS/cm), some differences are observed for 0.1A and 0.2A, when mixing was not applied ($G=0sec^{-1}$). Fig.6. shows the shows the differences in D_2 obtained at pH 5, for different conductivities, as a function of applied current, with and without applying a G.

The differences in D_2, between 1mS/cm and 8mS/cm, obtained for $G=0sec^{-1}$ and currents of 0.1A and 0.2A are directly related to the morphology of the kaolin aggregates, which do form even though mixing was not applied. The average D_2 obtained under these conditions is lower for 8mS/cm than for 1mS/cm. T-tests, comparing D_2 values obtained for same currents between sets (i.e. comparing 0.1A at 1mS/cm and 8mS/cm, at constant G), yielded probability values which indicated that differences could not be significant. However, one cannot ignore the images obtained under these conditions which show distinct differences in kaolin aggregation, as a function of conductivity. This

underlines the advantage of using image analysis techniques as a complementary technique to other macro techniques, for verifying the true nature of aggregates/flocs formed. Fig.7 shows the differences between images obtained after EF of suspensions with different conductivities (magnification x10).

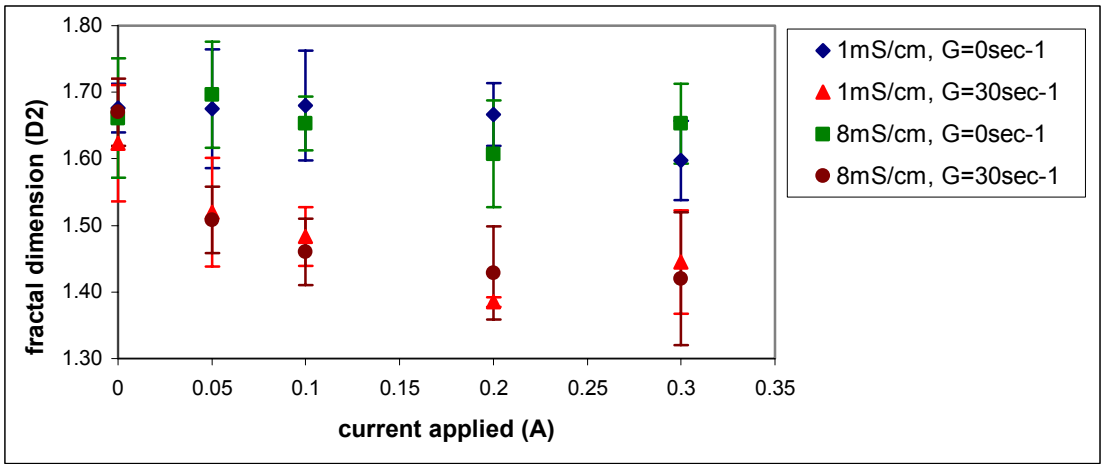

Fig.6. Fractal dimension, D_2, vs. current intensity, for G=0sec^{-1} and 30sec^{-1}, pH 5, 1mS/cm and 8mS/cm. Error bars represent one standard deviation.

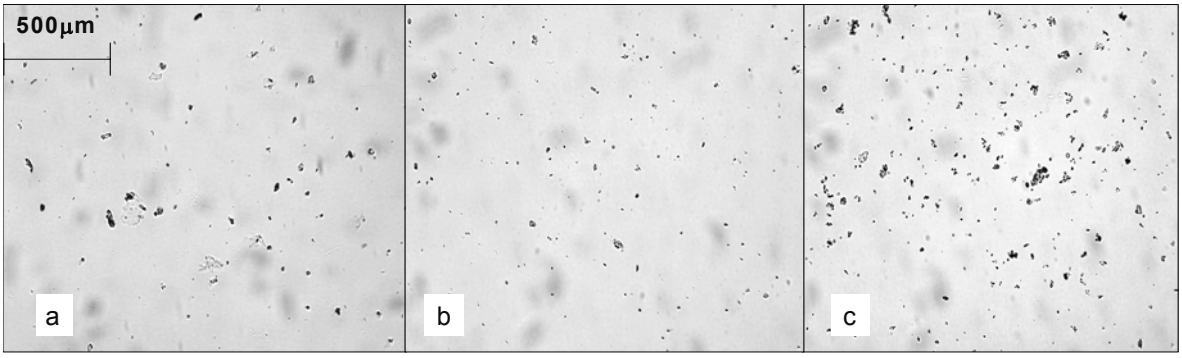

Fig.7. **a.** pH 5, 1mS/cm, 0.1A, G=0sec^{-1} **b.** pH 5, 8mS/cm, 0.05A, G=0sec^{-1} **c.** pH 5, 8mS/cm, 0.1A, G=0sec^{-1}

The images indicate that for higher conductivity values (8mS/cm), significant kaolin aggregation occurs, when a current is applied alone, without inducing mixing conditions. Minor $Al(OH)_3$ precipitation is observed, but evidently not sufficient to promote growth of flocs. The high level of electrolyte in solution, at 8mS/cm, coupled with an adequate aluminum dose (0.1A) has promoted flocculation via double layer compression and/or adsorption and charge neutralization. However, the size of the resulting aggregates (some up to 50µm) and the relatively short time span of the experiments (6 minutes total), pose questions regarding the primary transport mechanism which has enabled aggregation in these conditions – without inducing mixing conditions. Brownian diffusion exists, but it is unlikely it serves as the sole transport mechanism, enabling aggregation into large aggregates, within a short period of time. In EF, an electric field is induced, while the current passes through the cell. This could enhance particle transport which would explain the enhanced kaolin aggregation occurring without application of a G. For 8mS/cm, when both current and G are applied, transport via diffusion becomes negligible and similar D_2 results to those at lower conductivity values are obtained as increased $Al(OH)_3$ precipitation is observed.

Little literature exists on D_2 values of resulting aggregates/flocs in flocculation processes using alum; none exists on aggregates/flocs formed in EF. Gorczyca and Ganczarczyk (1996) reported D_2

values for alum flocs formed in inorganic clay and mineral suspensions to be between 1.71 and 1.97 (±0.05). Li and Ganczarczyk (1989) calculated fractal dimensions of alum flocs to be between 1.59 and 1.97, from measurements conducted by Tambo and Watanabe (1979). Chakraborti et al. (2003) found the D_2 values of flocs formed by flocculation of latex particles with alum to be between 1.94±0.18 and 1.48±0.08, depending on alum dose, shear rate, and observation times. Although some D_2 values of aggregates/flocs formed in the EF process fall within the ranges reported by authors, in general the values obtained after EF within the lower range. The unique physical-chemical conditions in EF, which differ from those created in conventional flocculation, affect coagulation/flocculation mechanisms and consequently the morphology of the resulting aggregates/flocs.

3.3.3 Particle Size Distribution

Particle size distribution analysis was carried out as a complementary procedure to image analysis, to maximize data on aggregate/floc formation in the EF process, and examine a connection between the fractal dimensions calculated and floc/aggregate size. From particle distribution measurements, a correlation can be observed between the D_2 and size. Fig.8. shows the undersize frequency % of sizes obtained at different currents (and densities) and dosing times.

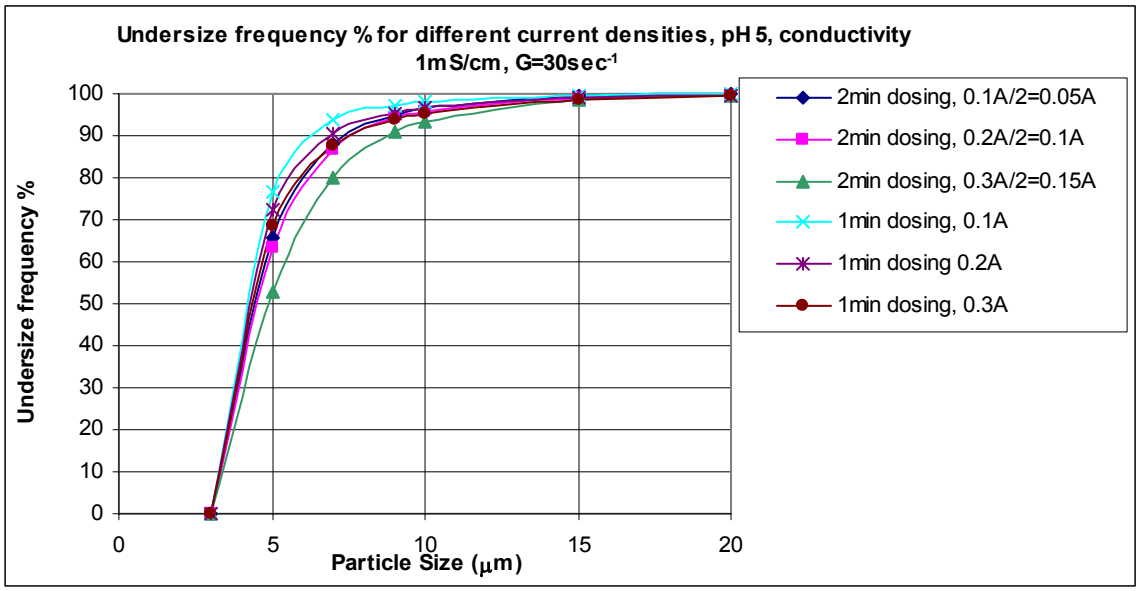

Fig.8. Undersize frequency %, pH 5, 1mS/cm, G=30sec^{-1}, varying currents (densities) and dosing times.

For 0.05A and 0.15A, a dosing period of 2 minutes, and G=30sec^{-1}, D_2 values were 1.46±0.05 and 1.41±0.05, respectively, although these differences are not considered significant. Particle size distributions show that for 0.15A, larger particles are obtained than for 0.05A. Thus, a trend can be detected in which lower D_2 values correspond to larger particle sizes. When comparing current densities, for equal total doses, a similar trend is observed. For a current density of 1.6mA/cm^2, 2 minutes dosing, the resulting D_2 value is 1.46±0.05. For 3.2mA/cm^2, 1 minute dosing, the average D_2 is 1.48±0.04. Particle counts show that higher current densities (shorter dosing periods) produce smaller sizes, which correspond to higher D_2 values.

When observing particles counts conducted on suspensions with different conductivities, without the application of a velocity gradient, the same trend is observed: larger particles produce smaller D_2 values. Fig.9. shows the undersize frequency % of sizes obtained at different currents for suspensions with different conductivities. For 0.2A, larger particles are observed at 8mS/cm than at 1mS/cm. In these conditions, the corresponding D_2 values were 1.61±0.08 and 1.67±0.05,

respectively. Although the differences in average D_2 obtained for different conductivities are not considered significant, a correlation is observed, which also corresponds to image analysis results. The connection between floc size and fractal dimension is typical of forming aggregates (Spicer and Pratsinis 1996; Kusters 1997; Chakraborti 2003). Aggregation models, which have been used to calculate theoretical fractal dimensions of aggregates are based on the assumption that primary

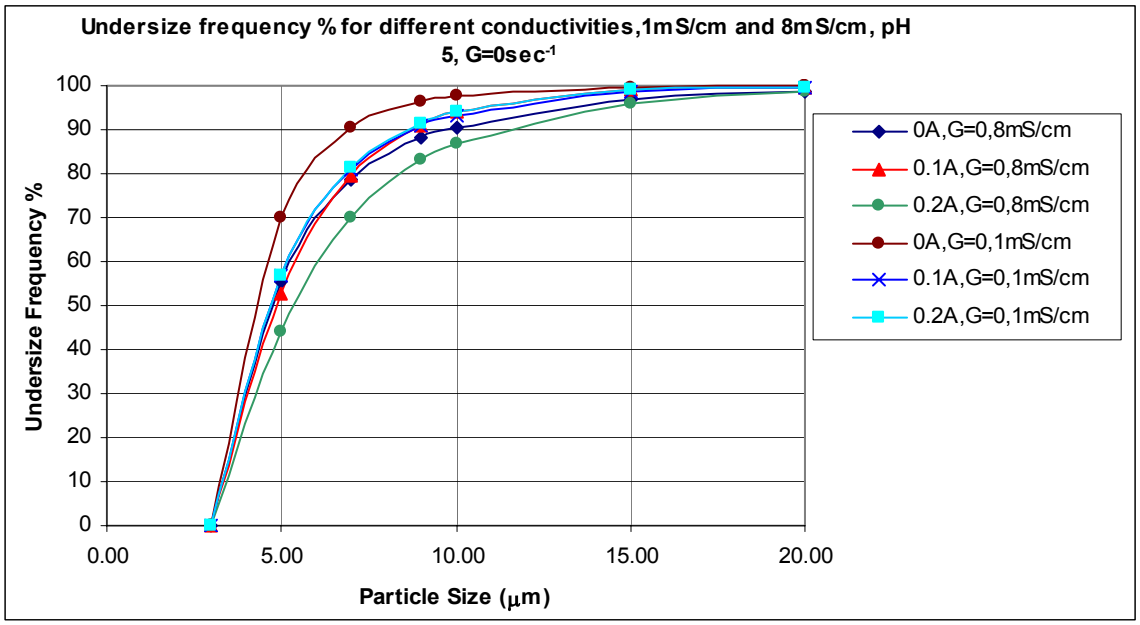

Fig.9. Undersize frequency %, pH 5, 1mS/cm and 8mS/cm, G=0sec^{-1}

particles are solid and have a fractal dimension of Euclidean value (i.e. D_2=2). In this case, as clusters begin to form, and aggregates grow, the fractal dimension will decrease as size increases, until a point where the aggregates are sufficiently large in comparison to the primary particles that comprise it (Meakin, 1988). At this point, any other addition of particles will not have an affect on structure, and the fractal dimension will not change.

4. Conclusions

1. EF is an alternative process to conventional flocculation, both are similar, but also somewhat different. These differences, small as they may be, are manifested in the chemical and physical characteristics of the treated suspension and resulting aggregates.
2. The final pH will always be higher than the initial pH, due to hydroxyl formation at the cathode. The pH increase can be controlled by applying a velocity gradient (G), which enhances aluminum hydroxide precipitation thus removing excess hydroxyl ions from the system. A low G (10sec^{-1}) is sufficient to create a relatively stable pH throughout the process.
3. The change in pH throughout the process causes a shift in the speciation of aluminum mononuclear species, and consequently a shift in the coagulation mechanisms. This is evident by the changes in ζ potential as a function of current, which is directly linked to the charge on the particles, and is indicative of the coagulant active species in solution.
4. The application of a current does have an apparent affect on particle transport. The electric field induced by passage of a current seems to affect aggregation, by enhancing particle transport. When lowering the diffusion barrier between primary particles, without inducing mixing conditions, aggregation of primary particles was observed when currents were applied. The extent of aggregation in these conditions is indicative of another transport mechanism other than Brownian diffusion.

5. Floc size increases as the current increases, as would be expected. Higher doses produce larger flocs, as also reported in conventional coagulation A higher current will increase precipitation of $Al(OH)_3$ (at pH 5 and 6.5) and consequently larger flocs will form.
6. The current density seems to affect floc growth, as lower current densities produced lower fractal dimension values for identical doses. This could be also a function of dosing periods, which were prolonged for lower current densities to achieve adequate total doses.
7. The fractal dimensions of the flocs obtained in EF are on average lower than those reported for conventional coagulation. This can be explained by the dynamic physical/chemical conditions EF generates including the changing speciation, rise in pH, bubble formation and the type of dosing regime.
8. A correlation exists between size and fractal dimension – lower fractal dimensions were obtained for larger aggregate sizes. This is consistent with flocculation models which have been developed based on conventional coagulation (i.e. Diffusion Limited Model (DLA) and its variants).

5. References

1. Adin, A. and Vescan, N. (2002) Electroflocculation for particle destabilization and aggregation for municipal water and wastewater treatment. Proceeding of the American Chemistry Society **42** (2), 537-541.
2. Amirtharajah, A. and O'Melia, C.R. (1990) Coagulation Processes: destabilization, mixing and flocculation. Water Quality and Treatment, New-York, McGraw-Hill.
3. Belongia, B. M., Haworth, P. D., Baygents, J. C., Raghavan, S. (1999) Treatment of alumina and silica chemical mechanical polishing waste by electrodecantation and electrocoagulation. Journal of The Electrochemical Society **146** (11), 4124-4130.
4. Chakraborti, R.K., Gardner, K.H., Atkinson, J.F., Van Benschoten J.E (2003) Changes in fractal dimension during aggregation. Water Research **37**, 873-883.
5. Clark, M.M, Srivastava, R.M., David, R. (1993) Mixing and aluminum precipitation. Environmental Science and Technology **27** (10), 2181-2189.
6. Derjaguin, B.V. and Landau, L., (1941) Theory of the stability of strongly charged lyophobic sols and of the adhesion of strongly charged particles in solutions of electrolytes. Acta Physicochim. URSS **14**, 633-662.
7. Do, J. S. and Chen, M. L. (1994) Decolorization of dye-containing solutions by electrocoagulation. Journal of Applied Electrochemistry **24**, 785-790.
8. Duan, J. and Gregory, J. (2003) Coagulation by hydrolyzing salts. Advances in Colloid and Interface Science **100-102**, 475-502.
9. Forrest, S.R. and Witten, T.A. (1979) Long-range correlations in smoke-particle aggregates. Journal of Physics A **12** (5), 109-117.
10. Gorczyca, B and Ganczarczyk J.J. (1996) Image analysis of alum coagulated mineral suspensions. Environmental Technology **17**, 1361-9.
11. Holt, P. K., Barton, G. W., Wark, M., Mitchell, C.A. (2002) A quantitative comparison between chemical dosing and electrocoagulation. Colloids and Surfaces A: Physicochemical Engineering Aspects **211**, 233-248.
12. Ivanshvili ,A. I., Przhegorlinskii, V. I. , Kalichenko, T. D. (1987) Comparative evaluation of the efficiency of electrocoagulation and reagent methods of clarifying wastewater. Soviet Journal of Water Chemistry and Technology **9** (5), 118-119.
13. Jullien, R. and Botet, R. (1987) Aggregation and Fractal Aggregates, Singapore: World Science
14. Klimpel, R.C. and Hogg, R. (1986) Effects of flocculation conditions on agglomerate structure. Journal of Colloid and Interface Science **113**, 121-131.

15. Kusters, K.A., Wijers, J.G., Thoenes, D (1997) Aggregation kinetics of small particles in agitated vessels. Chemical Engineering Science **52** (1), 107-121.
16. Letterman, R.D., Amirtharajah, A., O'Melia, C.R. (1999) Coagulation and Flocculation. In AWWA "Water Quality and Treatment", Letterman, R.D. (ed.)
17. Li, D., Ganczarczyk, J.J. (1989) Fractal geometry of particle aggregates generated in water and wastewater treatment processes. Environmental Science and Technology **23** (11), 1385-9.
18. Lin, M.Y., Lindsay, H.M., Weitz, D.A., Ball, R.C., Klein, R., Meakin, P. (1989) Universality in colloid aggregation. Nature **339**, 360-362.
19. Lyklema, J. (1978) Surface chemistry of colloids in connection with stability, Ives K. J. (Ed.). The Scientific Basis of Flocculation, Sijthoff and Noordhoff, The Netherlands.
20. Mameri, N., Yeddou, A.R., Louncin,i H., Belhocine ,D., Grib ,H., Bariou, B (1998) Defluoridation of Septentrional Sahara water of North Africa by electrocoagulation process using bipolar aluminum electrodes. Water Research **32** (5), 1604-1612.
21. Mandelbrot, B.B.(1975) Les Objets Fractals: Forme, Hasard et Dimension, Flammarion, Paris.
22. Matteson, M. J., Dobson, R. L., Glenn, R. W., Jr., Kukunoor, N. S., Waits, W. H. III., Clayfield, E. J. (1995) Electrocoagulation and separation of aqueous suspensions of ultrafine particles. Colloids and Surfaces A: Physicochemical Engineering Aspects **104**, 101-109.
23. Meakin, P. (1998) Fractal aggregates. Advances in Colloid and Interface Science. **28**, 249-331.
24. Mills, D. (2000) A new process for electrocoagulation. AWWA **92** (6), 34-43.
25. Mollah, A. Y. A., Schennech, R., Parga, J. R. and Cocke, D. L. (2001) Electrocoagulation (EC) – Science and applications. Journal of Hazardous materials **B84**, 29-41.
26. Oles, V.(1992) Shear-induced aggregation and breakup of polystyrene latex particles. Journal of Colloid and Interface Science **154**, 351-358.
27. O'Melia, C.R. (1972) Coagulation and flocculation. In Physicochemical Processes for Water Quality Control W.J., Weber Jr. (ed.), Wiley Interscience, New York.
28. Picard, T., Cathalifaud-Feuillade, G., Mazet, M., Vandensteendam ,C. (2000) Cathodic dissolution in the electrocoagulation process using aluminum electrodes. Journal of Environmental Monitoring **2**, 77-80.
29. Pouet, M. F. and Grasmick, A. (1995) Urban wastewater treatment by electrocoagulation and flotation. Water Science and Technology **31** (3-4), 275-283.
30. Spicer, P.T. and Pratsinis, S.E. (1996) Shear-induced flocculation: The evolution of floc structure and the shape of the size distribution at steady-state. Water Research **30** (5), 1049-1056.
31. Sposito, G. (1996) The environmental chemistry of aluminum. Second, CRC Press Ltd., Florida.
32. Tambo, N. and Watanabe, Y. (1979) Physical characteristics of flocs I: the floc density and aluminum floc. Water Research **13**, 409-419.
33. Verwey, E. J. W. and Overbeek, J. Th G. (1948) Theory of stability of lyphobic colloids, Elsevier, Amsterdam.
34. Vik, E. A., Carlson, D. A., Eikum, A. S., Gjessing, E. T. (1984) Electrocoagulation of potable water. Water Research **18** (11), 1355-1360.
35. Zhang, J. and Buffle, J. (1996) Multi-method determination of the fractal dimension of hematite aggregates. Colloids and Surfaces A: Physicochemical and Engineering Aspects **107**,175-187.

Size and structure evolution of kaolin-$Al(OH)_3$ flocs in the electroflocculation process: A study using static light scattering

T. Harif, M. Hai and A. Adin

Soil &Water Sciences Department, Faculty of Agricultural, Food and Environmental Quality Sciences, The Hebrew University of Jerusalem, POB 12, Rehovot 71612, Israel. E-mail: tharif@vms.huji.ac.il; dariels@pob.huji.ac.il; adin@vms.huji.ac.il

Abstract Electroflocculation (EF) is gaining recognition as an alternative process to conventional coagulation/flocculation. The electrical current applied in EF to generate the active coagulant species creates a unique chemical/physical environment in which competing redox reactions occur - notably hydrolysis. As such, hydroxyl is generated at the cathode which causes the pH to continuously rise and coagulation/flocculation mechanisms to shift. This impacts the formation of a sweep floc regime which relies on precipitation of metal hydroxide and its growth into floc. The size and structural evolution of kaolin-$Al(OH)_3$ flocs using static light scattering techniques was examined in aim of understanding kinetic aspects of the process. An EF cell was operated in batch mode and comprised of two electrodes - a stainless steel cathode (inner electrode) and an aluminum anode (outer electrode).The cell was run at constant current between 0.042A-0.22A, and analysis performed at different time intervals. The results show that EF is able to generate a range of flocs, exhibiting different growth rates and structural characteristics, depending on the conditions of operation. Growth patterns were sigmoidal with higher growth rates obtained for higher currents. The dependency of growth rate on current can be related to initial pH and a higher dependency was observed for initial optimal sweep floc regime. All flocs exhibited a fragile nature and undergo compaction and structural fluctuations during growth.
Keywords Electroflocculation; coagulation; aluminum; floc; structure; scattering exponent

1. Introduction

Electroflocculation (EF) can be considered an alternative to conventional coagulation/flocculation processes, although substantial differences between the two exist. EF generates active coagulant species in situ by electrolytic oxidation of an appropriate anode material, thus differing from the conventional process in which chemical coagulants such as metal salts or polymers and polyelectrolytes are used. The use of electrolysis creates a unique coagulation and flocculation environment as the dosing regime is additive over time, negative counter-ions are not introduced, and competing redox reactions occur simultaneously – the first and foremost being hydrolysis. With regard to coagulation/flocculation mechanisms, the applied current in fact has a "double" affect as it both governs the dissolution of metal coagulant into the system, and also causes the pH to rise, due to hydroxyl formation at the cathode, a product of hydrolysis. As coagulation mechanisms depend primarily on factors such as pH and coagulant dosage, which govern speciation of the active mononuclear species (Amirtharajah and O'Melia, 1990; Letterman et al., 1999), in EF the coagulation mechanisms shift throughout the process, depending on the speciation at each given time, until the current is stopped, enabling the pH to stabilize and the species to reach equilibrium. This has a profound impact on the generation of a stable sweep floc regime which is of utmost importance in particle removal in water treatment and relies on precipitation of metal hydroxide and its growth into floc.

Research into EF, although not extensive, has examined colloidal and organic matter removal (Vik et. al., 1984; Matteson et. al., 1995; Holt et al., 2002) and explored a wide range of applications such as urban and industrial wastewater treatment (Do and Chen, 1994; Pouet and Grasmick, 1995;

Belongia et. al., 1999; Mollah et. al., 2000; Adin and Vescan, 2002). However, in-depth research is still required into the mechanisms of coagulation and flocculation in EF, which are directly affected by the unique conditions the process creates. This study utilizes static light scattering techniques to measure the size and structural evolution of aluminum hydroxide flocs formed in EF, in aim of understanding kinetic aspects of the process.

EF technology and coagulants

In its simplest form, an EF reactor may be made up of an electrolytic cell containing one anode and one cathode. The anode metals most commonly used are aluminum or iron because when electrochemically oxidized they produce the most commonly used ionic coagulants, Al^{+3} and Fe^{+3} (or Fe^{+2}) respectively**.**

The redox reactions that occur with aluminum anodes are described in Eqs. (1)-(3):

(-) Cathode: $2H_2O + 2e^- \rightarrow H_{2\,(g)} + 2OH^-_{(aq)}$ (1)

(+) Anode: $2H_2O \rightarrow O_{2\,(g)} + 4H^+_{(aq)} + 4e^-$ (2)

(+) Anode: $Al_{(s)} \rightarrow Al^{3+}_{(aq)} + 3e^-$ (3)

In the case of Al^{+3}, the water molecules in the primary hydration shell are polarized because of the high charge on the metal ion, leading to their replacement by hydroxyl ions (Duan and Gregory, 2003) and the formation of aluminum hydroxide mononuclear species, which have a lower positive charge as described by Eqs. (4)-(7). The hydrolysis proceeds as the pH is increased, giving first the doubly- and single-charged cationic species and then uncharged aluminum hydroxide, $Al(OH)_3$, which is of very low solubility and precipitates at intermediate pH values.

$Al^{+3}_{(aq)} + H_2O \rightarrow AlOH^{+2}_{(aq)} + H^+_{(aq)}$ (4)

$AlOH^{+2}_{(aq)} + H_2O \rightarrow Al(OH)_2^+{}_{(aq)} + H^+_{(aq)}$ (5)

$Al(OH)_2^+{}_{(aq)} + H_2O \rightarrow Al(OH)_{3(s)} + H^+_{(aq)}$ (6)

$Al(OH)_{3(s)} + H_2O \rightarrow Al(OH)_4^-{}_{(aq)} + H^+_{(aq)}$ (7)

The solubility boundary denotes the thermodynamic equilibrium that exists between the dominant aluminum species and solid aluminum hydroxide, at a given pH. The minimum solubility, 0.03mg/l Al^{+3}, occurs at pH 6.3, with solubility increasing as the solution becomes more acidic or alkaline. Although dimeric, trimeric and polynuclear hydrolysis products of Al^{+3} can form, these can often be ignored, especially in dilute solutions, and may not affect the overall speciation. As such, this paper will assume that mononuclear hydrolyzed species adequately predict aluminum hydroxide precipitation.

Flocculation, floc size and structure

The classical expression by von Smoluchowski (1917) has formed the core of almost all subsequent research into flocculation modeling. The model he developed shows the rate of irreversible aggregation of flocs containing *i*- and *j*- number of particles, to form aggregates with *m*-particles, where $m=i+j$:

$$dn_m/dt = \tfrac{1}{2} \sum_{i=1,\, j=m-i}^{i=m-1} \alpha_{ij}\beta_{ij}n_i n_j - n_m \sum_{i=1}^{i=\infty} \alpha_{im}\beta_{im}n_i \qquad (8)$$

n_{ij} is the number concentration, α_{ij} and β_{ij}, are the collision efficiency and frequency, respectively. The basic simplifying assumptions for this equation (such as every collision is successful ($\alpha_{ij}=1$), monodispersity and both particle and floc are spherical) rendering its relevance to practical systems limited. As such, modifications have been added while taking into account the presence of short-ranged forces, $\alpha_{ij}<1$, polydispersity and floc structure (Jiang and Logan, 1991; Kusters et al., 1997).

Several phases of floc growth occur during flocculation. Initially, particle growth is dominant, in which particles combine by coagulation and their size increases rapidly. As flocculation continues the flocs form large, porous and open structures that are more susceptible to fragmentation by fluid shear (Tambo, 1991). After a characteristic time, a steady state is reached between aggregation and

fragmentation, characterized by an aggregate size distribution that does not change with time and is unique to each system (Spicer and Pratsinis, 1996). Aggregate structure has been found to impact the kinetics of the flocculation process, as a more open structure has a larger collision profile (Kusters et al., 1997). Moreover, porous aggregates are fragmented by fluid shear stresses more rapidly than compact mass equivalent particles (Potanin, 1991; Flesch et al., 1999). Aggregate restructuring can also occur, by re-aggregation of fragments or by shear interactions that rearrange the structure (Oles, 1992).

The structures of a range of aggregate types can be characterized using fractal mathematics (Mandelbrot, 1987), in which the expression of fractal dimension is used to describe the irregularity of a self similar form. One should note that in reality aggregates do not exhibit an exact fractal structure, and the fractal dimension is but a method of quantification, which gives an indication of aggregate compactness. The mass fractal dimension, D_f, describes the relationship between the characteristic length, l, of an aggregate and its mass M:

$$M \propto l^{D_f} \quad (9)$$

D_f can have values between 1 (a line of particles) to 3 (a compact sphere of particles).

The measurement of floc structure can be conducted using techniques such as static light scattering (Guan et al., 1998; Lo et al., 2000) and image analysis (Tence, 1986; Clark and Flora, 1991; Chakraborti et al., 2003). The former will be used in this research, and is considered advantageous due to the non- interfering nature of the technique, however, assumptions concerning data interpretation can be limiting (Thill et al., 2000).

Light Scattering Techniques

The basic principle of scattering techniques is that particles, when illuminated by a radiation source, will scatter secondary radiation in all directions due to reflection, refraction and diffraction. The scattering patterns are specific for different particle sizes, and they are influenced by the shape, homogeneity, the relative refractive index of particles to medium, and by the wavelength of the incoming radiation. These scattering intensities can be detected by a specific detector array and are translated into a measure of the particle size, according to available approximations that were developed for particles of different sizes and optical properties (Sorensen, 1997). The scattering patterns are related to the scattering angle in a way which can also be used to obtain information on the structure of the aggregates. The magnitude of the wave number or the momentum transfer, q, in relation to the scattering angle, θ, is (Sorensen, 1997):

$$q = (4\pi n/\lambda)\sin(\theta/2) \quad (10)$$

where θ is the scattering angle, λ is the *in vacuo* wavelength of the incident beam, and n is the refractive index of the medium. The inverse of this variable (q^{-1}) indicates the length scale of the scattering experiment.

The angular scattering intensity, I(q), of a fractal aggregate with no multiple scattering is the product of the form factor, P(q), which represents the scattered intensity function from a single primary particle, and the structure factor, S(q), that describes additional scattered intensity due to the spatial correlation between the particles in the aggregate:

$$I(q) \propto S(q)P(q) \quad (11)$$

The form factor, P(q), is constant at small q, so that I(q) solely depends on the aggregate structure at large length scales ($q^{-1} >> r_s$, primary particle/scatterer radius). The structure factor, S(q), is constant at large q, and therefore I(q) depends on the primary particles at the low length scale of the aggregate.

In the range of fractal geometry, S(q) is a power law function of the form (Thill et al., 2000):

$$S(q) \propto q^{-D_f} \quad (12)$$

For: $r_s << q^{-1} << \xi$, where r_s is the scatterer radius and ξ is the distance above which the mass distribution inside the aggregate cannot be considered fractal.

The above equation can be used for structural measurements if applying the Raleigh-Gans-Debye (RGD) approximation, which assumes that elementary units (primary particles) within the scattering body (aggregate) all scatter independently. The approximation is valid for non-absorbing particles in the limit that both:

$$|m-1| \ll 1 \qquad (13a)$$

$$(4\pi n/\lambda)L|m-1| \ll 1 \qquad (13b)$$

where m is the relative refractive index of the scatterers (primary particles) and L is the length of the scattering body (the diameter of the primary particles).

The measure of D_f assuming RGD approximation is acquired from the slope of the logarithmic plot of I(q) versus q. However, in reality the measured scattering intensity is in fact contributed to by all the aggregates in the scattering volume, and not only a single aggregate composed of equal sized particles as approximated by the scattering theories. Albeit in a dispersion all aggregates contribute differently to S(q) due to variation in their sizes (and therefore also in the validity limit ξ), and therefore the global slope of the structure factor is not strictly the fractal dimension. In light of this, the absolute slope of the logarithmic plot of I(q) versus q will be referred to as the scattering exponent (SE), as it may not necessarily represent the real mass fractal dimension of the aggregates. The SE, however, does still portray structural properties, and higher SE values will indicate more compact aggregates – and vice versa (Guan et al., 1998; Waite, 1999).

The system presented in this study represents a complex water system, thus the light scattering results presented for a mixture of aluminum hydroxide and kaolin should be interpreted with caution. However, for relatively narrow distributions, polydispersity effects are expected to be insignificant (Lawler, 1997; Bushell and Amal, 1998).

2. Materials and methods

Colloidal suspension

1.2gr of kaolin ($AlSi_2O_5(OH)_4$) was suspended in 20 liters of distilled water (60mg/l final concentration) and homogenized using an Ultraturax 2000.1.66gr of $NaHCO_3$ was added (final concentration 83mg/l), the pH was corrected to 5 and 6.5 with NaOH or H_2SO_4, and conductivity was increased to 1mS/cm with $NaNO_3$.

EF cell

An EF batch unit was designed (Fig. 1.).It consisted of a plexyglass cap, which could be fitted onto a 1 L chemical glass and to which the electrodes were attached. The inner electrode, the cathode, was made from stainless steel and concentric in form (H=10cm, D=2.5cm). It was fitted onto the arm of the magnetic stirrer, and stationary throughout all the experiments. The outer electrode, the anode, was made from aluminum and could be used in two sizes, for applying different current densities: a concentric electrode (H=10cm, D=9.5cm) and two separate electrodes, with a total effective area of 1/4 of the former electrode. The electrodes were connected to a DC external power source. Mixing conditions within the cell were achieved with the magnetic stirrer and a constant mixing speed of 145 rpm was used for all experiments.

Floc size and structure analysis

Size distributions and structural information of kaolin-$Al(OH)_3$ flocs were determined as a function of time using a Malvern Mastersizer Microplus, which ascertains size by analysis of forward scattered light. The size distribution data given by the instrument covers the size range of 50nm to 500μm.A He-Ne laser light (λ = 633nm) was passed through a 2.0mm-width measurement cell in which the sample flowed. The beam was converged by a 300mm focusing lens and 42 detectors enabling the collection of light scattered from 0.03^o to 46.4^o. The plane of polarization of the laser beam is parallel to the detector axis (vertical). Size distribution information was obtained using supplied software which uses Mie theory to develop a scattering pattern that matches the scattering pattern of the sample being measured. Information on distribution size is presented in this paper as the volume mean diameter:

$$D(V, 0.5) = \Sigma_i (V_i d_i)/\Sigma_i V_i \qquad (14)$$

Where V_i is the relative volume in size class i with mean class diameter d_i.
Information on floc structure was obtained by measuring the intensity of light (I) at all detectors and plotting log I versus log q (eq. 10). Information regarding the angles of the detectors and intensity correction data, based on the geometric configuration of the detectors, was supplied by Malvern Instruments.

Image Analysis

Image analysis was used in conjunction with scattering measurements as a complementary analysis to ascertain floc properties over time. The aggregates resulting from the process were photographed using an Olympus digital camera *model DP11* (3.0 mega pixel resolution) which was mounted on an Olympus Stereoscope *model SZX12*. All photographs were taken at magnification x 50.

ζ Potential

The ζ potential of the suspension was measured using a Malvern *Zetamaster S*. Each result was an average of three readings. It is an indirect measurement of the charge on particles, and its value determines the extent of the electrostatic forces of repulsion between charged particles which change with the addition of a coagulant.

Experimental Procedure

The EF apparatus was fixed onto a 1L chemical glass containing 800ml of kaolin suspension, the electrodes submerged in the suspension. A current was applied for various time intervals (3, 6 and 10 minutes) at the end of which samples were analyzed (for pH, size distribution, ζ potential and image analysis). The complete dose of aluminum was achieved at 10 minutes, for each applied current, after which additional aluminum was not introduced into solution. At this stage samples underwent continuous mixing and measurements were taken at two more time intervals: 15 and 20 minutes. For all size distribution measurements, the Malvern Microplus was operated at a gentle pump speed of 400, so to minimize disruption of floc structure. The EF cell was operated in galvanostatic mode: the current was set and the potential found its own value dependent on the system's overall resistance. This ensured coagulant production at a predetermined rate, defined by Faraday's law. The currents used for the experiments were 0.042A, 0.11A and 0.22A, yielding aluminum doses of 2.43mg/l, 6.48mg/l and 12.96mg/l respectively. These doses are equivalent to aluminum content in 30mg/l, 80 mg/l and 160 mg/l commercial alum (8.1% of the total molecule).Current densities were altered by changing the anode size. These are summarized in table 1.

Current applied	Current density (full anode)	Current density (1/4 anode)
0.042A	0.197mA/cm^{2}a	0.788mA/cm^2
0.11A	0.516mA/cm^2	2.062mA/cm^2
0.22A	1.031mA/cm^2	4.125mA/cm^2

Table 1. Current densities used for experiments.

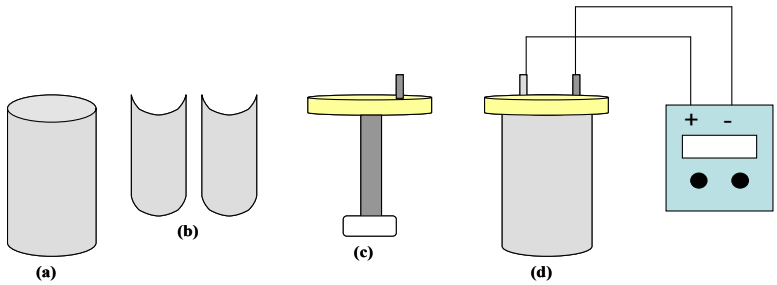

Fig.1. Components of the EF batch cell: a. Full aluminum anode (213.3cm^2) b. 2 aluminum anodes, 1/4 total area of full anode (53.33cm^2) c. Stainless steel cathode fitted onto magnetic stirrer arm and attached to plexyglass cap d. Complete EF apparatus fixed onto a 1L chemical glass.

3. Results and Discussion

Size distributions

The initial stages of floc growth in the EF process were examined. Unlike conventional flocculation, in EF the aluminum dosing is additive over time (until the current is stopped) while simultaneously generating hydroxyl ions. Aluminum super-saturation leading to aluminum hydroxide precipitation depends primarily on aluminum dose and pH (Sposito, 1996) and therefore in the initial stages of EF, mass is continuously being added to the system, as dosing continues and the pH rises. The employed initial pH values were chosen to cover the pH range in which aluminum hydroxide precipitation would occur and floc evolution could be measurable. Fig.2. shows the evolution of size distributions over time for currents of 0.042A and 0.22A (maximum anode area), at initial pH 5 and 6.5. The size distribution graphs show the evolution of size over time, with modal diameters at the end of the process reaching above 200μm, with the spread reaching the upper detection limit of the instrument. For 0.042A, the growth appears similar for the initial 3 minutes of the process, for both pH values, while after 6 minutes, at pH 6.5 it is accelerated, resulting in a wider distribution spread. This behavior is also evident for 0.22A - the initial 3 minutes show similar size distributions after which at pH 6.5 an accelerated growth rate is observed. The initial 3 minutes appear to be an induction period, in which the aluminum hydroxide precursor particles are developing into sizes which will lead to enhanced aggregation as the process progresses. This period is considerably shorter for 0.22A and pH 6.5, as after only 3 minutes sizes as large as 100μm are already observed. The size distributions indicate that while growth into larger floc is occurring, smaller particles are simultaneously being formed, and thus a wider distribution spread. For 0.042A and pH 5 the size distribution narrows after 15 minutes, whereas at pH 6.5 after 10 minutes. For 0.22A, this occurs at pH 5 and 6.5, after 10 and 6 minutes respectively. Although colloidal particles of aluminum hydroxide are continuously being formed until the current is stopped, at 10 minutes, their presence in solution, as colloidal matter, depends on contact opportunities. A higher number of particles would increase the number of collisions, leading to formation of larger particles and providing additional contact opportunities for the submicron particles (Chowdry et al., 1991). At pH 6.5 precipitation of aluminum hydroxide is considered optimal, therefore larger amounts of precursor particles are

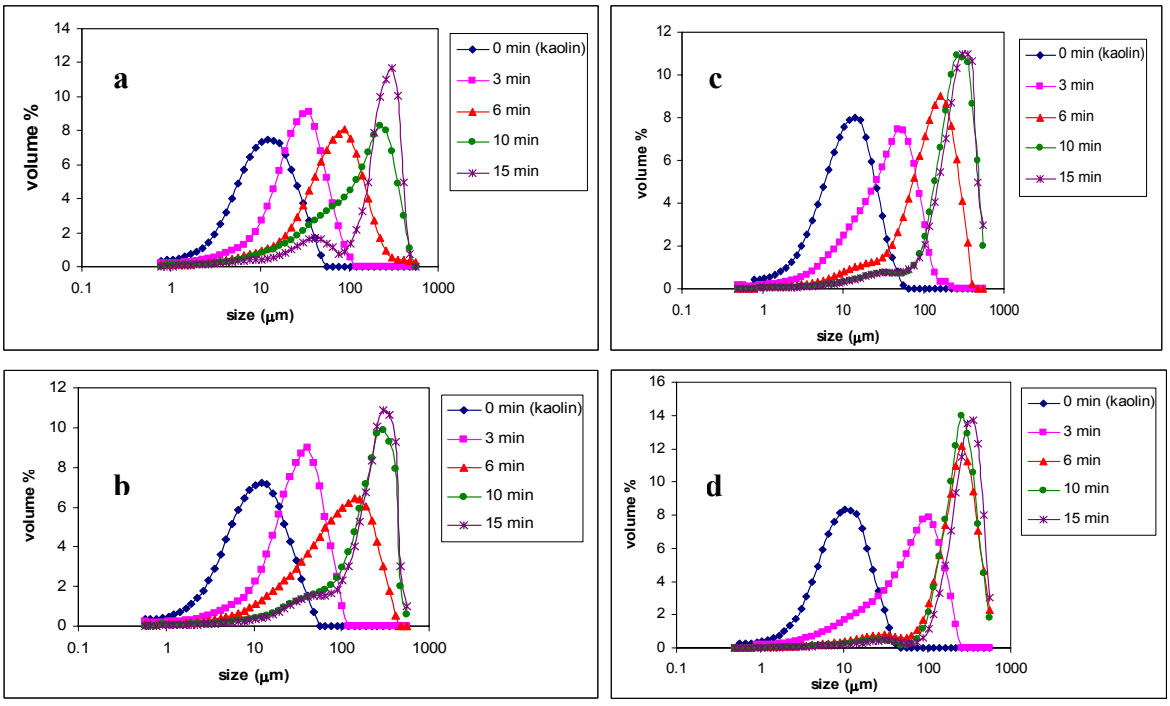

Fig.2. a. 0.042A, pH 5 b. 0.042A, pH 6.5 c. 0.22A, pH 5 d. 0.22A, pH 6.5.

formed and for both currents, at this pH a more rapid growth rate is observed. Moreover, for higher currents (0.22A) a significantly shorter induction period is observed. The higher growth rate observed for 0.22A, is due to increased dosage of aluminum, which will increase at this pH the precipitation of aluminum hydroxide, resulting in larger amounts of precursor particles.

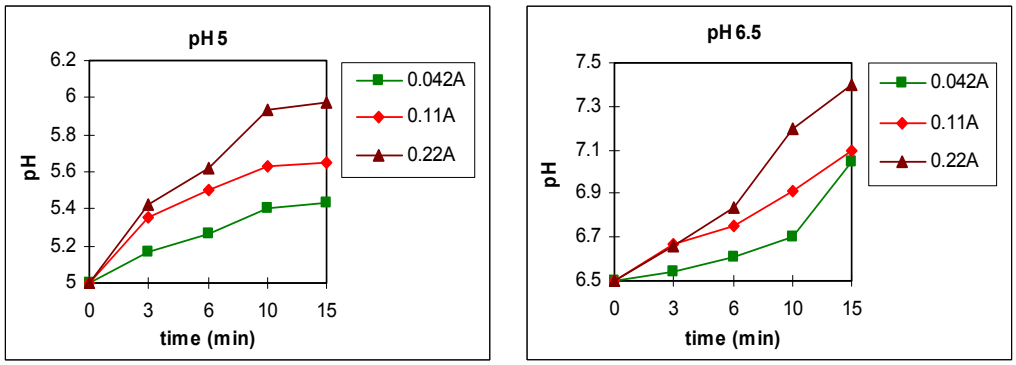

Fig.3. Change in pH for each time interval, initial pH 5 and 6.5.

Although pH 5 is not considered an optimal sweep floc regime (Amirtharajah and O'Melia, 1990), the addition of hydroxyl ions into the solution coupled with the continuous aluminum dosing pushes the equilibrium towards enhanced aluminum hydroxide precipitation and substantial growth is observed – even so, at a reduced rate compared to pH 6.5. At pH 5 the positive soluble aluminum mononuclear species govern the solution (Duan and Gregory, 2003), although as the process progresses, the pH rises and conditions become favorable for aluminum hydroxide precipitation (transition *into* sweep-floc regime), which stabilizes the pH after 10 minutes (Fig.3.) due to the removal of the excess hydroxyl ions from solution. However, at pH 6.5, the pH increases rapidly at end of process compared to the beginning, due to the move *out* of sweep floc regime as speciation shifts towards soluble negative mononuclear species. Under these conditions removal of the excess hydroxyl ions is limited, as aluminum hydroxide precipitation is no longer favorable, hence the sharper rise in pH. Despite the increase in pH and shift away from optimal precipitation conditions at the end of the process, the growth at pH 6.5 is more rapid than at pH 5.

Growth of particles into larger flocs is not only dependent on particle precursor numbers, but also on their ability to form stable bonds. Surface charge also plays a role in determining floc evolution (Nowostawska et al., 2005) which is measured here in the form of ζ potential - indicating electrostatic repulsive forces in the suspension (Fig.4.). The initial values of the kaolin suspension are -30 and -34 mV, which are the ζ potentials of the kaolin suspension at initial pH 5 and 6.5 respectively.

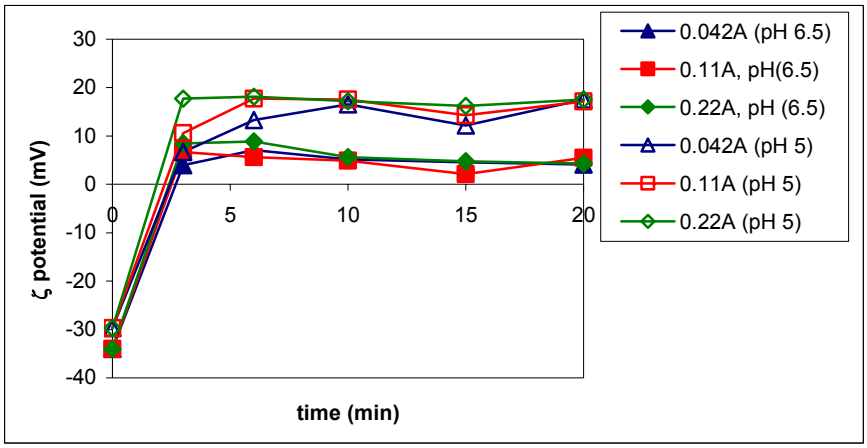

Fig. 4. ζ potential changes over time for 0.042A, 0.11A, 0.11A and pH 5 and 6.5

Within 3 minutes of EF, for both pH values, the ζ potential "jumps" to positive values which is indicative of the positive aluminum ions generated in solution, and the hydrolyzed species subsequently formed. In the initial stages, at pH 5, positive soluble aluminum mononuclear species in solution are dominant, and the ζ potential of the suspension in these conditions becomes more positive compared to pH 6.5. Stabilization occurs at 3, 6 and 10 minutes for 0.22A, 0.11A and 0.042A respectively - as conditions become favorable for aluminum hydroxide precipitation. For the pH values reached from initial pH 5, for each current, the aluminum hydroxide will be charged positively, as its iso-electric point (i.e.p) is between pH 8-9 (Sposito, 1996). At initial pH 6.5 the process commences from optimal sweep floc conditions while shifting the speciation towards negative soluble aluminum mononuclear species as it progresses. The ζ potential in these conditions is less positive than at pH 5, as less positive mononuclear species are present throughout the (initial) stages. The aluminum hydroxide surface charge is still positive, but nearer its i.e.p. A slight drop in the ζ potential is measured for all currents after 6 minutes, where speciation towards the negative mononuclear species begins to impact (also indicated by a sharper rise in pH (Fig.3.), as less hydroxyl ion is removed from solution in the form of aluminum hydroxide precipitate).

Floc growth stages

Several stages of floc growth occur during flocculation. Initially, precursor particle growth is dominant, after which particles combine and their size increases rapidly. As flocculation continues, the flocs form large, porous and open structures that are more susceptible to fragmentation by fluid shear (Tambo, 1991). As a result, the final floc size distribution is a balance between particle growth and breakage (Spicer and Pratsinis, 1996). Fig.5. shows the evolution of the volume mean diameter with time, for 0.042A and 0.22A with different current densities and pH values.

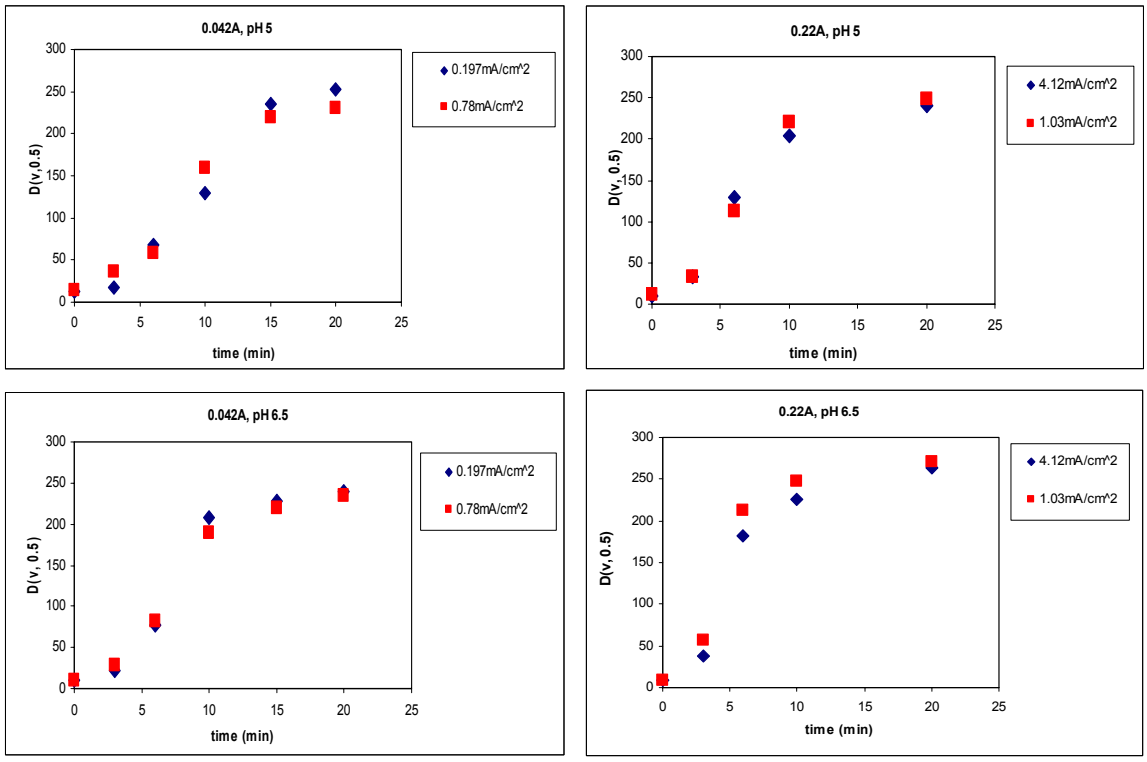

Fig.5. Evolution of the volume mean diameter for various current densities and pH values.

The graphs show that the current density does not affect the growth pattern of the flocs, within the ranges used in this experiment. Hence, all results now will refer to experimental data obtained using full anode area. Within the experimental conditions, the total dose of aluminum dictates the growth pattern, and factors such as current density and voltage (which is dependant on current density) do

not impact floc development. All graphs exhibit sigmoidal behaviour and three development stages. The first stage is the induction of aluminum hydroxide precursor particles, and limited growth due to primary collisions between those particles. Stage two exhibits enhanced growth of an exponential type, and in stage three the flocculation rate diminishes because of aggregate break up. These stages have been observed elsewhere (Kusters et al., 1997; Flesch et al., 1999). For both currents stage two commences at similar times (after 3 minutes), after which enhanced growth rates are observed for 0.22A, more so at pH 6.5. The transition to steady state (stage three) occurs when the flocs have reached a volume mean diameter of approximately 200μm, a size where disruption is caused by hydrodynamic stresses and fragmentation begins to dominate. The time of transition depends on the growth rate. For 0.042A and pH 5, this transition occurs at 15 minutes, while at pH 6.5 at an earlier time of 10 minutes. For 0.22A, pH 5 and 6.5 these times are 10 and 6 minutes respectively. In addition, for 0.22A and pH 6.5, the floc size obtained at steady state is larger than for all other conditions (above 250 μm). The increased aluminum dosing with this current, at an initial pH where aluminum hydroxide precipitation is optimal, increases the floc growth rate and apparently the strength of linkage between the particles comprising the floc, making it more resistant to breakage. This is in agreement with other studies (Francois, 1988), which found an increase both in floc growth rate and the collision efficiency with increased alum concentration during kaolin flocculation. Although at initial pH 5, the aluminum equilibrium shifts into sweep floc regime as the process progresses, this has less impact on the growth rates, than when starting out in optimal sweep floc regime, where initial nucleation and growth are maximized.

In the growth stages (induction and exponential), before transition to a steady state due to fragmentation, the connection between the volume mean diameter and time can be written as:

$$\mathbf{D(V,0.5) = Ke^{bt}} \qquad (15)$$

where K is a fitting parameter and b is the growth factor, dependent on the unique flocculation conditions.

By fitting the initial growth curves with a simple exponential regression, b can be calculated.

Table 2 summarizes the various growth factors obtained for various currents and pH values.

Initial pH	b (0.042A)	R^2	b (0.11A)	R^2	b (0.22A)	R^2
5.0	0.236	0.98	0.303	0.92	0.381	0.99
6.5	0.297	0.98	0.329	0.94	0.528	0.99

Table 2. Growth factors calculated from initial growth curves.

Fig. 6 shows the connection between growth factor and current, for each initial pH. A good degree of linearity is observed between the growth factor and applied current, within the current range used, higher currents producing higher growth factors. pH 6.5 yields not only higher growth factors, but also a higher growth dependency on current - which is larger by approximately 1.7 than that obtained at pH 5. These differences are most likely connected to the generation of mass into the system in the primary stages of the process, where at initial pH 6.5 aluminum hydroxide early precipitation is increased more with increase in current, relatively to initial pH 5. However, the primary mass generated is not necessarily the sole reason for the differences observed, as surface forces also play a role in particle coagulation enabling growth into larger floc. Moreover, floc structure has been found to affect the growth profile as a larger collision profile (a more open structure), enhances the collision frequency (Kusters et al., 1997; Flesch et al., 1999). Different alum doses have been shown to generate different floc structures (Tambo and Watanabe, 1979), thus the current applied in EF should also have a similar effect. However, in EF, the current does not only control the coagulant dosage, but it also creates a dynamic physical/chemical environment in which speciation shifts as the pH rises, while micro-bubbles are being simultaneously formed as gaseous

hydrolysis products are generated at the electrodes. All these are likely to have a profound effect on the evolving floc as floc structure is a crucial factor in understanding size evolution.

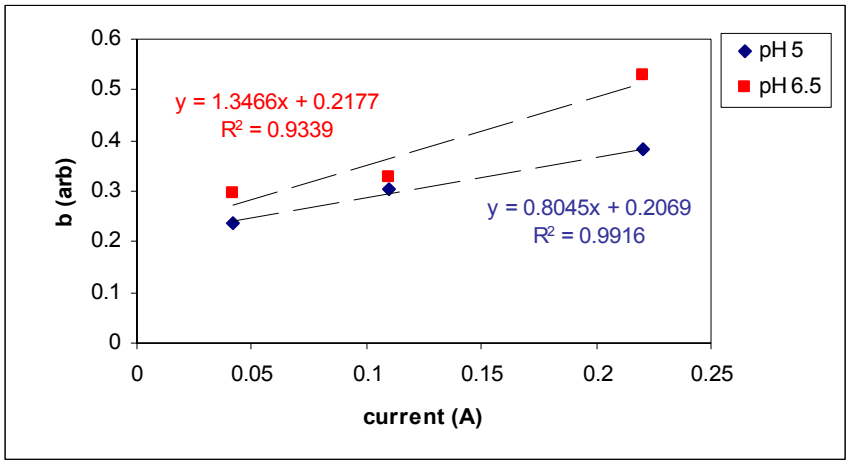

Fig.6. Dependency of growth factor on current at different pH values.

Structural evolution

Flocs undergo a series of processes including aggregation, fragmentation and, in some cases, structural rearrangement. The evolution of floc structure throughout the flocculation process depends on various factors such as floc size, formation and break-up rates, bonding forces and hydrodynamic forces (Selomulya et al., 2003). The change in floc structure can be quantified by monitoring the variation in the fractal dimension, or the scattering exponent (SE). As mentioned in the introduction, the SE will be used in this research to define the structural properties of the flocs.

To interpret scattering plots to obtain structural data on the flocs, the question whether the primary particles maintain independent scattering must be raised beforehand, that is if the RGD approximation is valid (eq. 13a and 13b). Precipitation of aluminum hydroxide precursor particles and their growth has been studied (Li et al., 2005). It has been shown that detectable precursors/nuclei appear in the range of 100nm. Due to the uncertainty of the aluminum hydroxide precursor particles nucleating, a refractive index of 1.59 can be used as an approximation, based on the refractive index range of other aluminum hydroxide crystals (Li et al., 2005). In this case, the limitations for assuming RGD approximation for structural interpretation of scattering plots of the flocs are fulfilled:

$m = n_{Al(OH)3}/n_{water} = 1.59/1.33 = 1.195$. $|m-1| = 0.195$ and

$(4\pi n_{water}/\lambda_{laser})L\,|m-1| = (4\pi 1.33/633)*100*0.195 = 0.5$

Fig.7. shows typical scattering graphs of flocs at different time intervals. The graphs obtained for 0.22A, at both pH values, show that transition into an angle independent scattering region at low q is hardly apparent. A mild transition does occur at the beginning of the process, at 3 minutes, after which the graphs exhibit a dependency on q, even in the low range. This is presumably a result of the large size of the flocs obtained for 0.22, after 6 minutes and above, for both pH values. For 0.042A, the transition is more apparent, and occurs for most time intervals, at both pH values, except at pH 6.5 after 10 and 15 minutes, again due to the size of the flocs. For all graphs, one decade of linearity is observed for: $1.4*10^{-4}<q<1.6*10^{-3}$. This region will be used to calculate the SE, from the slope of the scattering plots.

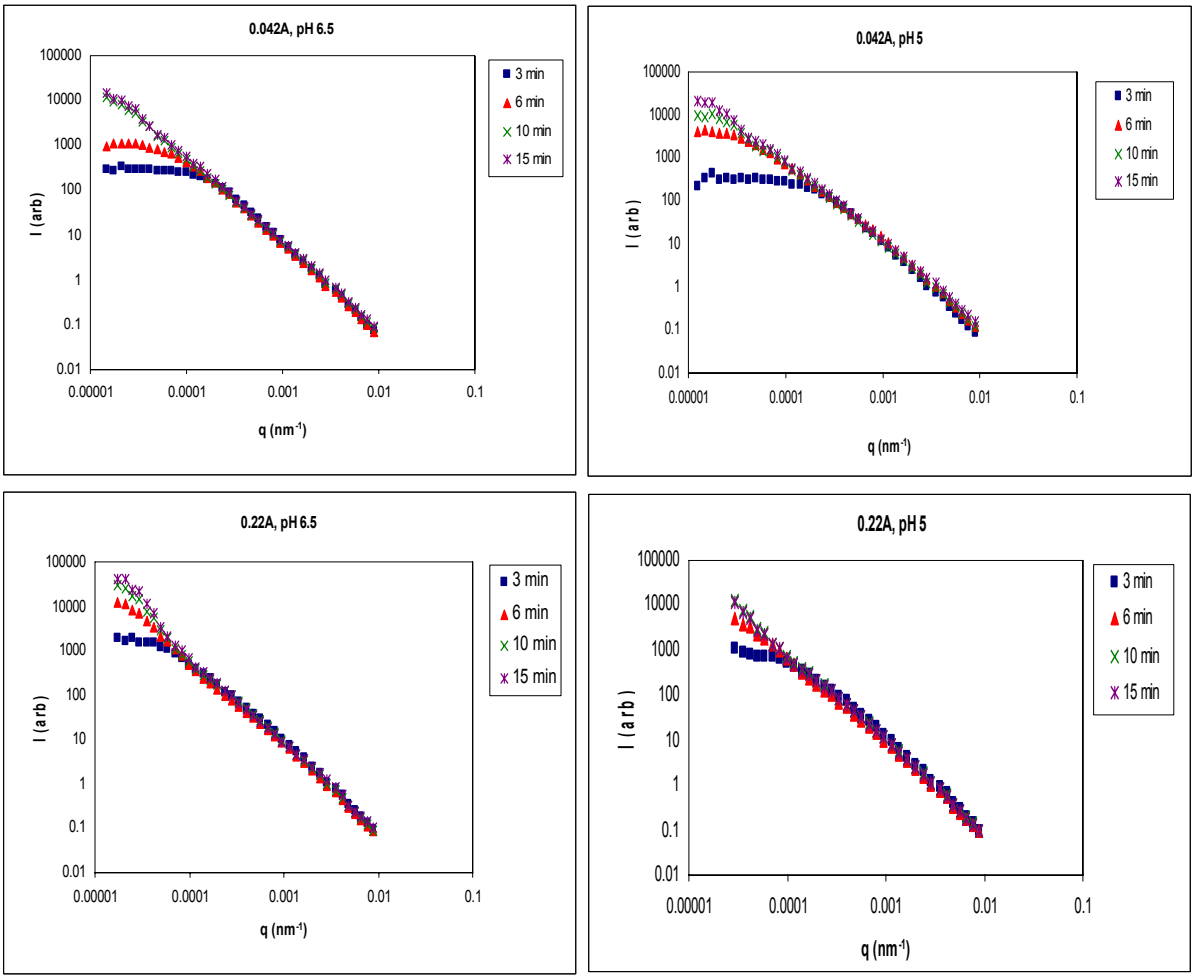

Fig.7. Conventional static light scattering plots (log(I) vs. log(q)) for $Al(OH)_3$ flocs forming as a function of time.

Time (min)	**SE**, pH 6.5			**SE**, pH 5		
	0.042A	0.11A	0.22A	0.042A	0.11A	0.22A
3	1.83±0.04	1.78±0.02	1.77±0.02	1.75±0.06	1.86±0.02	1.78±0.03
6	1.93±0.01	1.95±0.01	1.78±0.01	1.78±0.02	1.81±0.02	1.84±0.02
10	1.89±0.01	1.88±0.02	1.81±0.02	1.88±0.01	1.90±0.01	1.87±0.02
15	1.93±0.01	1.93±0.01	1.86±0.01	1.87±0.01	1.87±0.01	1.87±0.02

Table 3. Scattering exponents obtained for various currents and pH values.

The results show that for all currents and pH values compaction occurs during the process, resulting in a final SE, at 15 minutes, which is lower than that obtained during the initial 3 minutes. In some

conditions, fluctuations in the structural evolution are observed. This indicates the extreme fragile nature of the flocs.
For 0.042A, the flocs formed at pH 6.5 are more compact than those at pH 5. However, for 0.22A, the differences between the two pH values are not as distinct. From comparing 0.22A to 0.042A, at pH 6.5 it is evident that the higher current (aluminum dose) produced less compact flocs, throughout all stages of the process. This also impacts the growth rate which has been observed to be higher at

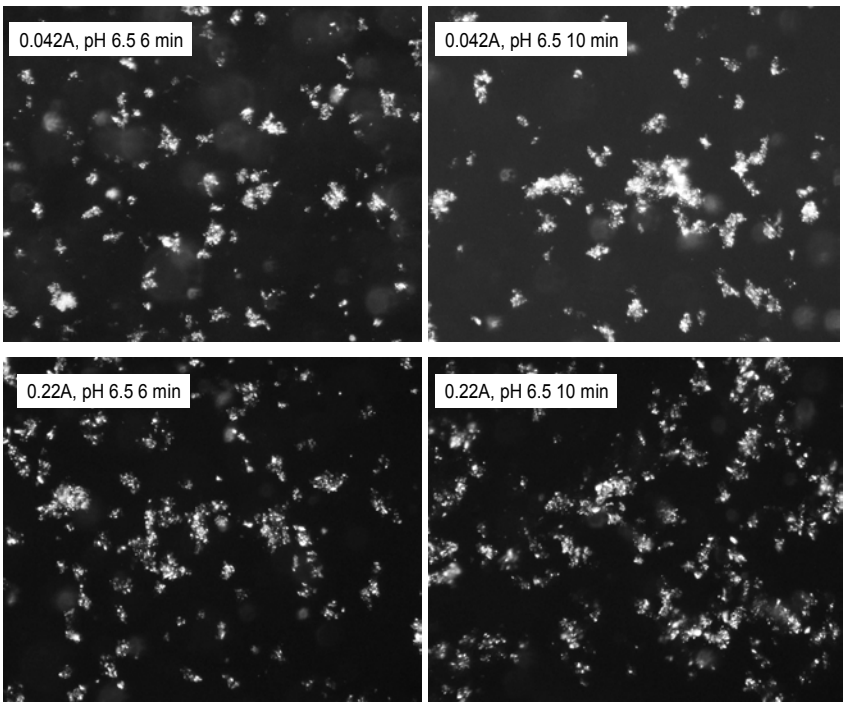

Fig.8. Floc structures obtained at pH 6.5 for 0.042A and 0.22A – 6 and 10 min.

0.22A, as the collision profile of the flocs forming is larger, and hence their collision frequency higher. Although for 0.22A, fragmentation starts at an earlier stage than for 0.042A (fig.5.) the flocs still maintain a more open structure, and reach a larger size by 15 minutes, thus indicating stronger linkage between particles comprising the floc.
This could be a result of the extent of transition out of favorable precipitation conditions. For 0.22A, compared to 0.042A, this transition is sharper, with the final pH reaching 7.4 as opposed to 7.0 for 0.042A. This affects the surface charge of the particles, as a higher pH will reduce the surface charge of the aluminum hydroxide precipitate shifting it towards its iso-electric point. A lower surface charge would decrease electrostatic repulsive forces, resulting in a higher collision efficiency and a stronger floc (stronger bonds). Moreover, at 0.22A, the generation of hydrogen gas is increased and therefore more micro-bubbles are present. These are incorporated in the floc, thus creating a more porous structure. Fig.8. illustrates these differences visually. For 0.042A and pH 6.5, the flocs are well defined, and compact in structure, whereas 0.22A yields structures which are extremely tenuous displaying a porosity which seems even transparent in some regions. For pH 5, differences in the SE obtained at different currents are not appreciable, which exhibit a rather open structure, as indicated in Fig.9. At this pH, the transition into more favorable aluminum hydroxide precipitation conditions occurs at the later stages of the process (as the pH and aluminum dose rise), thus the mass introduced into the system is less than at pH 6.5. In this case, incorporation of the micro-bubbles into flocs containing less mass would probably result in a more open structure. The flocs also exhibit less strength, and despite their large collision profile do not reach the size obtained at pH 6.5 for 0.22A.

At pH 5, the surface charge of the aluminum hydroxide precipitating is more positive (further from the i.e.p) than at pH 6.5, indicating that repulsive electrostatic forces are stronger.

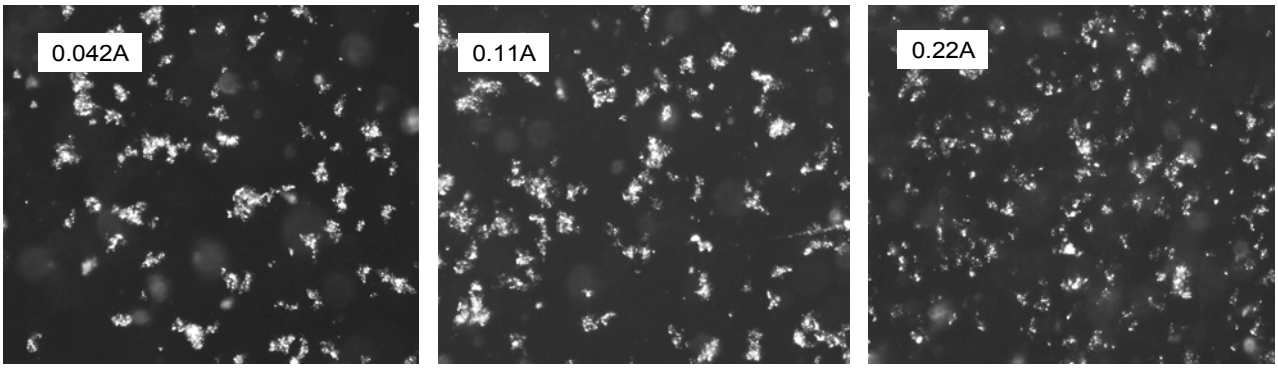

Fig.9. Floc structures obtained at pH 5, for various currents – 10 min.

The above data shows that size and structure evolution of flocs in EF of a colloidal suspension stems from a delicate balance between mass introduced (particle numbers) at the initial stages of the process and the amount of gaseous products (in the form of microbubbles) in solution – both are current dependent. The initial particle numbers are also a function of pH, which creates, in conjunction with the current, conditions favorable for aluminum hydroxide supersaturation and precipitation. However, these also affect the surface charge of the flocs forming, which in turn affects the strength of the bonds between the precursor particles and ultimately the collision efficiency and size of the floc. All these parameters, which are intertwined, are summarized in a conceptual model (Fig.10.) which predicts floc structure and size, with reference to the specific conditions studied here (EF of a model kaolin suspension).

At pH 5 less mass is generated as floc sweep regime is not optimal. The repulsive surface forces at this pH are stronger for all currents, therefore the collision efficiency (α) is lower. The floc structure depends on the ratio of microbubbles/mass, as more open structures evolve, as the ratio increases. For lower currents this ratio is maintained (a low current results both in low mass and less microbubbles), but the reduced mass will result in flocs exhibiting a lower collision efficiency (β) that evolve slowly – but still portray a porous structure. For higher currents, the collision frequency is higher as more mass is generated along with hydrolysis products, resulting in a more rapidly evolving porous structure.

At pH 6.5 more mass is generated as the conditions are optimal for aluminum hydroxide precipitation. The repulsive surface forces are weaker, indicated by a ζ potential which is nearer to the i.e.p of aluminum hydroxide – hence, the collision efficiency is higher. For lower currents, the microbubble/mass ratio is smaller, and coupled with the reduced mass will result in a more compact floc which evolves slowly. For higher currents, microbubble generation is increased, resulting in a more open structure, but exhibiting strength. These flocs have both a high collision frequency and high collision efficiency – hence, the increased growth dependency on current and increased growth rate.

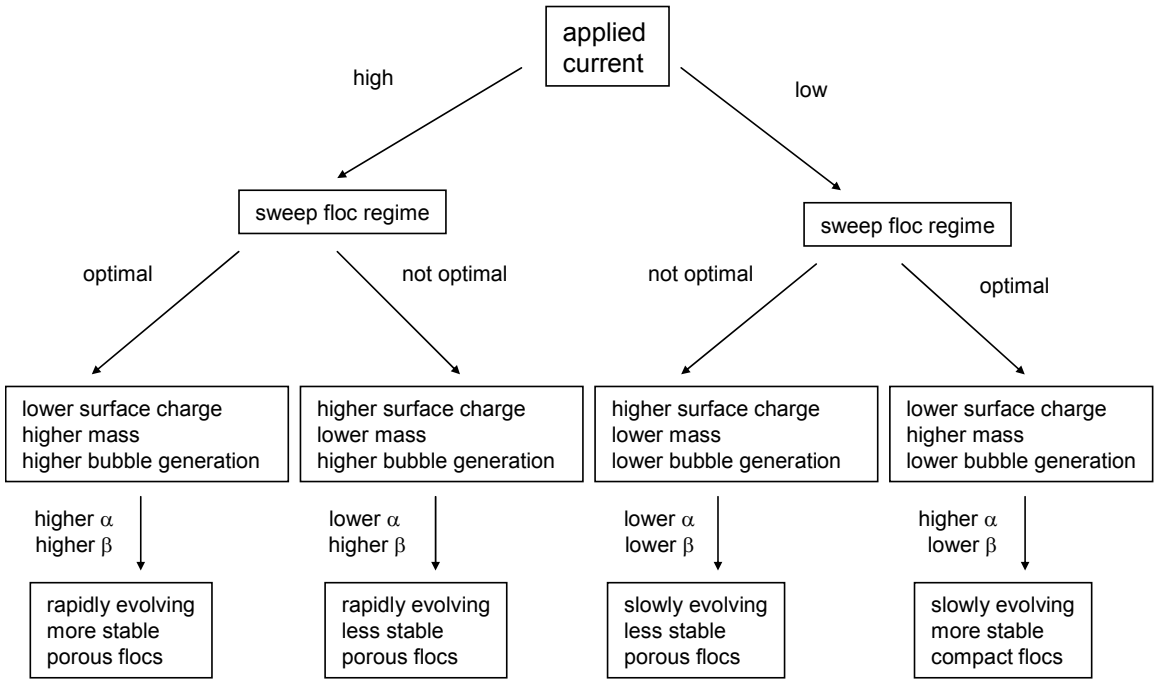

Fig. 10. Conceptual model predicting floc evolution – rate and structure.

4. Conclusions

EF consists of synergistic processes which create a dynamic environment in which floc formation and growth occur. The system's response to current and pH change will dictate the kinetics of floc formation and growth in EF, and subsequently floc structure. The system studied serves as a model for natural occurring systems containing colloidal matter, and displayed kinetic behavior which can be connected to specific system characteristics, derived from operational parameters.

- Floc growth was found to be independent of current density, and only dependent on absolute current values (within the values examined).
- All evolution patterns, for all conditions, included three typical stages: induction, exponential growth and fragmentation, as found in conventional flocculation.
- Higher growth rates were obtained for higher currents.
- A higher dependency of growth rate on current occurred at pH 6.5, in optimal sweep floc regime. This appears to stem from the stronger linkage between particles at this pH, coupled with increased mass and microbubble generation for higher currents - resulting in larger collision efficiencies and enhanced growth rate.
- The flocs undergo compaction and in some cases structural fluctuation occurring during growth. This reflects somewhat their fragile nature.
- EF can generate range of flocs, exhibiting different structural characteristics, depending on the conditions of operation. This versatility has clear implications to many processes of importance in water and wastewater treatment as flocs can be "tailored" for specific processes, depending on their requirements.

Acknowledgements

The work was partially supported by BMBF Germany and Israeli ministry of Science. We gratefully acknowledge Dr. Rivka Amit and Mr. Yoav Nahamias from the Geological Survey of Israel for assistance with the Malvern Mastersizer Microplus, and other instrumentation. This work is part of the Ph.D thesis of Tali Harif.

5. References

1. Amirtharajah, A. and O'Melia, C.R. (1990) Coagulation Processes: destabilization, mixing and flocculation. Water Quality and Treatment, New-York, McGraw-Hill.
2. Letterman, R.D., Amirtharajah, A., O'Melia, C.R. (1999) Coagulation and Flocculation. In AWWA "Water Quality and Treatment", Letterman, R.D. (ed.)
3. Vik, E. A., Carlson, D. A., Eikum, A. S., Gjessing, E. T. (1984) Electrocoagulation of potable water. Water Research **18** (11), 1355-1360.
4. Matteson, M. J., Dobson, R. L., Glenn, R. W., Jr., Kukunoor, N. S., Waits, W. H. III., Clayfield, E. J. (1995) Electrocoagulation and separation of aqueous suspensions of ultrafine particles. Colloids and Surfaces A: Physicochemical Engineering Aspects **104**, 101-109.
5. Holt, P. K., Barton, G. W., Wark, M., Mitchell, C.A. (2002) A quantitative comparison between chemical dosing and electrocoagulation. Colloids and Surfaces A: Physicochemical Engineering Aspects **211**, 233-248.
6. Do, J. S. and Chen, M. L. (1994) Decolorization of dye-containing solutions by electrocoagulation. Journal of Applied Electrochemistry **24**, 785-790.
7. Pouet, M. F. and Grasmick, A. (1995) Urban wastewater treatment by electrocoagulation and flotation. Water Science and Technology **31** (3-4), 275-283.
8. Belongia, B. M., Haworth, P. D., Baygents, J. C., Raghavan, S. (1999) Treatment of alumina and silica chemical mechanical polishing waste by electrodecantation and electrocoagulation. Journal of the Electrochemical Society **146** (11), 4124-4130.
9. Mollah, A. Y. A., Schennech, R., Parga, J. R. Cocke, D. L. (2001) Electrocoagulation (EC) – Science and applications. Journal of Hazardous materials **B84**, 29-41.
10. Adin, A. and Vescan, N. (2002) Electroflocculation for particle destabilization and aggregation for municipal water and wastewater treatment. Proceeding of the American Chemistry Society **42** (2), 537-541.
11. Smoluchowski, M. (1917) Versuch einer mathematischen theorie der koagulations – kinetik kolloides losungen, Z. Physic. Chem. **92**, 129-168.
12. Duan, J. and Gregory, J. (2003) Coagulation by hydrolyzing salts. Advances in Colloid and Interface Science **100-102**, 475-502.
13. Jiang, Q. and Logan, B.E. (1991) Fractal dimensions of aggregates determined from steady state size distributions. Environmental Science and Technology **25**, 2031-2038.
14. Kusters, K.A., Wijers, J.G., Thoenes, D. (1997) Aggregation kinetics of small particles in agitated vessels. Chemical Engineering Science **52** (1), 107-121.
15. Tambo, N. (1991) Basic concepts and innovative turn of coagulation/flocculation. Water Supply **9**, 1-10.
16. Spicer, P.T. and Pratsinis, S.E. (1996) Shear-induced flocculation: The evolution of floc structure and the shape of the size distribution at steady-state. Water Research **30** (5), 1049-1056.
17. Potanin A. A. (1991) On the mechanism of aggregation and breakup of polystyrene. Journal of Colloid and Interface Science **145**, 140-157.
18. Flesch, J.C., Spicer, P.T., Pratsinis S.E. (1999) Laminar and turbulent shear-induced flocculation of fractal aggregates. AIChE Journal **45** (5), 1114-1124.
19. Oles, V. (1992) Shear-induced aggregation and breakup of polystyrene latex particles. Journal of Colloid and Interface Science **154**, 351-358.
20. Mandelbrot, B. B. (1987) The fractal geometry of nature. Freeman, New-York.
21. Guan, J., Waite T.D., Amal R. (1998) Rapid structure characterization of bacterial aggregates. Environmental Science and Technology **32**, 3735-3742.
22. Lo B. and Waite, T.D. (2000) Structure of hydrous ferric oxide aggregates. Journal of Colloid and Interface Science **222**, 83-89.

23. Tence, M., Chevalier J. P., Jullien R. (1986) On the measurement of the fractal dimension of aggregated particles by electron-microscopy experimental method, corrections and comparison with numerical models. Journal De Physique **47** (11), 1989-1998.
24. Clark, M.M. and Flora, J.R.V. (1991) Floc restructuring in varied turbulent mixing. Journal of Colloid and Interface Science **147**, 407-421.
25. Chakraborti, R.K., Gardner, K.H., Atkinson, J.F., Van Benschoten J.E (2003) Changes in fractal dimension during aggregation. Water Research **37**, 873-883.
26. Thill, A., Lambert, S., Moustier, S., Ginestet, P., Audic, J.M., Bottero, J.Y. (2000) Structural interpretations of static light scattering patterns of aggregates II. Experimental study. Journal of Colloid and Interface Science **228**, 386-392.
27. Sorensen C.M. (1997) Surface and colloid chemistry: Birdi, K.S., Ed., CRC Press: Boca Raton, FL, Chapter 13, 533-558.
28. Lawler, D.F. (1997) Particle size distributions in treatment processes: theory and practice. Journal of Water Science and Technology **36** (4), 15-23.
29. Bushell, G. and Amal, R. (1998) Fractal aggregates of polydisperse particles. Journal of Colloid and Interface Science **205**, 459-469.
30. Chowdhury, Z.K., Amy, G.L., Bales R.C. (1991) Coagulation of submicron colloids in water treatment by incorporation into aluminum hydroxide floc. Journal of Environmental Science and Technology **25**, 1766-1773.
31. Nowostawska, U., Sander, S.G., McGrath, K.M., Hunter K.A. (2005) Effects of coagulants on the surface forces of colloidal alumina under water treatment conditions. Colloids and Surfaces A; Physicochemical Engineering Aspects **266**, 214-222.
32. Francois, R.J. (1988) Growth kinetics of hydroxide flocs. American Water Works Association **80**, 92-96.
33. Tambo, N. and Watanabe, Y. (1979) Physical characteristics of flocs I: the floc density and aluminum floc. Water Research **13**, 409-419.
34. Selomulya, C., Bushell, G., Amal, R., Waite, T.D. (2003) Understanding the role of restructuring in flocculation: The application of a population balance model. Chemical Engineering Science **58**, 327-338.
35. Li, H., Addai-Mensah, J., Thomas, J.C., Gerson, A.R. (2005) The influence of Al(III) supersaturation and NaOH concentration on the rate of crystallization of $Al(OH)_3$ precursor particles from sodium aluminate solutions. Journal of Colloid and Interface Science **286**, 511-519.